

1 **The esophageal epithelium in systemic sclerosis: cellular and molecular**  
2 **dysregulation revealed by single-cell RNA sequencing**

3  
4 Matthew Dapas<sup>1</sup>, Margarette H. Clevenger<sup>2</sup>, Hadijat M. Makinde<sup>1</sup>, Tyler Therron<sup>1</sup>, Dustin A.  
5 Carlson<sup>2</sup>, Mary Carns<sup>1</sup>, Kathleen Aren<sup>1</sup>, Cenfu Wei<sup>2</sup>, Lutfiyya N. Muhammad<sup>3</sup>, Carrie L.  
6 Richardson<sup>1</sup>, John E. Pandolfino<sup>2</sup>, Harris R. Perlman<sup>1\*</sup>, Deborah R. Winter<sup>1\*</sup>, Marie-Pier  
7 Tetreault<sup>2\*</sup>

8  
9  
10 **Affiliations:**

- 11 1. Division of Rheumatology, Department of Medicine, Northwestern University Feinberg School of  
12 Medicine, Chicago, IL  
13 2. Division of Gastroenterology & Hepatology, Department of Medicine, Northwestern University  
14 Feinberg School of Medicine, Chicago, IL  
15 3. Department of Preventive Medicine, Northwestern University Feinberg School of Medicine, Chicago,  
16 IL

17  
18  
19  
20  
21

\*These authors jointly supervised the work

22 **ABSTRACT**

23

24 Systemic sclerosis (SSc) is a rare autoimmune disease characterized by vasculopathy and progressive

25 fibrosis of the skin and internal organs. Individuals with SSc often suffer from chronic acid reflux and

26 dysphagia due to loss of esophageal motility. However, the pathogenesis of esophageal dysmotility in SSc

27 is poorly understood. To determine whether distinct changes in esophageal epithelial cells contribute to

28 impaired motility in SSc, we investigated the stratified squamous esophageal epithelium using single-cell

29 RNA sequencing (n=306,372 cells) in individuals with SSc compared those with gastroesophageal reflux

30 disease (GERD) as well as healthy controls. The proportion of epithelial cells in the outermost, superficial

31 compartment of the esophageal epithelium was significantly reduced in SSc (9.4% vs 21.6% in HCs).

32 Differential gene expression in SSc was primarily limited to the superficial compartment (3,572 genes vs.

33 232 in all other compartments), with significant upregulation of extracellular matrix and keratinization

34 genes. These cellular and molecular changes in SSc were highly correlated with those seen in GERD,

35 indicating they were secondary to reflux; however, their magnitudes were more pronounced in the proximal

36 esophagus, suggesting that esophageal dysmotility leads to greater proximal acid exposure, which may

37 contribute to aspiration. SSc-specific gene dysregulation implicated immunoregulatory pathways likely

38 pertinent to pathogenic mechanisms. By offering a comprehensive view of transcriptional dysregulation at

39 single-cell resolution in human esophageal epithelial cells in SSc compared to GERD and healthy tissue,

40 this work clarifies the state of epithelial cells in SSc-induced esophageal dysfunction.

## 41 INTRODUCTION

42 Systemic sclerosis (SSc), also known as scleroderma, is an immune-mediated rheumatic disease of  
43 unknown etiology that causes progressive fibrosis of the skin and internal organs. Although uncommon  
44 (18-26 per 100,000 people)<sup>1-4</sup>, SSc is one of the deadliest autoimmune disorders<sup>5</sup>, with a 10-year survival  
45 rate of 45-68% following diagnosis<sup>4,6,7</sup>. Over 90% of individuals with SSc report gastrointestinal (GI)  
46 dysfunction<sup>8</sup>, with esophageal dysmotility being the most common GI manifestation<sup>9</sup>. Individuals with SSc  
47 and esophageal involvement typically suffer from chronic acid reflux and dysphagia due to loss of  
48 esophageal motility and are at much greater risk of esophageal stricture and Barrett's esophagus<sup>8,10,11</sup>. The  
49 rate of esophageal involvement was nearly twice as high in individuals with SSc who died within 5 years  
50 of diagnosis<sup>12</sup>.

51 There are multiple, interrelated mechanisms that may cause esophageal dysmotility in SSc.  
52 Vascular damage and neurogenic impairment lead to smooth muscle cell fibrosis<sup>13</sup>, but esophageal muscle  
53 atrophy has also been observed in SSc without vasculopathy or fibrosis<sup>14</sup>. Inflammatory signatures<sup>15</sup>,  
54 absence of anti-centromere antibodies<sup>16</sup>, and presence of anti-topoisomerase I antibodies are associated with  
55 esophageal complications, as well<sup>8</sup>. Complicating research efforts is significant clinical and molecular  
56 heterogeneity observed between SSc patients<sup>17-19</sup> and difficulty distinguishing between effects from  
57 autoimmune processes and secondary factors such as severe reflux. Consequently, the pathogenesis of  
58 esophageal disease in SSc remains poorly understood.

59 Molecular investigations of SSc esophageal involvement have primarily focused on canonical  
60 pathways in submucosal and muscle layers<sup>20</sup>. However, the mucosa is no less essential for normal  
61 esophageal transport<sup>21,22</sup>, and recent studies have suggested that esophageal epithelial cells (EECs) may  
62 play a more central role in the pathogenesis of SSc esophageal involvement than previously thought<sup>20</sup>.  
63 Mouse models with epithelial-cell-specific knockout of *Fli1*, an Ets transcription factor implicated in SSc  
64 pathogenesis<sup>23</sup>, spontaneously develop dermal and esophageal fibrosis and interstitial lung disease<sup>24</sup>.  
65 Importantly, the resultant lung disease is mediated by T-cell autoimmunity, but fibrosis of the skin and

66 esophagus persist in mice additionally lacking mature T and B cells, suggesting that the fibrosis is  
67 principally driven by the epithelia<sup>20,24</sup>.

68 Most studies implicating epithelial cells in SSc esophageal dysmotility have been performed in  
69 mice or *in vitro*, and molecular analyses in humans have so far been limited to bulk tissues<sup>15</sup>. Furthermore,  
70 single-cell gene expression studies performed in other diseases of the esophagus, including squamous cell  
71 carcinoma<sup>25,26</sup> and allergic eosinophilic esophagitis<sup>27,28</sup>, have identified substantial cellular and molecular  
72 changes in EECs compared to healthy tissue, such as significant expansion of non-proliferative suprabasal  
73 cells<sup>27,28</sup>. Therefore, to comprehensively investigate the effects of SSc on the esophageal epithelium, we  
74 performed single-cell RNA sequencing (scRNA-seq) of esophageal mucosal biopsies from SSc patients  
75 with clinically significant esophageal involvement and compared EEC distributions and gene expression  
76 signatures to individuals with gastroesophageal reflux disease (GERD) and healthy controls (HCs). By  
77 examining gene expression profiles from human tissue at single-cell resolution, this work sheds essential  
78 light on the cellular roots of esophageal dysfunction in SSc by clarifying the pathogenic role of the  
79 squamous epithelium, one of the most integral tissues supporting healthy esophageal function.

80

## 81 **METHODS**

82

### 83 **Subjects**

84 The SSc study population were recruited from adult patients aged 18 to 89 diagnosed with SSc according  
85 to the 2013 ACR/EULAR classification criteria, who visited the Northwestern Medicine Esophageal Center  
86 for esophageal symptom evaluation and motility testing, as described previously<sup>29</sup>, between 2020 and 2021.  
87 Patients with GERD were recruited at the primary visit following positive Bravo pH testing<sup>28</sup>. Patients with  
88 technically inadequate panometry or manometry studies, previous foregut surgeries (including prior  
89 pneumatic dilation), or mechanical obstructions in the esophagus such as esophageal stricture, eosinophilic  
90 esophagitis, severe reflux esophagitis (Los Angeles classification C or D), or hiatal hernias larger than 5  
91 cm were excluded. HCs met asymptomatic criteria including lack of esophageal symptoms, no history of

92 alcohol dependency or tobacco use, body mass index less than 30kg/m<sup>2</sup>, and no previous antacid or proton  
93 pump inhibitor treatment<sup>28</sup>. The study protocol received approval from the Northwestern University  
94 Institutional Review Board.

95

## 96 **Symptom evaluation and motility testing**

97 Esophageal function testing included functional lumen imaging probe (FLIP) panometry during sedated  
98 endoscopy, high-resolution manometry (HRM), and in some subjects, 24-hour pH-impedance or timed-  
99 barium esophagram, which were completed and interpreted as previously described<sup>30-33</sup>. HRM  
100 classifications were based on the application of the Chicago Classification v4.0 to 10 supine and 5 upright  
101 test swallows<sup>34</sup>. FLIP panometry classifications were based on previous evaluation of asymptomatic  
102 volunteers and patients<sup>35-37</sup>. During endoscopy (same encounter as HRM/FLIP), esophageal mucosal  
103 biopsies were obtained at approximately 5-cm (“distal esophagus”) and 15-cm (“proximal esophagus”)  
104 proximal to the squamocolumnar junction. Acid exposure was measured as the percentage of time with  
105 esophageal pH<4 over a monitoring period of 24 hours. Most patients also completed validated symptom-  
106 questionnaires (patient-reported outcomes) on the day of esophageal motility testing with FLIP or HRM,  
107 including the Brief Esophageal Dysphagia Questionnaire (BEDQ), the Gastroesophageal Reflux Disease  
108 Questionnaire (GerdQ), and the Northwestern esophageal quality of life (NEQOL) survey.<sup>38-40</sup>

109

## 110 **Sample processing and sequencing**

111 Esophageal mucosal biopsies from proximal and distal esophagus were processed for scRNA-seq as  
112 described in Clevenger et al<sup>28</sup>. Briefly, following tissue digestion and filtering, cell suspensions met 85%  
113 minimum viability via Cellometer Auto2000 (Nexcelom Bioscience). Cells were loaded into a Chromium  
114 iX controller (10X Genomics) on a Chromium Next GEM Chip G (10X Genomics) to capture  
115 approximately 10,000 cells per sample and were processed for encapsulation following the manufacturer’s  
116 protocol. Cell barcoding and library construction were performed using the 10X Genomics Chromium  
117 Next GEM Single Cell 3’ Reagents Kits v3.1 and Dual Index Kit TT Set A according to the manufacturer’s

118 protocol. Sequencing was performed by the NUseq Core using the Illumina Novaseq 6000. Paired-end  
119 reads consisting of a 28-base-pair read for cell barcodes and unique molecular identifiers and a 90-base-  
120 pair read for transcripts were aligned to the GRCh38 reference transcriptome using Cell Ranger v6.1.2.

121

### 122 **Sample and cell quality control**

123 Samples with high ambient RNA (<70% of sequencing reads mapped to cells) were removed from  
124 consideration. Gene expression counts generated by Cell Ranger were analyzed using Seurat v4.3.0<sup>41</sup>. Cells  
125 with low gene diversity (<200 unique genes), low unique molecular identifier counts (<500), or excessive  
126 counts (>100,000) were removed from consideration. Cells with high proportions of mitochondrial DNA  
127 reads, indicative of apoptosis or lysis, were removed using the bivariate regression models implemented in  
128 the miQC package<sup>42</sup>. Cells were filtered if their proportion of reads mapped to mitochondrial DNA  
129 exceeded 0.05 and their posterior probability of belonging to a compromised cell distribution was greater  
130 than 0.75 according to miQC. Doublets, in which more than one cell is clumped together in a single droplet,  
131 were predicted and removed using scDblFinder<sup>43</sup> with an expected, additive doublet rate of 0.01 per  
132 thousand cells with standard deviation of 0.01.

133

### 134 **Sample integration and cell type annotation**

135 Individual samples were normalized and integrated on 3,000 variable features using Seurat's SCTransform  
136 procedure<sup>44</sup> with v2 regularization<sup>45</sup> and canonical correlation analysis dimension reduction. Integration  
137 anchors were determined using a reference consisting of three pairs of proximal and distal samples from  
138 HCs. Principal component (PC) analysis was performed on the transformed and integrated expression  
139 counts. Uniform manifold approximation and projection (UMAP)<sup>46</sup> embeddings were calculated on the top  
140 40 PCs with n=200 neighbors. Cell clustering was performed using Seurat's modularity-based clustering  
141 on a shared nearest neighbor (SNN) graph with k=25 on the top 40 PCs. Clusters were annotated according  
142 to the expression of established cell-specific gene markers (**Supplemental Table 1, Supplemental Figure**

143 1). For annotation of smaller cell clusters, we first filtered out the epithelial, myeloid, lymphoid, and  
144 endothelial cell clusters and then recomputed PCs and re-clustered the subset (PCs = 25, k=15).

145

### 146 **Epithelial cell characterization**

147 After isolating the subset of epithelial cell clusters, we further filtered cells with disproportionately low  
148 read counts ( $\leq 3,500$ ; **Supplemental Figure 2, A-C**). The samples were then re-integrated using the  
149 procedure described above. UMAP embeddings were calculated on the top 35 PCs with n=100 neighbors.

150 Epithelial compartments (basal, suprabasal, and superficial) were identified according to expression of  
151 established markers (**Supplemental Figure 4D**)<sup>27,28,47-50</sup>. For each compartment, we computed composite

152 gene signature scores using Seurat's AddModuleScore() function (**Supplemental Figure 2E**). Cells were  
153 initially clustered on an SNN graph with k=50 with resolution=0.25 (**Supplemental Figure 2F**), but

154 because the modularity optimization clustering implemented in Seurat grouped proliferating cells across  
155 different epithelial compartments and inconsistently distinguished suprabasal and superficial cells, we

156 applied K-means clustering on the expression of the compartment-specific markers to delineate epithelial  
157 compartments. We performed separate K=2 K-means clustering on 1) the Seurat clusters containing basal

158 and early suprabasal cells (clusters 1-5) to distinguish basal from suprabasal compartments and 2) the Seurat  
159 clusters containing late suprabasal and superficial cells (clusters 6-8) to demarcate suprabasal and

160 superficial compartments (**Supplemental Figure 2, G-H**). Proliferating epithelial cells were identified  
161 using Seurat's CellCycleScoring() function. Cells predicted as being in S or G2/M phases based on the

162 relative expression of corresponding markers<sup>51</sup> were labeled as proliferating cells (**Supplemental Figure**  
163 **2I**). We tested for statistical differences in proportions of epithelial cell populations between conditions

164 using MASC<sup>52</sup>. To derive a continuous epithelial differentiation score for each cell (**Supplemental Figure**  
165 **3**), we combined the compartment-specific module scores as follows :

$$166 \quad EDS_C = score_{suprabasal} + score_{superficial} - score_{basal}$$

167

168 Where  $EDS_C$  is the epithelial differentiation score for a given cell. This  $EDS_C$  was then scaled between 0  
169 and 1:

170

$$171 \quad EDS_{C,scaled} = \frac{EDS_C - \min(EDS_1, \dots, EDS_n)}{\max(EDS_1, \dots, EDS_n) - \min(EDS_1, \dots, EDS_n)}$$

172

### 173 **Gene expression analysis**

174 To identify dysregulated pathways in SSc, we first calculated differential gene expression between  
175 conditions within each epithelial compartment, considering each cell as a sample. Differential gene  
176 expression was calculated using the FindMarkers() function in Seurat with the Wilcoxon rank-sum test on  
177 log-normalized RNA counts for genes expressed in at least 1% of cells by compartment. We adjusted for  
178 multiple testing using a Bonferroni correction accounting for the number of genes tested. Genes with an  
179 adjusted  $P < 0.05$  and absolute  $\log_2$  fold change  $> 0.1$  were considered significantly differentially expressed.

180 <sup>53,54</sup> Genes were then ranked by the magnitude and statistical certainty of their expression differences:

181

$$182 \quad Weight = -\log_{10}(p) * abs(\log_2[FC])$$

183

184 Gene set enrichment was calculated using 3,795 canonical pathway gene sets from the Human Molecular  
185 Signatures Database<sup>55</sup> using gene set enrichment analysis (GSEA)<sup>53,54</sup>. Statistical gene set enrichment was  
186 calculated using one-way positive enrichment with 100,000 permutations on pathways with at least 10  
187 genes. Mitochondrial and ribosomal genes were excluded from the GSEA.

188 To more robustly characterize gene expression differences between conditions<sup>56</sup>, we performed  
189 pseudo-bulk differential expression analysis by aggregating RNA counts per sample within epithelial  
190 compartments. Genes with at least one count per million detected in at least 75% of samples in at least one  
191 condition per epithelial compartment were analyzed. To mitigate outlier-driven signals, genes with log-  
192 transformed expression greater than 3 standard deviations from the mean in exactly one individual were



193 excluded. Differential gene expression was evaluated using edgeR v3.42.4<sup>57-59</sup>. Gene expression was  
194 modeled using a quasi-likelihood negative binomial generalized linear model, with global negative-  
195 binomial trended dispersion estimated across all samples and gene-specific quasi-likelihood dispersions  
196 estimated within each epithelial compartment. Differences in gene expression across conditions were  
197 assessed using quasi-likelihood F-tests with false-discovery rate (FDR) adjustment. We conducted tests  
198 combining both proximal and distal esophageal regions, as well as separate tests for each esophageal region.

199 Transcription factor enrichment analyses were conducted on the pseudo-bulk results using the  
200 enricher() function from clusterProfiler v4.8.3<sup>60</sup>. We used consensus results from ENCODE<sup>61</sup> and ChEA<sup>62</sup>,  
201 as curated by the Ma'ayan Lab<sup>63</sup> and available at <http://amp.pharm.mssm.edu/Enrichr/><sup>64</sup> to test for the  
202 enrichment of transcription factor target genes from among genes that were differentially expressed  
203 between SSc, GERD, and HCs with Bonferroni-adjusted  $p < 0.05$ . Background gene sets were comprised of  
204 the genes included in the pseudo-bulk differential expression analyses for each epithelial compartment.  
205 Transcription factors absent from the background gene set were removed as candidate transcription factors.  
206 Separate enrichment tests were performed for all differentially expressed genes (DEGs) and those that were  
207 upregulated or downregulated in SSc. Enrichment results were adjusted using a Bonferroni correction  
208 accounting for the number of transcription factors with more than 2 genes in the significant DEG list .

209

### 210 **Pseudo-bulk sample permutation**

211 Because of the sample size imbalance by disease state, which inherently yields different statistical power  
212 for different tests across conditions, we permuted differential expression testing with equivalent sample  
213 sizes to better evaluate the relative extent of dysregulation by EEC compartment and biopsy location  
214 between SSc and GERD. We permuted all possible combinations of SSc samples with sample size  $n=4$  for  
215 both the proximal and distal regions and used the median statistics in the SSc vs. HCs tests to more directly  
216 compare the results with those observed in GERD vs. HCs.

217

### 218 **Gene expression trajectory analysis**

219 To model gene expression as a continuous function along the axis of epithelial cell differentiation, we  
220 utilized the framework implemented in Lamian<sup>65</sup>, with the epithelial differentiation score serving as the  
221 underlying pseudotime metric. Lamian fits a polynomial B-spline curve with the number of knots  
222 determined by minimization of the Bayesian Information Criterion. With few cells near the lower and upper  
223 limits of our epithelial differentiation score and the interpolation range bound by the minimum and  
224 maximum pseudotime values, the B-spline models produced erratic fits near the interpolation boundaries.  
225 Therefore, we instead modeled natural cubic splines, which are constrained to linearity at the boundaries  
226 (second derivative is zero), and we excluded the lowest and highest 1% of cells from the interpolation  
227 interval. Using these modeled gene expression trajectories, we performed hierarchical clustering of  
228 differential gene trajectories for all genes that were significantly differentially expressed between SSc and  
229 HC in single-cell-level differential expression testing.

230

### 231 **Clinical phenotype associations**

232 To test for associations with categorical measures of esophageal function (FLIP, HRM, NM), we performed  
233 ordinal logistic regression that modeled likelihoods of increasing clinical severity. We excluded individuals  
234 with achalasia or esophagogastric junction outflow obstruction (EGJOO) from ordinal regression modeling  
235 motility. For FLIP we combined the “borderline/diminished” and “impaired/disordered” phenotypes. For  
236 NM we combined the Stage I and Stage II ineffective motility phenotypes. The resultant ordering for the  
237 ordinal regression was “normal” < “ineffective” < “absent” for HRM; “normal” < “borderline/diminished  
238 & impaired/disordered” < “absent” for FLIP; and “normal” < “stages I & II – ineffective” < “stage III –  
239 absent” for NM.

240 For association testing with quantitative clinical measures in SSc, we first performed a principal  
241 components analysis (PCA) on a set of nine quantitative clinical traits: HRM mean distal contractile interval  
242 (DCI), HRM basal esophagogastric junction (EGJ) pressure, HRM EGJ contractile index, HRM median  
243 integrated relaxation pressure (IRP), FLIP intra-balloon pressure at 60ml, FLIP EGJ distensibility index,  
244 the GerdQ impact score, the BEDQ score, and the NEQOL score. Missing values were imputed with the

245 mean. We then modeled associations with the first two PCs using linear regression. Gene expression was  
246 represented using log-transformed counts.

247

248

## 249 **RESULTS**

250 Whole tissue single-cell RNA sequencing (scRNA-seq) was performed on paired proximal and distal  
251 mucosal biopsies from ten patients with systemic sclerosis (SSc), four with gastroesophageal reflux disease  
252 (GERD), and six healthy controls (HCs). All participants but one in each group were female (**Table 1**). SSc  
253 patients were significantly older than HCs (54.9 vs 27.0 years;  $P < 0.001$ ). Among SSc patients, six had the  
254 limited cutaneous subtype, three had the diffuse cutaneous subtype, and one had sine scleroderma with no  
255 cutaneous symptoms (**Supplemental Table 1**). Mean SSc disease duration at the time of biopsy was 132  
256 months. All SSc patients had positive serum antinuclear antibody and impaired esophageal motility.  
257 Following sample-level quality control (**Supplemental Table 2**), 39 samples were retained for analysis,  
258 including 19 from the proximal esophagus and 20 from the distal esophagus.

259

### 260 **Characterization of esophageal mucosal cell populations**

261 A total of 306,372 esophageal cells (7,856 mean cells per sample) were retained for cell clustering and gene  
262 expression analysis (**Figure 1**). Each cell type was identified according to the expression of established  
263 cell-specific gene markers including *KRT6A*, *KRT13*, and *KRT15* for epithelial cells (**Supplemental Table**  
264 **3, Supplemental Figure 1**). Epithelial cells comprised the bulk of the sample ( $n=264,858$ ; 86.45%),  
265 followed by lymphoid cells ( $n=25,129$ ; 8.20%), myeloid cells ( $n=10,019$ ; 3.27%), endothelial cells  
266 ( $n=4,027$ ; 1.31%), and all other cell types ( $n=2,339$ ; 0.76%).

267

### 268 **Significant loss of superficial EECs in SSc**

269 Following isolation of the epithelial cell cluster and additional quality control (**Supplemental Figure 2, A-**  
270 **C**), we characterized the remaining 230,720 esophageal epithelial cells (EECs) according to their

271 differentiation and cell cycling states (**Figure 2A**). We classified the EECs into five primary compartments:  
272 basal (n=55,818; 24%), proliferating basal (n=36,439; 16%), proliferating suprabasal (n=25,314; 11%),  
273 suprabasal (n=82,283; 36%), and superficial (n=30,866; 13%) based on relative expression of canonical  
274 epithelial genes and cell cycle markers (**Figure 2, B-C; Supplemental Figure 2, D-E**). Roughly 40% of  
275 basal cells and 24% of suprabasal cells were proliferating, and the fractions of cells that were proliferating  
276 did not differ by disease (**Figure 2D; Supplemental Figure 2, F-I**). Proportions of basal and suprabasal  
277 cells were not significantly different across conditions, but there were significantly fewer superficial cells  
278 in SSc compared to HCs ( $\mu_{SSc}=0.10$ ,  $\mu_{HC}=0.21$ ,  $P=0.003$ , **Figure 2E**). The reduction of superficial cells in  
279 SSc was further apparent when examining EEC differentiation score distributions (**Supplemental Figure**  
280 **3**) and projecting UMAP embeddings separately by disease state (**Figure 3**).

281

### 282 **EEC gene dysregulation highly correlated in SSc and GERD, limited to superficial cells**

283 Overall, the gene expression correlation between biopsy locations was extremely high, ranging from  $r=0.98$   
284 to  $r=0.99$  for the 2,000 most variable genes (**Supplemental Figure 4A**) aggregated by condition and  
285 epithelial compartment (**Supplemental Figure 4B; Supplemental Table 4**). Inter-sample expression  
286 correlations indicated that the greatest gene expression heterogeneity was in the superficial compartment  
287 (mean=0.94, std. dev.=0.027), followed by the basal compartment (mean=0.94, std. dev.=0.018; **Figure 4,**  
288 **A-B**). Differential gene expression between conditions was most predominant in the superficial  
289 compartment (**Figure 4, C-E**). At the single-cell level, about 6.6% and 4.1% of expressed genes were  
290 significantly differentially expressed between SSc and HCs in the superficial compartment in the proximal  
291 and distal regions, respectively, compared to just 1.3-1.4% and 1.3-3.0% in non-proliferating basal and  
292 suprabasal cells (**Supplemental Tables 5-6**). Most differentially expressed genes (DEGs) were only  
293 differentially expressed in one epithelial compartment (**Figure 4, C-D**). We observed more suprabasal  
294 differential expression in the distal esophagus than in the proximal esophagus for both SSc and GERD  
295 (**Figure 4, C-E**). Many of the same genes were significantly dysregulated in both SSc and GERD compared  
296 to HCs (**Supplemental Table 5**). Depending on the compartment and biopsy location, 22-44% of

297 significantly dysregulated genes in SSc or GERD were differentially expressed in both conditions (**Figure**  
298 **4E**). Consequently, the DEGs in SSc and GERD were significantly enriched for some of the same pathways,  
299 particularly those related to the extracellular matrix and keratinization (**Figure 4F**). Clustered trajectories  
300 of relative gene expression (SSc vs. HCs) by epithelial differentiation score for all single-cell-level DEGs  
301 revealed distinct patterns of differential expression (**Figure 4, G-H**), which were principally distinguished  
302 by the direction of gene expression change in superficial cells. Gene expression changes were more  
303 pronounced in the most terminally differentiated superficial cells in the proximal esophagus (**Figure 4G**),  
304 whereas in the distal esophagus the differences appeared more in late-stage suprabasal and early-stage  
305 superficial cells (**Figure 4H**).

306 Six pathways were significantly enriched among DEGs between SSc and HCs: matrisome  
307 (suprabasal, distal  $P_{FDR}=2.3\times 10^{-4}$ , **Figure 4H**; superficial, distal  $P_{FDR}=2.6\times 10^{-2}$ ) and matrisome-associated  
308 genes (suprabasal, distal  $P_{FDR}=4.4\times 10^{-4}$ ); cornified envelope formation (suprabasal, distal  $P_{FDR}=2.1\times 10^{-3}$ ;  
309 superficial, distal  $P_{FDR}=4.7\times 10^{-2}$ ), and keratinization genes (suprabasal, distal  $P_{FDR}=2.1\times 10^{-3}$ ; superficial,  
310 distal  $P_{FDR}=5.0\times 10^{-2}$ ); developmental biology-related genes (suprabasal, distal  $P_{FDR}=4.1\times 10^{-4}$ ; superficial,  
311 distal  $P_{FDR}=9.2\times 10^{-3}$ ); and innate immune system genes ( $P_{FDR}=2.8\times 10^{-2}$ , **Figure 4G**). No pathways were  
312 significantly enriched among genes differentially expressed between SSc and GERD in any epithelial  
313 compartment. The leading edges of significantly enriched pathways (**Supplemental Table 7**) contained  
314 recurring genes from shared protein families, including serine protease inhibitors (serpins, **Supplemental**  
315 **Figure 4C**), keratins (**Supplemental Figure 4D**), S100 proteins (**Supplemental Figure 4E**), and small  
316 proline-rich proteins (SPRRs, **Supplemental Figure 4F**). The most frequent gene in leading edges of  
317 significantly enriched pathways was *PI3* (**Supplemental Figure 4G**), including all pathways enriched in  
318 SSc. Among the other most enriched pathways specific to SSc were those related to the regulation of metal  
319 and immune homeostasis (**Figure 4F, Supplemental Table 7**).

320 Upon aggregating single-cell expression counts by sample for each EEC compartment, we found  
321 that gene expression patterns clustered by EEC compartment (**Supplemental Figure 5A**) and that  
322 differential expression between conditions was nearly exclusively limited to superficial cells (**Figure 5, A-**

323 **B; Supplemental Figure 5B**). There were 3,572 genes differentially expressed between SSc and HCs with  
324 FDR  $q < 0.05$  in the superficial compartment, compared to just 232 total in all other compartments, including  
325 only 172 that were not also differentially expressed in the superficial compartment (**Supplemental Table**  
326 **8**). The differential expression observed in SSc was again highly correlated with the changes seen in GERD  
327 (**Figure 5, C-D**). The correlations in  $\log_2$  fold change between SSc and GERD vs. HCs were consistently  
328 between 0.40-0.53 in all compartments except for superficial cells, where we observed much stronger  
329 correlation in the proximal region ( $r=0.82$ ) than in the distal region ( $r=0.36$ ; **Supplemental Figure 5C**).

330 We detected 2,103 genes that were significantly differentially expressed in SSc but not GERD in  
331 the proximal esophagus and 282 in the distal esophagus, of which 170 were differentially expressed only  
332 in the distal region (**Figure 5, C-D; Supplemental Table 9**). Among the most upregulated SSc-specific  
333 genes (**Figure 5, C-E; Supplemental Figure 5, C-D**) were genes related to inflammation (*PTGES*,  
334 *MFGE8*)<sup>66,67</sup>, innate immune response (*FCGBP*, *BST2*, *CD44*, *APOBEC3A*)<sup>68-71</sup>, immune cell migration  
335 (*C10orf99*, *LTB4R*, *ACKR3*)<sup>72-74</sup>, antigen presentation (*HLA-B*, *CD74*, *TAP1*, *PSMB8*, *PSMB9*)<sup>75</sup>, natural  
336 killer cell activation (*CLEC2B*)<sup>76</sup>, and fibroproliferation (*SGK1*, *HBEGF*)<sup>77,78</sup>. Four of the top five and eight  
337 of the top 20 most downregulated SSc-specific genes by fold change in superficial EECs in the proximal  
338 esophagus were metallothioneins (*MT1A*, *MT1E*, *MT1F*, *MT1G*, *MT1H*, *MT1M*, *MT1X*, *MT2A*). The  
339 metallothioneins comprised the bulk of three pathways uniquely enriched in SSc with  $P < 0.001$ : zinc  
340 homeostasis, copper homeostasis, and cellular responses to stimuli (**Figure 4F**). The most down-regulated  
341 SSc-specific gene across both the proximal and distal esophagus was the *H19* lncRNA. Interestingly, the  
342 most down-regulated gene by fold change in GERD, *MUC22*, was not differentially expressed in SSc. One  
343 gene, *SLC8A1-AS1*, was significantly differentially expressed in both GERD and SSc, but in opposite  
344 directions (**Figure 5, C-E; Supplemental Table 9**).

345 More genes were significantly differentially expressed in SSc than in GERD, but in terms of  
346 relative fold change vs. HCs, we observed greater expression changes in GERD (**Supplemental Figure**  
347 **5C**). We therefore performed all possible sample permutations with equal numbers of SSc and GERD  
348 samples ( $n=4$ ) and repeated differential gene expression testing to more directly compare the relative

349 number of DEGs in both conditions (**Figure 5F**). In superficial cells from the proximal esophagus, there  
350 were more DEGs in SSc in 60% of permutations, but the relative FC differences were greater in GERD in  
351 61% of permutations (**Supplemental Table 10**). In the distal region, there were more DEGs in GERD in  
352 62% of permutations, and the relative FC differences were greater in GERD in all permutations. The  
353 correlations between SSc and GERD in terms of relative gene expression changes were consistently much  
354 higher in the proximal region permutations than in the distal region (**Figure 5, G-H**). The permutation  
355 results confirmed that the differences in gene expression observed in SSc relative to GERD were not simply  
356 due to differences in sample size.

357 In summary, the gene expression changes measured in SSc and GERD were highly correlated. In  
358 the distal esophagus, differential expression was more pronounced in GERD than in SSc, whereas in the  
359 proximal esophagus there were more DEGs in SSc. In both conditions, differential gene expression was  
360 most prevalent in the superficial compartment, but the expression changes appeared comparatively earlier  
361 in the differentiation of distal EECs relative to proximal EECs.

362

### 363 **Transcription factor enrichment analysis**

364 We next examined whether DEGs in SSc superficial cells were significantly enriched for targets of specific  
365 transcription factors. Among genes differentially expressed in SSc compared to GERD, the target genes of  
366 IRF1 were significantly enriched (**Table 2**). IRF1 targets were significantly enriched among all proximal  
367 superficial DEGs ( $p_{\text{adj}}=0.021$ ) and among only those that were downregulated ( $p_{\text{adj}}=0.0024$ ). However,  
368 *IRF1* was not itself differentially expressed in superficial cells in SSc compared to GERD. Compared to  
369 HCs, three transcription factors were significantly enriched in SSc in the proximal esophagus, including  
370 MYC ( $p_{\text{adj}}=2.1\times 10^{-7}$ ) and E2F4 ( $p_{\text{adj}}=5.5\times 10^{-5}$ ) for upregulated DEGs and NFE2L2 for downregulated  
371 DEGs ( $p_{\text{adj}}=7.6\times 10^{-4}$ ). *MYC* and *E2F4* were also themselves differentially expressed in SSc compared to  
372 HCs in superficial cells ( $p_{\text{adj}}=7.8\times 10^{-5}$ ,  $p_{\text{adj}}=9.8\times 10^{-4}$ , respectively). *MYC* was the most enriched  
373 transcription factor in genes upregulated in GERD compared to HCs, but the enrichment was not significant

374 after adjusting for multiple testing ( $p_{\text{adj}}=0.11$ ). No transcription factors were significantly enriched in any  
375 pairwise comparison in the distal esophagus.

376

### 377 **Expression mapping in superficial EECs**

378 Examining the expression patterns within superficial cells from the proximal esophagus more closely, we  
379 identified five distinct clusters (**Figure 6A**) distinguished by unique expression marker patterns (**Figure**  
380 **6B, Supplemental Figure 6, Supplemental Table 11**) and varying degrees of differentiation (**Figure 6C**).  
381 Clusters 1 and 3 represent the outermost, terminally differentiated epithelial layers, as evidenced by their  
382 *FLG* expression<sup>79-81</sup>. They differed by the expression of metallothioneins, which were predominantly  
383 expressed in cluster 3 (**Figure 6, E-F**). Cluster 3 was less abundant in SSc compared to HC with  $P<0.05$   
384 (**Figure 6D**), but metallothionein expression was lower in other superficial clusters, as well (**Figure 6F**).  
385 Within the superficial EECs, the relative expression of metallothioneins was significantly correlated with  
386 the differentiation score ( $r=0.06$ ,  $P=2.3\times 10^{-23}$ ). Cluster 2 was distinguished by its relatively high *CTSV*  
387 expression. Clusters 4 and 5 were the least differentiated of the superficial cells and were distinguished by  
388 their relative expression of *GJB6* and *FGFBP1*, respectively, although neither gene was differentially  
389 expressed between conditions.

390 For the expression of the significantly enriched transcription factors (*IRF1*, *MYC*, *E2F4*, and  
391 *NFE2L2*; **Table 2**) and their targets, we observed two consistent patterns (**Figure 7**). First, the greatest  
392 magnitude differences in median target expression between SSc and HCs were seen in cluster 5. Second,  
393 in each of those instances, the median target expression in GERD was between that of SSc and HCs. The  
394 expression correlations between the enriched transcription factors and their targets were positive for *MYC*  
395 ( $r=0.42$ ) and *E2F4* ( $r=0.24$ ) and negative for *IRF1* ( $r=-0.20$ ) and *NFE2L2* ( $r=-0.18$ ).

396

### 397 ***FLII* expression in human EECs**

398 Deletion of the *Fli1* gene in epithelial cells in mice has been shown to recapitulate histological and  
399 molecular features of esophageal involvement in SSc<sup>24</sup>. Therefore, we investigated the expression of *FLII*



400 in our human esophageal samples. The expression of *FLII* in human EECs was negligible and did not meet  
401 the minimum expression thresholds for inclusion in our differential gene expression analysis. We did  
402 observe low *FLII* expression levels in endothelial cells (**Supplemental Figure 7A**), but the expression  
403 differences between SSc, HCs, and GERD was not significant (**Supplemental Figure 7B**). There were  
404 many *FLII* downstream targets among the proximal, superficial DEGs between SSc and HCs and seven  
405 between SSc and GERD (*ARPC2*, *RAB24*, *MTPN*, *PPIF* upregulated; *CEBPZ*, *TRMT10C*, *TBP*  
406 downregulated); however, the proportion of these genes among all DEGs was not different than what would  
407 be expected by chance ( $P>0.05$ ), and the average expression of *FLII* targets was higher in GERD and lower  
408 in HCs compared to the expression in SSc (**Supplemental Figure 7C**).

409

#### 410 **Correlations with clinical phenotypes**

411 We next evaluated whether the cellular and molecular changes we observed between SSc, GERD, and HCs  
412 were correlated with specific clinical measures of esophageal dysfunction (**Table 1**). To test for associations  
413 with esophageal motility phenotypes, we performed ordinal regression against increasing phenotype  
414 severity. To more efficiently model the covariance structure among quantitative, functional esophageal  
415 measures in SSc (**Figure 8A**), we performed PCA on a set of nine clinical metrics and tested for correlations  
416 with the first two PCs (**Figure 8B**). The first PC explained 45.5% of variance and was most correlated with  
417 FLIP intra-balloon pressure at 60ml ( $r=0.94$ ), The second PC explained 22.6% of variance and was most  
418 correlated with HRM basal EGJ pressure ( $r=0.74$ ).

419 We did not observe any significant correlations between epithelial cell compartment proportions in  
420 SSc and esophageal motility phenotypes. It appeared that the low proportion of superficial cells in the  
421 esophageal epithelium was a universal feature in SSc, regardless of phenotype (**Supplemental Figure 8A**).  
422 The proportion of superficial cells decreased with disease duration, but the trend was not statistically  
423 significant ( $P=0.1$ ; **Supplemental Figure 8B**). We also did not observe any significant correlations between  
424 EEC compartment proportions and quantitative trait PCs (**Figure 8C**).

425 We then tested for correlations with gene expression in superficial EECs for genes that were  
426 significantly differentially expressed in SSc compared to HCs ( $P_{\text{adj}} < 0.05$ ) and nominally differentially  
427 expressed in SSc compared to GERD ( $P < 0.05$ ). There were 433 genes that met these criteria in the proximal  
428 esophagus and 99 in the distal esophagus. Although no associations with esophageal motility phenotypes  
429 were statistically significant after adjusting for multiple testing, the strongest phenotypic correlation was  
430 with *TRIM11* ( $P_{\text{FLIP}} = 0.01$ ,  $P_{\text{HRM}} = 0.007$ , **Supplemental Figure 8C**), a gene recently found to attenuate Treg  
431 cell differentiation in  $CD4^+$  T cells in mice<sup>82</sup>. No associations with the top two clinical PCs were significant  
432 after adjusting for multiple testing. We also tested for clinical PC correlations with aggregate  
433 metallothionein gene expression and transcription factor target expression for IRF1, MYC, E2F4, and  
434 NFE2L2. We observed one nominal association between the mean metallothionein module score and PC1  
435 ( $P = 0.02$ , **Figure 8D**). Notably, within superficial cells we also observed a strong correlation between the  
436 proportion of metallothionein-expressing cluster 3 cells and PC1 in the distal esophagus (**Figure 8E**). This  
437 indicates that not only is this population of cells reduced in SSc, but its relative decrease is further correlated  
438 with more severe esophageal involvement (**Figure 8F**). Therefore, our findings suggest that increased  
439 esophageal dysmotility in SSc is associated with a decline in metallothionein-expressing superficial EECs,  
440 which coincides with lower overall metallothionein expression in superficial cells.

441

442

## 443 **DISCUSSION**

444 Esophageal dysfunction is extremely common in SSc and is significantly associated with increased  
445 mortality and lower quality of life<sup>83,84</sup>. The causal mechanisms by which SSc affects the esophagus,  
446 however, have not been conclusively determined. Here, we sought to clarify the role of epithelial cells in  
447 SSc esophageal dysfunction by using scRNA-seq to quantify cellular and transcriptional changes relative  
448 to HCs and individuals with GERD. While our findings indicate that epithelial changes in SSc result  
449 primarily from chronic acid exposure, they also highlight immunoregulatory pathways uniquely altered in  
450 SSc that may be linked to pathogenic aberrations.

451 With epithelial layers of the skin and internal organs being primary sites of injury in SSc, the  
452 pathogenic role of epithelial cells in SSc has long been an ongoing area of research. When damaged,  
453 epithelial cells release signals that help induce fibroblast activation to promote wound healing<sup>85</sup>. In SSc,  
454 epidermal keratinocyte characteristics resemble a pro-fibrotic, activated state<sup>86</sup>. SSc epidermal cells were  
455 also found to stimulate fibroblasts in culture<sup>87</sup>, and some signs related to epithelial-mesenchymal transition  
456 (EMT) have been observed in the SSc epidermis<sup>88</sup>. The FLI1 (friend leukemia integration 1) transcription  
457 factor, in particular, has received much attention for its potential role in epithelial-cell-mediated SSc  
458 pathogenesis<sup>20</sup>. Lower FLI1 expression was observed in the epidermis of diffuse cutaneous SSc, and  
459 inactivation of FLI1 in human keratinocytes in vitro induced gene expression changes characteristic of  
460 SSc<sup>24</sup>. Furthermore, conditional deletion of *Fli1* in epithelial cells produced an SSc-like phenotype in  
461 mice<sup>24</sup>. Importantly, the epithelial-cell-specific *Fli1* knockout further recapitulated the esophageal  
462 involvement of SSc, with increased collagen deposition in the lamina propria combined with atrophy of the  
463 circular muscle layer, and the esophageal changes were not mediated by T-cell autoimmunity<sup>24</sup>. In contrast  
464 to these previous studies in mice and epidermal keratinocytes, we did not observe *FLII* expression in EECs  
465 in any condition. *FLII* was expressed at low levels in endothelial cells, but the expression differences  
466 between SSc, HCs, and GERD were not significant. We did observe significantly increased expression in  
467 SSc and GERD of the *PI3* gene, which encodes trappin-2/elafin, previously found to be induced by Fli1  
468 silencing in human dermal microvascular endothelial cells<sup>89</sup>. However, this association is unlikely to be  
469 pathogenic, as the increase in gene expression was greater in GERD, and a growing body of evidence  
470 indicates that trappin-2/elafin is expressed to promote tissue repair in response to gastrointestinal tissue  
471 inflammation<sup>90</sup>.

472 While there have been many studies of epithelial cells in skin in SSc, molecular study of the human  
473 esophagus in SSc had heretofore been limited to one array-based gene expression study in bulk tissue  
474 conducted by Taroni and colleagues<sup>15</sup>, in which they identified distinct expression signatures among  
475 variable genes between 15 individuals with SSc that were similar to those seen in skin<sup>91</sup>. These signatures  
476 were independent of clinically defined SSc subsets<sup>15</sup>, suggestive of inter-individual heterogeneity in SSc.

477 They also found that gene expression patterns between upper and lower esophageal biopsies within  
478 individuals were nearly identical. They did not observe statistical associations between inflammatory gene  
479 expression signatures and GERD, but the study was underpowered for such an analysis, and GERD was  
480 defined based on histological evidence for basal cell hyperplasia and intraepithelial lymphocyte counts.

481 The gene expression differences we observed in SSc epithelial cells were highly correlated with  
482 those seen in GERD, and nearly all differential gene expression was limited to the superficial layers of the  
483 epithelium. These observations suggest that the primary driver of differential gene expression in EECs in  
484 SSc is chronic acid exposure. The genes with the strongest mutual upregulation in SSc and GERD were  
485 primarily related to keratinization/cornification, including small proline-rich proteins (SPRRs), serine  
486 protease inhibitors (serpins), S100 proteins, late cornified envelope (LCE) genes, and keratins associated  
487 with terminal epithelial differentiation, namely *KRTDAP* and *KRT*. *KRT1* helps maintain epithelial barrier  
488 function in gastrointestinal epithelial cells, and its overexpression was shown to attenuate IL-1 $\beta$ -induced  
489 epithelial permeability<sup>92</sup>. The mutual upregulation of these genes in the outer layers of the epithelium  
490 therefore likely represent a protective response to chronic acid exposure.

491 While the overall gene expression differences were highly correlated between SSc and GERD,  
492 there were sets of genes disproportionately upregulated in SSc that hint at disease-related immune response  
493 aberrations, including genes that have previously been implicated in SSc pathogenesis. For example,  
494 *PTGES*, which encodes prostaglandin E synthase, was previously found to be significantly upregulated in  
495 SSc fibroblasts<sup>93</sup> and inflammatory non-classical monocytes<sup>94</sup>, and *Ptges*-null mice were resistant to  
496 bleomycin-induced fibrosis<sup>93</sup>. CD44 and CD74 form the receptor complex for the macrophage inhibitory  
497 factor (MIF), an inflammatory cytokine that promotes fibroblast migration and has been implicated in SSc  
498 pathogenesis<sup>95</sup>. LTB4R (Leukotriene B4 Receptor, or BLT1) has been found to activate AKT/mTOR  
499 signaling and knockdown of *LTB4R* attenuated fibrosis in bleomycin-induced SSc in murine models<sup>96</sup>.  
500 Serum HBEGF (heparin-binding epidermal growth factor) levels and fibroblast *HBEGF* expression were  
501 both significantly elevated in SSc<sup>97</sup>. Copy number variation of *APOBEC3A* was significantly associated  
502 with SSc in a Han Chinese population<sup>98</sup>. Finally, the SSc-specific upregulation of genes involved in antigen

503 processing and presentation (*HLA-B*, *CD74*, *TAP1*, *PSMB8*, *PSMB9*) are suggestive of increased human  
504 leukocyte antigen (HLA) class I activity in superficial EECs in SSc. Notably, *TAP1*, *PSMB8*, and *PSMB9*  
505 are located immediately adjacent to one another in the class II region of the HLA locus, which is the  
506 genomic region with the strongest genetic associations with SSc<sup>99</sup>, and SSc-associated HLA-B alleles have  
507 also been identified<sup>100,101</sup>.

508 The most striking set of genes that were uniquely downregulated in SSc were metallothioneins.  
509 The expression of detected metallothioneins (*MT1A*, *MT1E*, *MT1F*, *MT1G*, *MT1H*, *MT1M*, *MT1X*, *MT2A*)  
510 was strongly induced in the superficial compartment of EECs, but significantly less so in SSc and,  
511 interestingly, only in the proximal esophagus. We further observed a nominal association between relative  
512 metallothionein expression in the proximal esophagus and the first PC of esophageal dysmotility among  
513 SSc patients, with lower expression of metallothioneins correlated with greater EGJ distensibility and  
514 weaker contractility. The proportion of the primary metallothionein-expressing cluster within superficial  
515 EECs was likewise significantly associated with clinical PC1. The metallothioneins are a family of well-  
516 conserved, metal-binding proteins that regulate zinc and copper homeostasis, prevent heavy metal  
517 poisoning, and combat oxidative stress<sup>102,103</sup>. Their study in a wide array of physiological conditions and  
518 immune-mediated diseases has revealed the proteins play central roles in innate and adaptive immunity,  
519 including autoimmunity, but their immunoregulatory behavior is highly complex and context-specific<sup>102,103</sup>.  
520 Given their import in immune regulation, their associations with SSc and esophageal motility reported in  
521 this study, and the connection between SSc and heavy metal exposure<sup>104</sup>, the metallothioneins are  
522 compelling candidates that warrant further study in SSc.

523 Interestingly, there was greater relative gene dysregulation in the proximal esophagus compared to  
524 the distal esophagus in SSc, but the opposite was true for GERD. This discrepancy suggests that esophageal  
525 dysmotility in SSc leads to greater acid exposure in the proximal esophagus, since refluxed gastric acid  
526 typically affects the distal esophagus significantly more than the proximal esophagus<sup>105</sup> and abnormal  
527 peristalsis prolongs acid clearance<sup>106</sup>. This finding coincides with a bulk RNA-seq study of esophageal  
528 mucosa of achalasia patients<sup>107</sup>, which likewise identified more differential expression in the proximal

529 esophagus than in the distal esophagus, including significant enrichment of matrisome-associated genes  
530 and lower expression of genes associated with reactive oxygen species metabolism<sup>107</sup>. Due to differences  
531 in innervation depth<sup>108</sup>, the epithelium of the proximal esophagus has more nociceptive sensitivity than the  
532 distal esophagus, which likely contributes to the association between gastrointestinal symptoms and lower  
533 quality of life in SSc<sup>109</sup>. Proximal acid exposure increases the risk of aspiration<sup>110</sup> and is significantly more  
534 prevalent in SSc patients with idiopathic lung fibrosis<sup>111</sup>.

535         Targets for several transcription factors, including IRF1, MYC, E2F4, and NFE2L2 (or NRF2),  
536 were significantly enriched among DEGs in superficial EECs from the proximal esophagus. IRF1 is  
537 involved in innate immune responses, but while IRF1 targets were enriched in DEGs between SSc and GERD,  
538 the enrichment appeared to be driven by upregulation in GERD. IRF1 targets were not enriched in DEGs  
539 between SSc and HCs, nor was *IRF1* significantly differentially expressed in SSc. MYC, E2F4, and  
540 NFE2L2 all participate in different stages of the cell cycle<sup>112-114</sup>, and expression of each was highest in  
541 either the proliferating basal or suprabasal compartments, but these proteins may also play a role in terminal  
542 differentiation of EECs, particularly under conditions of stress. In the least differentiated superficial cluster  
543 (cluster 5), where the expression differences relative to HCs for each of these transcription factors and their  
544 targets was most pronounced, the expression level changes in GERD were correlated with those observed  
545 in SSc. Furthermore, *Myc* ablation in *Krt14*-expressing tissues in mice led to abnormal terminal  
546 differentiation of epithelial cells<sup>115</sup>, and a study of the esophageal epithelium in *Nrf2* knockout mice  
547 indicated that *Nrf2* regulates cornification of keratinized epithelial cells under conditions of stress<sup>116</sup>.

548         There are important limitations to consider when interpreting this study. First, this study only  
549 focused on squamous epithelial cells. There may be relevant changes in other cell types within the  
550 esophageal mucosa that correlate with SSc and dysmotility, but such analyses are ongoing and were outside  
551 the scope of this investigation. Second, the relatively small patient sample size of this study combined with  
552 the heterogeneity of SSc subtypes and dysmotility phenotypes limited our power to detect clinical  
553 associations between cell type proportions or gene expression changes and specific clinical phenotypes.  
554 Heterogeneous molecular profiles in SSc esophagus samples have been described previously<sup>15</sup>, but we

555 grouped all SSc patients together in our analyses for comparisons against GERD and HCs. We applied  
556 ordinal logistic regression on motility classifications and performed principal components analysis on  
557 reflux- and motility-related quantitative traits to increase our power to detect clinical associations but were  
558 nonetheless statistically limited by sample size. Third, we did not examine imaging data in the SSc  
559 esophageal mucosa. Therefore, we cannot make conclusions on the morphological states that accompany  
560 the transcriptional and cellular proportion changes that we observed. Future studies utilizing larger, more  
561 homogeneous cohorts with imaging data may be able to detect more esophageal epithelial changes  
562 associated with dysmotility in SSc.

563 In summary, esophageal complications are common in individuals with SSc and can greatly impact  
564 quality of life and lifespan. In this study, we sought to clarify the role of the epithelium in SSc esophageal  
565 involvement. Through a thorough, single-cell-level transcriptomic investigation, we identified the unique  
566 cellular and transcriptional differences present in the SSc esophageal epithelium. There were significantly  
567 fewer terminally differentiated epithelial cells in the outermost, superficial layers in both the proximal and  
568 distal esophagus, but otherwise epithelial compartment proportions were similar to healthy controls,  
569 including proliferating cell proportions. Significant differences in gene expression were likewise almost  
570 exclusively found in the superficial compartment, and these changes were highly correlated with those seen  
571 in individuals with GERD, indicating that the primary driver of differential gene expression in the SSc  
572 esophageal epithelium is chronic acid exposure. Transcriptional differences were also more prominent in  
573 the proximal esophagus of SSc patients, suggesting that esophageal dysmotility leads to greater proximal  
574 exposure. Genes that were most disproportionately dysregulated in SSc compared to GERD belonged to  
575 immune-related pathways, including innate and adaptive response, antigen presentation, and metal  
576 homeostasis, and may therefore point to pathogenic immune dysfunction. Future studies investigating these  
577 pathways in non-epithelial cell populations in more homogeneous SSc cohorts may further resolve the  
578 pathogenic mechanisms driving esophageal involvement in SSc. By serving as an atlas for the human  
579 esophageal epithelium in SSc, this study can guide future efforts to address remaining gaps in our

580 understanding of the SSc esophagus, to ultimately uncover pathogenic mechanisms and identify actionable  
581 targets.



## 582 REFERENCES

- 583 1. Bairkdar, M., Rossides, M., Westerlind, H., Hesselstrand, R., Arkema, E.V., and Holmqvist, M.  
584 (2021). Incidence and prevalence of systemic sclerosis globally: a comprehensive systematic review  
585 and meta-analysis. *Rheumatology (Oxford)* 60, 3121-3133. 10.1093/rheumatology/keab190.
- 586 2. Fan, Y., Bender, S., Shi, W., and Zoz, D. (2020). Incidence and prevalence of systemic sclerosis and  
587 systemic sclerosis with interstitial lung disease in the United States. *J Manag Care Spec Pharm* 26,  
588 1539-1547. 10.18553/jmcp.2020.20136.
- 589 3. Tian, J., Kang, S., Zhang, D., Huang, Y., Zhao, M., Gui, X., Yao, X., and Lu, Q. (2023). Global,  
590 regional, and national incidence and prevalence of systemic sclerosis. *Clin Immunol* 248, 109267.  
591 10.1016/j.clim.2023.109267.
- 592 4. Pope, J.E., Quansah, K., Hassan, S., Seung, S.J., Flavin, J., and Kolb, M. (2021). Systemic Sclerosis  
593 and Associated Interstitial Lung Disease in Ontario, Canada: An Examination of Prevalence and  
594 Survival Over 10 Years. *J Rheumatol* 48, 1427-1434. 10.3899/jrheum.201049.
- 595 5. Li, J.X. (2022). Secular Trends in Systemic Sclerosis Mortality in the United States from 1981 to  
596 2020. *Int J Environ Res Public Health* 19. 10.3390/ijerph192215088.
- 597 6. Rubio-Rivas, M., Royo, C., Simeon, C.P., Corbella, X., and Fonollosa, V. (2014). Mortality and  
598 survival in systemic sclerosis: systematic review and meta-analysis. *Semin Arthritis Rheum* 44, 208-  
599 219. 10.1016/j.semarthrit.2014.05.010.
- 600 7. Bairkdar, M., Chen, E.Y., Dickman, P.W., Hesselstrand, R., Westerlind, H., and Holmqvist, M.  
601 (2023). Survival in Swedish patients with systemic sclerosis: a nationwide population-based matched  
602 cohort study. *Rheumatology (Oxford)* 62, 1170-1178. 10.1093/rheumatology/keac474.
- 603 8. Li, B., Yan, J., Pu, J., Tang, J., Xu, S., and Wang, X. (2021). Esophageal Dysfunction in Systemic  
604 Sclerosis: An Update. *Rheumatol Ther* 8, 1535-1549. 10.1007/s40744-021-00382-0.
- 605 9. Emmanuel, A. (2016). Current management of the gastrointestinal complications of systemic  
606 sclerosis. *Nat Rev Gastroenterol Hepatol* 13, 461-472. 10.1038/nrgastro.2016.99.
- 607 10. Ahuja, N.K., and Clarke, J.O. (2021). Scleroderma and the Esophagus. *Gastroenterol Clin North Am*  
608 50, 905-918. 10.1016/j.gtc.2021.08.005.
- 609 11. Denaxas, K., Ladas, S.D., and Karamanolis, G.P. (2018). Evaluation and management of esophageal  
610 manifestations in systemic sclerosis. *Ann Gastroenterol* 31, 165-170. 10.20524/aog.2018.0228.
- 611 12. Foocharoen, C., Thinkhamrop, W., Chaichaya, N., Mahakkanukrauh, A., Suwannaroj, S., and  
612 Thinkhamrop, B. (2022). Development and validation of machine learning for early mortality in  
613 systemic sclerosis. *Sci Rep* 12, 17178. 10.1038/s41598-022-22161-9.
- 614 13. Sjogren, R.W. (1994). Gastrointestinal motility disorders in scleroderma. *Arthritis Rheum* 37, 1265-  
615 1282. 10.1002/art.1780370902.
- 616 14. Roberts, C.G., Hummers, L.K., Ravich, W.J., Wigley, F.M., and Hutchins, G.M. (2006). A case-  
617 control study of the pathology of oesophageal disease in systemic sclerosis (scleroderma). *Gut* 55,  
618 1697-1703. 10.1136/gut.2005.086074.
- 619 15. Taroni, J.N., Martyanov, V., Huang, C.C., Mahoney, J.M., Hirano, I., Shetuni, B., Yang, G.Y.,  
620 Brenner, D., Jung, B., Wood, T.A., et al. (2015). Molecular characterization of systemic sclerosis  
621 esophageal pathology identifies inflammatory and proliferative signatures. *Arthritis Res Ther* 17, 194.  
622 10.1186/s13075-015-0695-1.
- 623 16. Roman, S., Hot, A., Fabien, N., Cordier, J.F., Miossec, P., Ninet, J., Mion, F., and Reseau  
624 Sclerodermie des Hospices Civils de, L. (2011). Esophageal dysmotility associated with systemic  
625 sclerosis: a high-resolution manometry study. *Dis Esophagus* 24, 299-304. 10.1111/j.1442-  
626 2050.2010.01150.x.
- 627 17. Noviani, M., Chellamuthu, V.R., Albani, S., and Low, A.H.L. (2022). Toward Molecular  
628 Stratification and Precision Medicine in Systemic Sclerosis. *Front Med (Lausanne)* 9, 911977.  
629 10.3389/fmed.2022.911977.
- 630 18. Carlson, D.A., Crowell, M.D., Kimmel, J.N., Patel, A., Gyawali, C.P., Hinchcliff, M., Griffing, W.L.,  
631 Pandolfino, J.E., and Vela, M.F. (2016). Loss of Peristaltic Reserve, Determined by Multiple Rapid

- 632 Swallows, Is the Most Frequent Esophageal Motility Abnormality in Patients With Systemic  
633 Sclerosis. *Clin Gastroenterol Hepatol* 14, 1502-1506. 10.1016/j.cgh.2016.03.039.
- 634 19. Kimmel, J.N., Carlson, D.A., Hinchcliff, M., Carns, M.A., Aren, K.A., Lee, J., and Pandolfino, J.E.  
635 (2016). The association between systemic sclerosis disease manifestations and esophageal high-  
636 resolution manometry parameters. *Neurogastroenterol Motil* 28, 1157-1165. 10.1111/nmo.12813.
- 637 20. Asano, Y., Takahashi, T., and Saigusa, R. (2019). Systemic sclerosis: Is the epithelium a missing  
638 piece of the pathogenic puzzle? *J Dermatol Sci* 94, 259-265. 10.1016/j.jdermsci.2019.04.007.
- 639 21. Durcan, C., Hossain, M., Chagnon, G., Peric, D., Karam, G., Bsiesy, L., and Girard, E. (2022).  
640 Experimental investigations of the human oesophagus: anisotropic properties of the embalmed  
641 mucosa-submucosa layer under large deformation. *Biomech Model Mechanobiol* 21, 1685-1702.  
642 10.1007/s10237-022-01613-1.
- 643 22. Kou, W., Pandolfino, J.E., Kahrilas, P.J., and Patankar, N.A. (2017). Simulation studies of the role of  
644 esophageal mucosa in bolus transport. *Biomech Model Mechanobiol* 16, 1001-1009. 10.1007/s10237-  
645 016-0867-1.
- 646 23. Asano, Y., Bujor, A.M., and Trojanowska, M. (2010). The impact of Fli1 deficiency on the  
647 pathogenesis of systemic sclerosis. *J Dermatol Sci* 59, 153-162. 10.1016/j.jdermsci.2010.06.008.
- 648 24. Takahashi, T., Asano, Y., Sugawara, K., Yamashita, T., Nakamura, K., Saigusa, R., Ichimura, Y.,  
649 Toyama, T., Taniguchi, T., Akamata, K., et al. (2017). Epithelial Fli1 deficiency drives systemic  
650 autoimmunity and fibrosis: Possible roles in scleroderma. *J Exp Med* 214, 1129-1151.  
651 10.1084/jem.20160247.
- 652 25. Dinh, H.Q., Pan, F., Wang, G., Huang, Q.F., Olingy, C.E., Wu, Z.Y., Wang, S.H., Xu, X., Xu, X.E.,  
653 He, J.Z., et al. (2021). Integrated single-cell transcriptome analysis reveals heterogeneity of  
654 esophageal squamous cell carcinoma microenvironment. *Nat Commun* 12, 7335. 10.1038/s41467-  
655 021-27599-5.
- 656 26. Zhang, X., Peng, L., Luo, Y., Zhang, S., Pu, Y., Chen, Y., Guo, W., Yao, J., Shao, M., Fan, W., et al.  
657 (2021). Dissecting esophageal squamous-cell carcinoma ecosystem by single-cell transcriptomic  
658 analysis. *Nat Commun* 12, 5291. 10.1038/s41467-021-25539-x.
- 659 27. Rochman, M., Wen, T., Kotliar, M., Dexheimer, P.J., Ben-Baruch Morgenstern, N., Caldwell, J.M.,  
660 Lim, H.W., and Rothenberg, M.E. (2022). Single-cell RNA-Seq of human esophageal epithelium in  
661 homeostasis and allergic inflammation. *JCI Insight* 7. 10.1172/jci.insight.159093.
- 662 28. Clevenger, M.H., Karami, A.L., Carlson, D.A., Kahrilas, P.J., Gonsalves, N., Pandolfino, J.E.,  
663 Winter, D.R., Whelan, K.A., and Tetreault, M.P. (2023). Suprabasal cells retain progenitor cell  
664 identity programs in eosinophilic esophagitis-driven basal cell hyperplasia. *JCI Insight* 8.  
665 10.1172/jci.insight.171765.
- 666 29. Carlson, D.A., Prescott, J.E., Germond, E., Brenner, D., Carns, M., Correia, C.S., Tetreault, M.P.,  
667 McMahan, Z.H., Hinchcliff, M., Kou, W., et al. (2022). Heterogeneity of primary and secondary  
668 peristalsis in systemic sclerosis: A new model of "scleroderma esophagus". *Neurogastroenterol Motil*  
669 34, e14284. 10.1111/nmo.14284.
- 670 30. Carlson, D.A., Gyawali, C.P., Khan, A., Yadlapati, R., Chen, J., Chokshi, R.V., Clarke, J.O., Garza,  
671 J.M., Jain, A.S., Katz, P., et al. (2021). Classifying Esophageal Motility by FLIP Panometry: A Study  
672 of 722 Subjects With Manometry. *Am J Gastroenterol* 116, 2357-2366.  
673 10.14309/ajg.0000000000001532.
- 674 31. Koop, A.H., Kahrilas, P.J., Schauer, J., Pandolfino, J.E., and Carlson, D.A. (2023). The impact of  
675 primary peristalsis, contractile reserve, and secondary peristalsis on esophageal clearance measured  
676 by timed barium esophagogram. *Neurogastroenterol Motil*, e14638. 10.1111/nmo.14638.
- 677 32. Yadlapati, R., Kahrilas, P.J., Fox, M.R., Bredenoord, A.J., Prakash Gyawali, C., Roman, S., Babaei,  
678 A., Mittal, R.K., Rommel, N., Savarino, E., et al. (2021). Esophageal motility disorders on high-  
679 resolution manometry: Chicago classification version 4.0((c)). *Neurogastroenterol Motil* 33, e14058.  
680 10.1111/nmo.14058.
- 681 33. Stern, E.K., Carlson, D.A., Falmagne, S., Hoffmann, A.D., Carns, M., Pandolfino, J.E., Hinchcliff,  
682 M., and Brenner, D.M. (2018). Abnormal esophageal acid exposure on high-dose proton pump

- 683 inhibitor therapy is common in systemic sclerosis patients. *Neurogastroenterol Motil* 30.  
684 10.1111/nmo.13247.
- 685 34. Yadlapati, R., Kahrilas, P.J., Fox, M.R., Bredenoord, A.J., Prakash Gyawali, C., Roman, S., Babaei,  
686 A., Mittal, R.K., Rommel, N., Savarino, E., et al. (2021). Esophageal motility disorders on high-  
687 resolution manometry: Chicago classification version 4.0(©). *Neurogastroenterol Motil* 33, e14058.  
688 10.1111/nmo.14058.
- 689 35. Rooney, K.P., Baumann, A.J., Donnan, E., Kou, W., Triggs, J.R., Prescott, J., Decorrevont, A.,  
690 Dorian, E., Kahrilas, P.J., Pandolfino, J.E., and Carlson, D.A. (2021). Esophagogastric Junction  
691 Opening Parameters Are Consistently Abnormal in Untreated Achalasia. *Clin Gastroenterol Hepatol*  
692 19, 1058-1060.e1051. 10.1016/j.cgh.2020.03.069.
- 693 36. Carlson, D.A., Baumann, A.J., Donnan, E.N., Krause, A., Kou, W., and Pandolfino, J.E. (2021).  
694 Evaluating esophageal motility beyond primary peristalsis: Assessing esophagogastric junction  
695 opening mechanics and secondary peristalsis in patients with normal manometry. *Neurogastroenterol*  
696 *Motil* 33, e14116. 10.1111/nmo.14116.
- 697 37. Carlson, D.A., Kou, W., Lin, Z., Hinchcliff, M., Thakrar, A., Falmagne, S., Prescott, J., Dorian, E.,  
698 Kahrilas, P.J., and Pandolfino, J.E. (2019). Normal Values of Esophageal Distensibility and  
699 Distension-Induced Contractility Measured by Functional Luminal Imaging Probe Panometry. *Clin*  
700 *Gastroenterol Hepatol* 17, 674-681 e671. 10.1016/j.cgh.2018.07.042.
- 701 38. Jonasson, C., Wernersson, B., Hoff, D.A., and Hatlebakk, J.G. (2013). Validation of the GerdQ  
702 questionnaire for the diagnosis of gastro-oesophageal reflux disease. *Aliment Pharmacol Ther* 37,  
703 564-572. 10.1111/apt.12204.
- 704 39. Taft, T.H., Riehl, M., Sodikoff, J.B., Kahrilas, P.J., Keefer, L., Doerfler, B., and Pandolfino, J.E.  
705 (2016). Development and validation of the brief esophageal dysphagia questionnaire.  
706 *Neurogastroenterol Motil* 28, 1854-1860. 10.1111/nmo.12889.
- 707 40. Bedell, A., Taft, T.H., Keefer, L., and Pandolfino, J. (2016). Development of the Northwestern  
708 Esophageal Quality of Life Scale: A Hybrid Measure for Use Across Esophageal Conditions. *Am J*  
709 *Gastroenterol* 111, 493-499. 10.1038/ajg.2016.20.
- 710 41. Hao, Y., Hao, S., Andersen-Nissen, E., Mauck, W.M., 3rd, Zheng, S., Butler, A., Lee, M.J., Wilk,  
711 A.J., Darby, C., Zager, M., et al. (2021). Integrated analysis of multimodal single-cell data. *Cell* 184,  
712 3573-3587 e3529. 10.1016/j.cell.2021.04.048.
- 713 42. Hippen, A.A., Falco, M.M., Weber, L.M., Erkan, E.P., Zhang, K., Doherty, J.A., Vaharautio, A.,  
714 Greene, C.S., and Hicks, S.C. (2021). miQC: An adaptive probabilistic framework for quality control  
715 of single-cell RNA-sequencing data. *PLoS Comput Biol* 17, e1009290.  
716 10.1371/journal.pcbi.1009290.
- 717 43. Germain, P.L., Lun, A., Garcia Meixide, C., Macnair, W., and Robinson, M.D. (2021). Doublet  
718 identification in single-cell sequencing data using scDblFinder. *F1000Res* 10, 979.  
719 10.12688/f1000research.73600.2.
- 720 44. Hafemeister, C., and Satija, R. (2019). Normalization and variance stabilization of single-cell RNA-  
721 seq data using regularized negative binomial regression. *Genome Biol* 20, 296. 10.1186/s13059-019-  
722 1874-1.
- 723 45. Lause, J., Berens, P., and Kobak, D. (2021). Analytic Pearson residuals for normalization of single-  
724 cell RNA-seq UMI data. *Genome Biol* 22, 258. 10.1186/s13059-021-02451-7.
- 725 46. McInnes, L., Healy, J., and Melville, J. (2018). UMAP: Uniform Manifold Approximation and  
726 Projection for Dimension Reduction. arXiv:1802.03426. 10.48550/arXiv.1802.03426.
- 727 47. Clevenger, M.H., Karami, A.L., Carlson, D.A., Kahrilas, P.J., Gonsalves, N., Pandolfino, J.E.,  
728 Winter, D.R., Whelan, K.A., and Tetreault, M.P. (2023). Suprabasal cells retaining stem cell identity  
729 programs drive basal cell hyperplasia in eosinophilic esophagitis. *bioRxiv*.  
730 10.1101/2023.04.20.537495.
- 731 48. Busslinger, G.A., Weusten, B.L.A., Bogte, A., Begthel, H., Brosens, L.A.A., and Clevers, H. (2021).  
732 Human gastrointestinal epithelia of the esophagus, stomach, and duodenum resolved at single-cell  
733 resolution. *Cell Rep* 34, 108819. 10.1016/j.celrep.2021.108819.

- 734 49. Kabir, M.F., Karami, A.L., Cruz-Acuna, R., Klochkova, A., Saxena, R., Mu, A., Murray, M.G., Cruz,  
735 J., Fuller, A.D., Clevenger, M.H., et al. (2022). Single cell transcriptomic analysis reveals cellular  
736 diversity of murine esophageal epithelium. *Nat Commun* *13*, 2167. 10.1038/s41467-022-29747-x.
- 737 50. Okumura, T., Shimada, Y., Imamura, M., and Yasumoto, S. (2003). Neurotrophin receptor p75(NTR)  
738 characterizes human esophageal keratinocyte stem cells in vitro. *Oncogene* *22*, 4017-4026.  
739 10.1038/sj.onc.1206525.
- 740 51. Tirosh, I., Izar, B., Prakadan, S.M., Wadsworth, M.H., 2nd, Treacy, D., Trombetta, J.J., Rotem, A.,  
741 Rodman, C., Lian, C., Murphy, G., et al. (2016). Dissecting the multicellular ecosystem of metastatic  
742 melanoma by single-cell RNA-seq. *Science* *352*, 189-196. 10.1126/science.aad0501.
- 743 52. Fonseka, C.Y., Rao, D.A., Teslovich, N.C., Korsunsky, I., Hannes, S.K., Slowikowski, K., Gurish,  
744 M.F., Donlin, L.T., Lederer, J.A., Weinblatt, M.E., et al. (2018). Mixed-effects association of single  
745 cells identifies an expanded effector CD4(+) T cell subset in rheumatoid arthritis. *Sci Transl Med* *10*.  
746 10.1126/scitranslmed.aag0305.
- 747 53. Mootha, V.K., Lindgren, C.M., Eriksson, K.F., Subramanian, A., Sihag, S., Lehar, J., Puigserver, P.,  
748 Carlsson, E., Ridderstrale, M., Laurila, E., et al. (2003). PGC-1alpha-responsive genes involved in  
749 oxidative phosphorylation are coordinately downregulated in human diabetes. *Nat Genet* *34*, 267-273.  
750 10.1038/ng1180.
- 751 54. Subramanian, A., Tamayo, P., Mootha, V.K., Mukherjee, S., Ebert, B.L., Gillette, M.A., Paulovich,  
752 A., Pomeroy, S.L., Golub, T.R., Lander, E.S., and Mesirov, J.P. (2005). Gene set enrichment analysis:  
753 a knowledge-based approach for interpreting genome-wide expression profiles. *Proc Natl Acad Sci U*  
754 *S A* *102*, 15545-15550. 10.1073/pnas.0506580102.
- 755 55. Liberzon, A., Birger, C., Thorvaldsdottir, H., Ghandi, M., Mesirov, J.P., and Tamayo, P. (2015). The  
756 Molecular Signatures Database (MSigDB) hallmark gene set collection. *Cell Syst* *1*, 417-425.  
757 10.1016/j.cels.2015.12.004.
- 758 56. Squair, J.W., Gautier, M., Kathe, C., Anderson, M.A., James, N.D., Hutson, T.H., Hudelle, R.,  
759 Qaiser, T., Matson, K.J.E., Barraud, Q., et al. (2021). Confronting false discoveries in single-cell  
760 differential expression. *Nat Commun* *12*, 5692. 10.1038/s41467-021-25960-2.
- 761 57. Chen, Y., Lun, A.T., and Smyth, G.K. (2016). From reads to genes to pathways: differential  
762 expression analysis of RNA-Seq experiments using Rsubread and the edgeR quasi-likelihood  
763 pipeline. *F1000Res* *5*, 1438. 10.12688/f1000research.8987.2.
- 764 58. McCarthy, D.J., Chen, Y., and Smyth, G.K. (2012). Differential expression analysis of multifactor  
765 RNA-Seq experiments with respect to biological variation. *Nucleic Acids Res* *40*, 4288-4297.  
766 10.1093/nar/gks042.
- 767 59. Robinson, M.D., McCarthy, D.J., and Smyth, G.K. (2010). edgeR: a Bioconductor package for  
768 differential expression analysis of digital gene expression data. *Bioinformatics* *26*, 139-140.  
769 10.1093/bioinformatics/btp616.
- 770 60. Wu, T., Hu, E., Xu, S., Chen, M., Guo, P., Dai, Z., Feng, T., Zhou, L., Tang, W., Zhan, L., et al.  
771 (2021). clusterProfiler 4.0: A universal enrichment tool for interpreting omics data. *Innovation*  
772 (Camb) *2*, 100141. 10.1016/j.xinn.2021.100141.
- 773 61. Consortium, E.P. (2012). An integrated encyclopedia of DNA elements in the human genome. *Nature*  
774 *489*, 57-74. 10.1038/nature11247.
- 775 62. Lachmann, A., Xu, H., Krishnan, J., Berger, S.I., Mazloom, A.R., and Ma'ayan, A. (2010). ChEA:  
776 transcription factor regulation inferred from integrating genome-wide ChIP-X experiments.  
777 *Bioinformatics* *26*, 2438-2444. 10.1093/bioinformatics/btq466.
- 778 63. Kou, Y., Chen, E.Y., Clark, N.R., Duan, Q., Tan, C.M., and Ma'ayan, A. (2013). ChEA2: Gene-Set  
779 Libraries from ChIP-X Experiments to Decode the Transcription Regulome. held in Berlin,  
780 Heidelberg, (Springer Berlin Heidelberg), pp. 416-430.
- 781 64. Chen, E.Y., Tan, C.M., Kou, Y., Duan, Q., Wang, Z., Meirelles, G.V., Clark, N.R., and Ma'ayan, A.  
782 (2013). Enrichr: interactive and collaborative HTML5 gene list enrichment analysis tool. *BMC*  
783 *Bioinformatics* *14*, 128. 10.1186/1471-2105-14-128.

- 784 65. Hou, W., Ji, Z., Chen, Z., Wherry, E.J., Hicks, S.C., and Ji, H. (2023). A statistical framework for  
785 differential pseudotime analysis with multiple single-cell RNA-seq samples. *Nat Commun* *14*, 7286.  
786 10.1038/s41467-023-42841-y.
- 787 66. Wang, Q., Li, Y., Wu, M., Huang, S., Zhang, A., Zhang, Y., and Jia, Z. (2021). Targeting microsomal  
788 prostaglandin E synthase 1 to develop drugs treating the inflammatory diseases. *Am J Transl Res* *13*,  
789 391-419.
- 790 67. Yi, Y.S. (2016). Functional Role of Milk Fat Globule-Epidermal Growth Factor VIII in Macrophage-  
791 Mediated Inflammatory Responses and Inflammatory/Autoimmune Diseases. *Mediators Inflamm*  
792 *2016*, 5628486. 10.1155/2016/5628486.
- 793 68. Oh, S., Bournique, E., Bowen, D., Jalili, P., Sanchez, A., Ward, I., Dananberg, A., Manjunath, L.,  
794 Tran, G.P., Semler, B.L., et al. (2021). Genotoxic stress and viral infection induce transient  
795 expression of APOBEC3A and pro-inflammatory genes through two distinct pathways. *Nat Commun*  
796 *12*, 4917. 10.1038/s41467-021-25203-4.
- 797 69. Tiwari, R., de la Torre, J.C., McGavern, D.B., and Nayak, D. (2019). Beyond Tethering the Viral  
798 Particles: Immunomodulatory Functions of Tetherin (BST-2). *DNA Cell Biol* *38*, 1170-1177.  
799 10.1089/dna.2019.4777.
- 800 70. Baaten, B.J., Li, C.R., and Bradley, L.M. (2010). Multifaceted regulation of T cells by CD44.  
801 *Commun Integr Biol* *3*, 508-512. 10.4161/cib.3.6.13495.
- 802 71. Liu, Q., Niu, X., Li, Y., Zhang, J.R., Zhu, S.J., Yang, Q.Y., Zhang, W., and Gong, L. (2022). Role of  
803 the mucin-like glycoprotein FCGBP in mucosal immunity and cancer. *Front Immunol* *13*, 863317.  
804 10.3389/fimmu.2022.863317.
- 805 72. Okamoto, Y., and Shikano, S. (2023). Emerging roles of a chemoattractant receptor GPR15 and  
806 ligands in pathophysiology. *Front Immunol* *14*, 1179456. 10.3389/fimmu.2023.1179456.
- 807 73. Subramanian, B.C., Moissoglu, K., and Parent, C.A. (2018). The LTB(4)-BLT1 axis regulates the  
808 polarized trafficking of chemoattractant GPCRs during neutrophil chemotaxis. *J Cell Sci* *131*.  
809 10.1242/jcs.217422.
- 810 74. Nguyen, H.T., Reyes-Alcaraz, A., Yong, H.J., Nguyen, L.P., Park, H.K., Inoue, A., Lee, C.S., Seong,  
811 J.Y., and Hwang, J.I. (2020). CXCR7: a beta-arrestin-biased receptor that potentiates cell migration  
812 and recruits beta-arrestin2 exclusively through Gbetagamma subunits and GRK2. *Cell Biosci* *10*, 134.  
813 10.1186/s13578-020-00497-x.
- 814 75. Kelly, A., and Trowsdale, J. (2019). Genetics of antigen processing and presentation.  
815 *Immunogenetics* *71*, 161-170. 10.1007/s00251-018-1082-2.
- 816 76. Bartel, Y., Bauer, B., and Steinle, A. (2013). Modulation of NK cell function by genetically coupled  
817 C-type lectin-like receptor/ligand pairs encoded in the human natural killer gene complex. *Front*  
818 *Immunol* *4*, 362. 10.3389/fimmu.2013.00362.
- 819 77. Lu, R.Q., Zhang, Y.Y., Zhao, H.Q., Guo, R.Q., Jiang, Z.X., and Guo, R. (2022). SGK1, a Critical  
820 Regulator of Immune Modulation and Fibrosis and a Potential Therapeutic Target in Chronic Graft-  
821 Versus-Host Disease. *Front Immunol* *13*, 822303. 10.3389/fimmu.2022.822303.
- 822 78. Li, Y., Su, G., Zhong, Y., Xiong, Z., Huang, T., Quan, J., Huang, J., Wen, X., Luo, C., Zheng, W., et  
823 al. (2021). HB-EGF-induced IL-8 secretion from airway epithelium leads to lung fibroblast  
824 proliferation and migration. *BMC Pulm Med* *21*, 347. 10.1186/s12890-021-01726-w.
- 825 79. Uhlen, M., Fagerberg, L., Hallstrom, B.M., Lindskog, C., Oksvold, P., Mardinoglu, A., Sivertsson,  
826 A., Kampf, C., Sjostedt, E., Asplund, A., et al. (2015). Proteomics. Tissue-based map of the human  
827 proteome. *Science* *347*, 1260419. 10.1126/science.1260419.
- 828 80. Politi, E., Angelakopoulou, A., Grapsa, D., Zande, M., Stefanaki, K., Panagiotou, I., Roma, E., and  
829 Syrigou, E. (2017). Filaggrin and Periostin Expression Is Altered in Eosinophilic Esophagitis and  
830 Normalized With Treatment. *J Pediatr Gastroenterol Nutr* *65*, 47-52.  
831 10.1097/MPG.0000000000001419.
- 832 81. Oshima, N., Ishihara, S., Fukuba, N., Mishima, Y., Kawashima, K., Ishimura, N., Ishikawa, N.,  
833 Maruyama, R., and Kinoshita, Y. (2017). Epidermal differentiation complex protein involucrin is  
834 down-regulated in eosinophilic esophagitis. *Esophagus* *14*, 171-177. 10.1007/s10388-016-0568-y.

- 835 82. Yu, T., Yang, X., Fu, Q., Liang, J., Wu, X., Sheng, J., Chen, Y., Xiao, L., Wu, Y., Nie, D., et al.  
836 (2023). TRIM11 attenuates Treg cell differentiation by p62-selective autophagic degradation of  
837 AIM2. *Cell Rep* 42, 113231. [10.1016/j.celrep.2023.113231](https://doi.org/10.1016/j.celrep.2023.113231).
- 838 83. Crowell, M.D., Umar, S.B., Griffing, W.L., DiBaise, J.K., Lacy, B.E., and Vela, M.F. (2017).  
839 Esophageal Motor Abnormalities in Patients With Scleroderma: Heterogeneity, Risk Factors, and  
840 Effects on Quality of Life. *Clin Gastroenterol Hepatol* 15, 207-213 e201. [10.1016/j.cgh.2016.08.034](https://doi.org/10.1016/j.cgh.2016.08.034).
- 841 84. Forbes, A., and Marie, I. (2009). Gastrointestinal complications: the most frequent internal  
842 complications of systemic sclerosis. *Rheumatology (Oxford)* 48 Suppl 3, iii36-39.  
843 [10.1093/rheumatology/ken485](https://doi.org/10.1093/rheumatology/ken485).
- 844 85. Krieg, T., Abraham, D., and Lafyatis, R. (2007). Fibrosis in connective tissue disease: the role of the  
845 myofibroblast and fibroblast-epithelial cell interactions. *Arthritis Res Ther* 9 Suppl 2, S4.  
846 [10.1186/ar2188](https://doi.org/10.1186/ar2188).
- 847 86. Aden, N., Shiwen, X., Aden, D., Black, C., Nuttall, A., Denton, C.P., Leask, A., Abraham, D., and  
848 Stratton, R. (2008). Proteomic analysis of scleroderma lesional skin reveals activated wound healing  
849 phenotype of epidermal cell layer. *Rheumatology (Oxford)* 47, 1754-1760.  
850 [10.1093/rheumatology/ken370](https://doi.org/10.1093/rheumatology/ken370).
- 851 87. Aden, N., Nuttall, A., Shiwen, X., de Winter, P., Leask, A., Black, C.M., Denton, C.P., Abraham,  
852 D.J., and Stratton, R.J. (2010). Epithelial cells promote fibroblast activation via IL-1alpha in systemic  
853 sclerosis. *J Invest Dermatol* 130, 2191-2200. [10.1038/jid.2010.120](https://doi.org/10.1038/jid.2010.120).
- 854 88. Nikitorowicz-Buniak, J., Denton, C.P., Abraham, D., and Stratton, R. (2015). Partially Evoked  
855 Epithelial-Mesenchymal Transition (EMT) Is Associated with Increased TGFbeta Signaling within  
856 Lesional Scleroderma Skin. *PLoS One* 10, e0134092. [10.1371/journal.pone.0134092](https://doi.org/10.1371/journal.pone.0134092).
- 857 89. Miyagawa, T., Asano, Y., Saigusa, R., Hirabayashi, M., Yamashita, T., Taniguchi, T., Takahashi, T.,  
858 Nakamura, K., Miura, S., Yoshizaki, A., et al. (2019). A potential contribution of trappin-2 to the  
859 development of vasculopathy in systemic sclerosis. *J Eur Acad Dermatol Venereol* 33, 753-760.  
860 [10.1111/jdv.15387](https://doi.org/10.1111/jdv.15387).
- 861 90. Deraison, C., Bonnart, C., Langella, P., Roget, K., and Vergnolle, N. (2023). Elafin and its precursor  
862 trappin-2: What is their therapeutic potential for intestinal diseases? *Br J Pharmacol* 180, 144-160.  
863 [10.1111/bph.15985](https://doi.org/10.1111/bph.15985).
- 864 91. Hinchcliff, M., Huang, C.C., Wood, T.A., Matthew Mahoney, J., Martyanov, V., Bhattacharyya, S.,  
865 Tamaki, Z., Lee, J., Carns, M., Podluszky, S., et al. (2013). Molecular signatures in skin associated  
866 with clinical improvement during mycophenolate treatment in systemic sclerosis. *J Invest Dermatol*  
867 133, 1979-1989. [10.1038/jid.2013.130](https://doi.org/10.1038/jid.2013.130).
- 868 92. Dong, X., Liu, Z., Lan, D., Niu, J., Miao, J., Yang, G., Zhang, F., Sun, Y., Wang, K., and Miao, Y.  
869 (2017). Critical role of Keratin 1 in maintaining epithelial barrier and correlation of its down-  
870 regulation with the progression of inflammatory bowel disease. *Gene* 608, 13-19.  
871 [10.1016/j.gene.2017.01.015](https://doi.org/10.1016/j.gene.2017.01.015).
- 872 93. McCann, M.R., Monemdjou, R., Ghassemi-Kakroodi, P., Fahmi, H., Perez, G., Liu, S., Shi-Wen, X.,  
873 Parapuram, S.K., Kojima, F., Denton, C.P., et al. (2011). mPGES-1 null mice are resistant to  
874 bleomycin-induced skin fibrosis. *Arthritis Res Ther* 13, R6. [10.1186/ar3226](https://doi.org/10.1186/ar3226).
- 875 94. Villanueva-Martin, G., Acosta-Herrera, M., Carmona, E.G., Kerick, M., Ortego-Centeno, N.,  
876 Callejas-Rubio, J.L., Mages, N., Klages, S., Borno, S., Timmermann, B., et al. (2023). Non-classical  
877 circulating monocytes expressing high levels of microsomal prostaglandin E2 synthase-1 tag an  
878 aberrant IFN-response in systemic sclerosis. *J Autoimmun* 140, 103097. [10.1016/j.jaut.2023.103097](https://doi.org/10.1016/j.jaut.2023.103097).
- 879 95. Unlu, B., Tursen, U., Rajabi, Z., Jabalameli, N., and Rajabi, F. (2022). The Immunogenetics of  
880 Systemic Sclerosis. *Adv Exp Med Biol* 1367, 259-298. [10.1007/978-3-030-92616-8\\_10](https://doi.org/10.1007/978-3-030-92616-8_10).
- 881 96. Liang, M., Lv, J., Jiang, Z., He, H., Chen, C., Xiong, Y., Zhu, X., Xue, Y., Yu, Y., Yang, S., et al.  
882 (2020). Promotion of Myofibroblast Differentiation and Tissue Fibrosis by the Leukotriene B(4) -  
883 Leukotriene B(4) Receptor Axis in Systemic Sclerosis. *Arthritis Rheumatol* 72, 1013-1025.  
884 [10.1002/art.41192](https://doi.org/10.1002/art.41192).

- 885 97. Hirabayashi, M., Asano, Y., Yamashita, T., Miura, S., Nakamura, K., Taniguchi, T., Saigusa, R.,  
886 Takahashi, T., Ichimura, Y., Miyagawa, T., et al. (2018). Possible pro-inflammatory role of heparin-  
887 binding epidermal growth factor-like growth factor in the active phase of systemic sclerosis. *J*  
888 *Dermatol* *45*, 182-188. 10.1111/1346-8138.14088.
- 889 98. Guo, S., Li, Y., Wang, Y., Chu, H., Chen, Y., Liu, Q., Guo, G., Tu, W., Wu, W., Zou, H., et al.  
890 (2016). Copy Number Variation of HLA-DQA1 and APOBEC3A/3B Contribute to the Susceptibility  
891 of Systemic Sclerosis in the Chinese Han Population. *J Rheumatol* *43*, 880-886.  
892 10.3899/jrheum.150945.
- 893 99. Lopez-Isac, E., Acosta-Herrera, M., Kerick, M., Assassi, S., Satpathy, A.T., Granja, J., Mumbach,  
894 M.R., Beretta, L., Simeon, C.P., Carreira, P., et al. (2019). GWAS for systemic sclerosis identifies  
895 multiple risk loci and highlights fibrotic and vasculopathy pathways. *Nat Commun* *10*, 4955.  
896 10.1038/s41467-019-12760-y.
- 897 100. Acosta-Herrera, M., Kerick, M., Lopez-Isac, E., Assassi, S., Beretta, L., Simeon-Aznar, C.P.,  
898 Ortego-Centeno, N., International, S.G., Proudman, S.M., Australian Scleroderma Interest, G., et al.  
899 (2021). Comprehensive analysis of the major histocompatibility complex in systemic sclerosis  
900 identifies differential HLA associations by clinical and serological subtypes. *Ann Rheum Dis* *80*,  
901 1040-1047. 10.1136/annrheumdis-2021-219884.
- 902 101. Hanson, A.L., Sahhar, J., Ngian, G.S., Roddy, J., Walker, J., Stevens, W., Nikpour, M., Assassi,  
903 S., Proudman, S., Mayes, M.D., et al. (2022). Contribution of HLA and KIR Alleles to Systemic  
904 Sclerosis Susceptibility and Immunological and Clinical Disease Subtypes. *Front Genet* *13*, 913196.  
905 10.3389/fgene.2022.913196.
- 906 102. Dai, H., Wang, L., Li, L., Huang, Z., and Ye, L. (2021). Metallothionein 1: A New Spotlight on  
907 Inflammatory Diseases. *Front Immunol* *12*, 739918. 10.3389/fimmu.2021.739918.
- 908 103. Subramanian Vignesh, K., and Deepe, G.S., Jr. (2017). Metallothioneins: Emerging Modulators  
909 in Immunity and Infection. *Int J Mol Sci* *18*. 10.3390/ijms18102197.
- 910 104. Marie, I. (2019). Systemic sclerosis and exposure to heavy metals. *Autoimmun Rev* *18*, 62-72.  
911 10.1016/j.autrev.2018.11.001.
- 912 105. Shaker, R., Dodds, W.J., Helm, J.F., Kern, M.K., and Hogan, W.J. (1991). Regional esophageal  
913 distribution and clearance of refluxed gastric acid. *Gastroenterology* *101*, 355-359. 10.1016/0016-  
914 5085(91)90011-9.
- 915 106. Diener, U., Patti, M.G., Molena, D., Fisichella, P.M., and Way, L.W. (2001). Esophageal  
916 dysmotility and gastroesophageal reflux disease. *J Gastrointest Surg* *5*, 260-265. 10.1016/s1091-  
917 255x(01)80046-9.
- 918 107. Patel, C.K., Kahrilas, P.J., Hodge, N.B., Tsikretsis, L.E., Carlson, D.A., Pandolfino, J.E., and  
919 Tetreault, M.P. (2022). RNA-sequencing reveals molecular and regional differences in the esophageal  
920 mucosa of achalasia patients. *Sci Rep* *12*, 20616. 10.1038/s41598-022-25103-7.
- 921 108. Woodland, P., Aktar, R., Mthunzi, E., Lee, C., Peiris, M., Preston, S.L., Blackshaw, L.A., and  
922 Sifrim, D. (2015). Distinct afferent innervation patterns within the human proximal and distal  
923 esophageal mucosa. *Am J Physiol Gastrointest Liver Physiol* *308*, G525-531.  
924 10.1152/ajpgi.00175.2014.
- 925 109. Sandqvist, G., and Hesselstrand, R. (2019). Validity of the Swedish version of the systemic  
926 sclerosis quality of life questionnaire (SSCQoL): A novel measure of quality of life for patients with  
927 systemic sclerosis. *Ann Rheum Dis* *78*, 855-857. 10.1136/annrheumdis-2018-214260.
- 928 110. Lee, A.S., Lee, J.S., He, Z., and Ryu, J.H. (2020). Reflux-Aspiration in Chronic Lung Disease.  
929 *Ann Am Thorac Soc* *17*, 155-164. 10.1513/AnnalsATS.201906-427CME.
- 930 111. Savarino, E., Bazzica, M., Zentilin, P., Pohl, D., Parodi, A., Cittadini, G., Negrini, S., Indiveri, F.,  
931 Tutuian, R., Savarino, V., and Ghio, M. (2009). Gastroesophageal reflux and pulmonary fibrosis in  
932 scleroderma: a study using pH-impedance monitoring. *Am J Respir Crit Care Med* *179*, 408-413.  
933 10.1164/rccm.200808-1359OC.
- 934 112. Conboy, C.M., Spyrou, C., Thorne, N.P., Wade, E.J., Barbosa-Morais, N.L., Wilson, M.D.,  
935 Bhattacharjee, A., Young, R.A., Tavaré, S., Lees, J.A., and Odom, D.T. (2007). Cell cycle genes are

- 936 the evolutionarily conserved targets of the E2F4 transcription factor. *PLoS One* 2, e1061.  
937 10.1371/journal.pone.0001061.
- 938 113. Garcia-Gutierrez, L., Delgado, M.D., and Leon, J. (2019). MYC Oncogene Contributions to  
939 Release of Cell Cycle Brakes. *Genes (Basel)* 10. 10.3390/genes10030244.
- 940 114. Lastra, D., Escoll, M., and Cuadrado, A. (2022). Transcription Factor NRF2 Participates in Cell  
941 Cycle Progression at the Level of G1/S and Mitotic Checkpoints. *Antioxidants (Basel)* 11.  
942 10.3390/antiox11050946.
- 943 115. Portal, C., Wang, Z., Scott, D.K., Wolosin, J.M., and Iomini, C. (2022). The c-Myc Oncogene  
944 Maintains Corneal Epithelial Architecture at Homeostasis, Modulates p63 Expression, and Enhances  
945 Proliferation During Tissue Repair. *Invest Ophthalmol Vis Sci* 63, 3. 10.1167/iovs.63.2.3.
- 946 116. Wruck, C.J., Wruck, A., Brandenburg, L.O., Kadyrov, M., Tohidnezhad, M., and Pufe, T. (2011).  
947 Impact of Nrf2 on esophagus epithelium cornification. *Int J Dermatol* 50, 1362-1365. 10.1111/j.1365-  
948 4632.2011.04989.x.
- 949 117. Jones, R., Junghard, O., Dent, J., Vakil, N., Halling, K., Wernersson, B., and Lind, T. (2009).  
950 Development of the GerdQ, a tool for the diagnosis and management of gastro-oesophageal reflux  
951 disease in primary care. *Aliment Pharmacol Ther* 30, 1030-1038. 10.1111/j.1365-2036.2009.04142.x.  
952



953 **FIGURES**

954 **Figure 1. ScRNA-seq sample composition by cell type. A)** Integrated UMAP embedding of all cells  
955 (n=306,372) labeled by cell type. **B)** Expression by cell type of canonical markers. **C)** Sample-wise (n=39)  
956 distribution of major cell types. **D)** Proportion of cells by cell type.

957

958 **Figure 2. Landscape of esophageal epithelial cells. A)** Histological summary of the human esophageal  
959 epithelium, adopted from Clevenger et al.<sup>28</sup> Alternatively shaded cells within the same layer represent  
960 proliferating cells. NOTE: The layers of replicating cells not attached to the basement membrane, labeled  
961 here as proliferating suprabasal cells, are sometimes referred to as epibasal cells<sup>28</sup>. **B)** Integrated UMAP  
962 embedding of all esophageal epithelial cells (EECs, n=230,720) labeled by epithelial compartment. **C)**  
963 Expression by EEC compartment and cell cycle markers. **C)** Proportion of proliferating basal and  
964 suprabasal cells by condition and biopsy location. **E)** Proportions of cells by condition, EEC compartment,  
965 and biopsy location. The bars denote the mean values, the vertical lines the standard deviations, and the  
966 points the individual sample proportions. Pairwise differences across conditions were evaluated statistically  
967 using MASC<sup>52</sup>. \*p<0.05; \*\*p<0.005.

968

969 **Figure 3. Distribution of esophageal epithelial cells by differentiation score and epithelial**  
970 **compartment. A)** Integrated UMAP embeddings of esophageal epithelial cells divided by disease state,  
971 colored by differentiation score. **B)** Swarm plots of esophageal epithelial cells by differentiation score,  
972 colored by epithelial compartment.

973

974 **Figure 4. Differential gene expression at single-cell resolution in esophageal epithelial cells. A)** Inter-  
975 sample expression correlations are shown for each epithelial compartment for the 2,000 most variable  
976 genes. **B)** The distribution of inter-sample expression correlations are shown by epithelial compartment. **C-**  
977 **D)** UpSet plots showing differential gene expression at the single-cell level by epithelial compartment for  
978 SSc vs HCs (purple) and GERD vs HCs (orange) in the proximal **(C)** and distal **(D)** esophagus. **E)** The  
979 number of significantly differentially expressed genes with  $|\log_2FC| > 0.1$  are shown for SSC vs. HCs and  
980 GERD vs. HCs, by non-proliferating epithelial compartment and biopsy location. **F)** Gene set enrichment

981 analysis results, showing all pathways enriched with  $P < 0.001$  (unadjusted) for SSc vs. HCs (purple) and  
982 GERD vs. HCs (orange), split by non-proliferating epithelial compartment and biopsy location. Pathways in  
983 bold had enrichment with  $P < 0.001$  in both SSc and GERD. Points circled in red indicate statistical  
984 significance after adjusting for the number of tested pathways ( $P_{FDR} < 0.05$ ). **G-H**) Relative gene expression  
985 (SSc vs. HCs) for all DEGs at the single-cell level were modeled using Lamian<sup>65</sup> and plotted against the  
986 epithelial differentiation score in the proximal (**G**) and distal (**H**) esophagus. These trajectories were  
987 clustered based on Euclidean distance using Ward's method. The lefthand color bar displays the blended  
988 color of all epithelial compartments in which each gene was differentially expressed. In **G**), labeled genes  
989 highlight the top 25 ranked genes in the leading edge of the innate immune system pathway enriched in  
990 SSc in the superficial compartment of the proximal esophagus. In **H**), the labeled genes mark the leading  
991 edge genes of the matrisome pathway enriched in SSc in the suprabasal compartment of the distal  
992 esophagus. **I-L**) Dot plots showing average gene expression, by condition and epithelial compartment, for  
993 the most highly represented protein families in the leading edges of significantly enriched pathways:  
994 keratins (**I**), S100 proteins (**J**), small proline-rich proteins (**K**), and serine protease inhibitors (**L**). **M**) Single-  
995 cell gene expression by condition, epithelial compartment, and esophageal region for *PI3*, the most frequent  
996 gene in leading edges of significantly enriched pathways.

997

998 **Figure 5. Differential gene expression aggregated by sample and EEC compartment. A-B)** Gene  
999 expression differences between SSc and HCs (**A**) and between SSc and GERD (**B**) are shown for each  
1000 EEC compartment. Significant DEGs ( $FDR < 0.05$ ) are highlighted in purple. The percentages of genes that  
1001 were significantly differentially expressed in each compartment are plotted in blue in along the secondary  
1002 Y axis. **C-D**) Gene expression differences in  $\log_2FC$  are shown for SSc vs. HCs (Y axis) against GERD vs.  
1003 HCs (X axis) within the superficial compartment in the proximal (**C**) and distal (**D**) regions. Significant DEGs  
1004 in both conditions are highlighted in blue, significant DEGs in SSC only are highlighted in purple, and  
1005 significant DEGs in GERD only are highlighted in orange. The correlation between comparisons is shown  
1006 in the upper left, and the slope and coefficient of determination for the modeled linear regression with  
1007 intercept=0 is displayed in the lower right. Trendlines with 95% confidence intervals are plotted in pink, and  
1008 the dashed grey lines denote where  $y=x$ . Encircled points highlight disease-specific DEGs that are

1009 referenced in the main text and plotted in **(E)**, which shows the distribution of expression aggregated by  
1010 sample in the superficial compartment across conditions and biopsy locations. Pairwise differential  
1011 expression was determined using edgeR's quasi-likelihood F-tests: \* $p < 0.05$ ; \*\* $p < 0.005$ ; \*\*\* $p < 0.0005$ . **F)** The  
1012 number of significant DEGs are shown for GERD vs. HCs (orange) and for all permutations of  $n=4$  samples  
1013 for SSc vs. HCs (purple) in superficial cells for both proximal and distal regions. The point within the SSc  
1014 distribution is the median value. **G-H)** The distributions of relative FC or slope  $m$  (**G**) and coefficient of  
1015 determination  $r^2$  (**H**) are shown for all permutations of  $n=4$  SSc samples, determined by modeling a linear  
1016 regression with intercept=0 for the  $\log_2FC$  of SSc vs. HCs against the  $\log_2FC$  of GERD vs. HCs for all  
1017 expressed genes in the superficial compartment for both proximal and distal regions. DEG, differentially  
1018 expressed gene; FC, fold change.

1019  
1020 **Figure 6. Landscape of superficial esophageal epithelial cells.** **A)** Integrated UMAP embedding of all  
1021 superficial EECs ( $n=30,866$ ) clustered by unique transcriptional signatures. **B)** Relative expression of  
1022 cluster-specific gene signatures. **C)** Epithelial differentiation score by superficial cell cluster. **D)** Proportion  
1023 of superficial cells by condition and cluster from the proximal esophagus. The bars denote the mean values,  
1024 the vertical lines the standard deviations, and the points the individual sample proportions. Pairwise  
1025 differences across conditions were evaluated statistically using MASC<sup>52</sup>. \* $p < 0.05$ ; \*\* $p < 0.005$ . **E)** Distribution  
1026 of metallothionein module score in proximal, superficial cells by condition. The metallothionein module  
1027 score included *MT1A*, *MT1E*, *MT1F*, *MT1G*, *MT1H*, *MT1M*, *MT1X*, and *MT2A*. **F)** Distribution of relative  
1028 metallothionein expression by cluster and condition in superficial cells from proximal esophagus. All  
1029 pairwise comparisons were between SSc and GERD were statistically significant, except for cluster 5.

1030  
1031 **Figure 7. Expression of enriched transcription factors and their targets in superficial EECs in**  
1032 **proximal esophagus.** The distributions of enriched transcription factor expression and target module  
1033 scores are shown proximal, superficial cells by condition and superficial cluster for **A)** IRF1, **B)** MYC, **C)**  
1034 E2F4, and **D)** NE2L2.

1035

1036 **Figure 8. Correlations with clinical phenotypes. A)** Heatmap of quantitative clinical traits organized using  
1037 agglomerative, complete hierarchical clustering on Euclidean distances, with pairwise Spearman  
1038 correlations shown in each cell. **B)** SSc cases are plotted on the first two PCs of the quantitative clinical  
1039 traits, colored by esophageal motility phenotype. The relative magnitude and direction of trait correlations  
1040 with the PCs are shown with black arrows. **C)** Correlations between EEC compartments and clinical trait  
1041 PCs in SSc cases. Linear regression trendlines with 95% confidence intervals are shown for each  
1042 compartment against PC1 and PC2. **D)** Correlations between aggregate, relative metallothionein  
1043 expression and clinical trait PCs in superficial cells in the proximal esophagus. Trendlines with 95%  
1044 confidence intervals are shown with the unadjusted correlation P-value. The metallothionein module score  
1045 included *MT1A*, *MT1E*, *MT1F*, *MT1G*, *MT1H*, *MT1M*, *MT1X*, and *MT2A*. **E)** Correlations between superficial  
1046 clusters (SCs) and clinical trait PC1 in SSc cases. Linear regression trendlines with 95% confidence  
1047 intervals are shown for each SC. The displayed P-values correspond to the highlighted correlations  
1048 between SC3 and PC1. **F)** Boxplots showing the proportion of SC3 in superficial cells by esophageal motility  
1049 phenotype in the proximal and distal esophagus, colored by disease state (HCs, grey; GERD, orange; SSc,  
1050 purple). AET, acid exposure time; BEDQ, brief esophageal dysphagia questionnaire; BMI, body mass index;  
1051 DCI, distal contractile integral; DI, distensibility index; EGJ, esophagogastric junction; EGJOO,  
1052 esophagogastric junction outflow obstruction; FLIP, functional luminal imaging probe panometry; HCs,  
1053 healthy controls; HRM, high-resolution manometry; IEM, ineffective esophageal motility; IQR, inter-quartile  
1054 range; IRP, integrated relaxation pressure; NEQOL, Northwestern esophageal quality of life; NM,  
1055 neuromyogenic model. NR, not reported.

1056 **SUPPLEMENTAL FIGURES**

1057 **Supplemental Figure 1. Cell clustering and cell type annotation. A)** Cell type module scores for 10  
1058 detected cell types, colored by relative gene expression of the listed genes. **B)** Projected UMAP  
1059 embeddings calculated on the top 40 PCs with n=200 neighbors. Cells are colored by cluster, which are  
1060 numbered in descending order by total cell count. Clusters were determined using Seurat's modularity-  
1061 based clustering on a shared nearest neighbor (SNN) graph with k=25 and resolution=0.25 on the top 40  
1062 PCs. **C)** Isolation of cluster 13 for annotation of cell types with smaller proportions of cells and projected  
1063 UMAP embeddings for cluster 13, colored by subcluster. **D)** Cell type module scores for 7 detected cell  
1064 types in subcluster 13, colored by relative gene expression of the listed genes.

1065

1066 **Supplemental Figure 2. Epithelial cell quality control and annotation. A)** Projected UMAP embeddings  
1067 for integrated, esophageal epithelial cells (EECs) calculated on the top 35 PCs with n=100 neighbors. Cells  
1068 are colored by cluster, which are numbered in descending order by total cell count. Clusters were  
1069 determined using Seurat's modularity-based clustering on a shared nearest neighbor (SNN) graph with  
1070 k=40 and resolution=0.50 on the top 40 PCs. **B)** EEC UMAP projection, colored by the number of unique  
1071 genes per cell. **C)** Distribution of number of UMIs detected per cell, split by cluster. EECs with <3500  
1072 UMIs/cell were removed from further analysis. **D)** EEC UMAPs colored by gene expression ( $\log(\text{counts}+1)$ )  
1073 for genes included in compartment-specific expression scores. **E)** EEC UMAPs colored by compartment  
1074 expression scores. **F)** Projected UMAP embeddings for post-quality-control EECs calculated on the top 35  
1075 PCs with n=100 neighbors. Cells are colored by cluster, which are numbered in descending order by total  
1076 cell count. Clusters were determined using Seurat's modularity-based clustering on a SNN graph with k=50  
1077 and resolution=0.25 on the top 35 PCs. **G)** Result of K-means clustering to distinguish suprabasal from  
1078 basal cells, based on expression of corresponding cluster markers (Supplemental Figure 4) in clusters 3,  
1079 4, and 5, with K=2. **H)** Result of K-means clustering to distinguish superficial from suprabasal cells, based  
1080 on expression of corresponding cluster markers (Supplemental Figure 4) in clusters 6, 7, and 8, with K=2.  
1081 **I)** Predicted classification of cell cycle state in EECs determined using Seurat's CellCycleScoring()  
1082 function.

1083

1084 **Supplemental Figure 3. Derivation of epithelial cell differentiation score.** **A)** Density plots of  
1085 esophageal epithelial cell compartment module scores by compartment annotation. **B)** Density plot of  
1086 epithelial cell differentiation score by annotated compartment. **C)** UMAP of esophageal epithelial cells  
1087 colored by differentiation score.

1088  
1089 **Supplemental Figure 4. Group-wise gene expression correlation for variable genes.** **A)** 2,000 most  
1090 variable genes among single cells across all samples, with top 20 labeled. **B)** Correlations of gene  
1091 expression aggregated by condition and biopsy location are shown for each epithelial compartment for the  
1092 2,000 most variable genes, with proximal samples along the Y axis and distal samples along the X axis.

1093  
1094 **Supplemental Figure 5. Differential gene expression aggregated by sample and esophageal**  
1095 **epithelial cell compartment.** **A)** Multidimensional scaling plots of aggregate gene expression samples  
1096 colored by sample, epithelial compartment, condition, and biopsy location. **B)** Volcano plots of differential  
1097 gene expression between SSc and GERD by epithelial compartment and biopsy location with significant  
1098 associations highlighted in red and outer significantly differentially expressed genes labeled. **C)** Gene  
1099 expression differences in  $\log_2FC$  are shown for SSc vs. HCs (Y axis) against GERD vs. HCs (X axis) for  
1100 each epithelial compartment in the proximal and distal regions. Outer significantly differentially expressed  
1101 genes are labeled, as well as immune-related genes uniquely differentially expressed in SSc. The  
1102 Spearman correlations between gene expression differences are shown in the upper right of each plot ( $r$ ),  
1103 the relative FC or slope ( $m$ ) and coefficient of determination ( $r^2$ ) are shown in the bottom right of each plot.  
1104 Trendlines with 95% confidence intervals are plotted in pink, and the dashed grey lines denote where  $y=x$ .  
1105 **D)** Distributions of aggregate gene expression by epithelial layer, biopsy location, and condition are shown  
1106 for top SSc-specific and GERD-specific differentially expressed genes.

1107  
1108 **Supplemental Figure 6. Expression of superficial esophageal epithelial cell markers.** UMAPs with  
1109 expression for the top superficial cluster markers are shown along with the epithelial differentiation score  
1110 for superficial cells.

1111

1112 **Supplemental Figure 7. *FLI1* expression in human esophageal mucosa. A)** UMAP of integrated  
1113 mucosal dataset, colored by *FLI1* expression. The distribution of *FLI1* expression by cell type is shown in  
1114 the upper right. **B)** Distribution of *FLI1* expression by cell type and disease state. Endothelial cells had the  
1115 highest *FLI1* expression, but the expression differences between diseases was not significant. **C)** Violin  
1116 plot of the relative expression of *FLI1* target genes in superficial cells.

1117  
1118 **Supplemental Figure 8. Epithelial cell compartment proportions and additional correlations by**  
1119 **motility phenotype. A-B)** Proportions of esophageal epithelial cell compartments by HRM (**A**) and FLIP  
1120 (**B**) esophageal dysmotility phenotypes are shown for the proximal and distal esophagus samples. The  
1121 bars denote the mean values, the vertical lines the standard deviations, and the points the individual  
1122 sample proportions. **C)** The relationship between the proportion of superficial cells and the SSc disease  
1123 duration is plotted for proximal and distal samples. Trendlines with 95% confidence intervals are plotted in  
1124 pink, and correlation P-values are displayed in the upper right corners. **D)** The distribution of normalized  
1125 gene expression values by esophageal motility phenotype are shown for the *TRIM11* gene for the FLIP,  
1126 HRM, and NM esophageal dysmotility classifications. Unadjusted ordinal regression p-values are  
1127 displayed in the upper left corners. *TRIM11* was the most strongly association gene with the dysmotility  
1128 phenotypes by p-value. HRM, high-resolution manometry; FLIP, functional luminal imaging probe  
1129 panometry; IEM, ineffective esophageal motility; EGJOO, esophagogastric junction outflow obstruction;  
1130 NM, neuromyogenic model.

1131 **TABLES**

**Table 1. Patient demographics and clinical characteristics**

	<b>HCs</b>		<b>SSc</b>		<b>GERD</b>	
<b>Demographics</b>	<b>N = 6</b>		<b>N = 10</b>		<b>N = 4</b>	
Sex – female	5 (83.3%)		9 (90%)		3 (75%)	
Race – white	5 (83.3%)		8 (80%)		2 (50%)	
Ethnicity – non-Hispanic	5 (83.3%)		8 (80%)		2 (50%)	
Race/ethnicity – unknown/NR	1 (16.7%)		2 (20%)		2 (50%)	
<b>Traits</b>	<b>N</b>	<b>Median (IQR)</b>	<b>N</b>	<b>Median (IQR)</b>	<b>N</b>	<b>Median (IQR)</b>
Age (yrs)	6	27 (25-29)	10	54 (47-70)	4	42 (30-56)
BMI (kg/m <sup>2</sup> )	6	23 (22-25)	10	22 (19-30)	4	24 (23-36)
<b>Esophageal motility</b>						
Mean DCI (mmHg•s•cm)	6	464.2 (386-6-1026.1)	10	57.5 (0.0-206.1)	2	509.6 (367.4-651.7)
Pressure 60ml (mmHg)	6	43.5 (38.3-54.5)	9	31.0 (30.5-40.3)	0	-
<b>EGJ barrier function</b>						
End-expiratory EGJ pressure (mmHg)	6	7 (4-8)	10	6 (3-10)	2	12 (11-12)
EGJ contractile index (mmHg•cm)	6	19.4 (15.2-29.0)	10	21.0 (19.1-27.5)	2	19.0 (10.8-27.1)
Median IRP (mmHg)	6	4 (3-9)	10	6 (4-12)	2	8 (6-9)
EGJ-DI (mm <sup>2</sup> /mmHg)	6	6.2 ( 5.2-8.5)	9	6.3 (4.1-9.2)	-	-
<b>Reflux severity</b>						
AET (%)	6	0.8 (0.5-2.8)	4	8.7 (3.3-14.5)	3	16.8 (13.9-17.3)
GerdQ <sup>117</sup> score	6	0 (0-0)	10	3 (1-4)	3	3 (3-4)
BEDQ <sup>39</sup> score	6	0 (0-0)	8	8 (3-14)	3	1 (1-1)
NEQOL <sup>40</sup> score	6	56 (56-56)	8	31 (23-47)	3	36 (29-46)

1132 AET, acid exposure time; BEDQ, brief esophageal dysphagia questionnaire; BMI, body mass index; DCI, distal contractile integral;

1133 DI, distensibility index; EGJ, esophagogastric junction; HCs, healthy controls; IQR, inter-quartile range; IRP, integrated relaxation

1134 pressure; NEQOL, Northwestern esophageal quality of life; NR, not reported



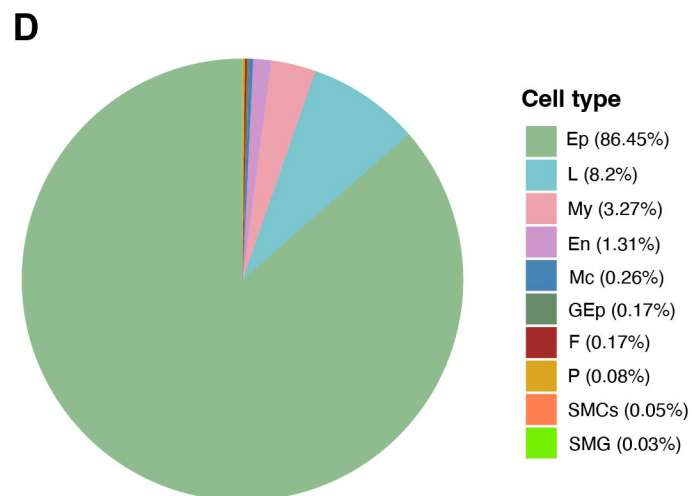
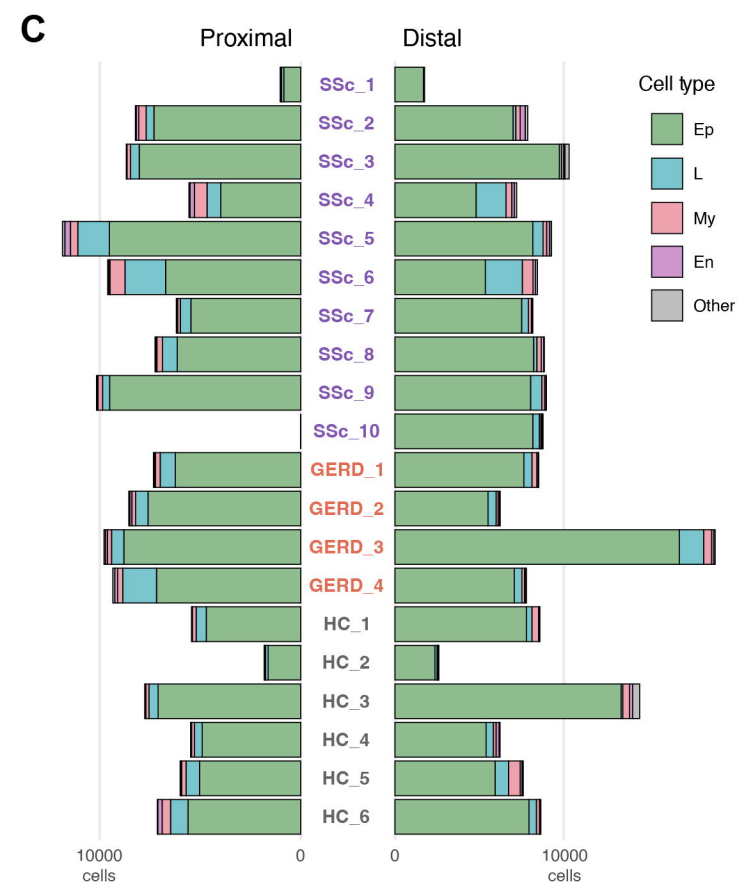
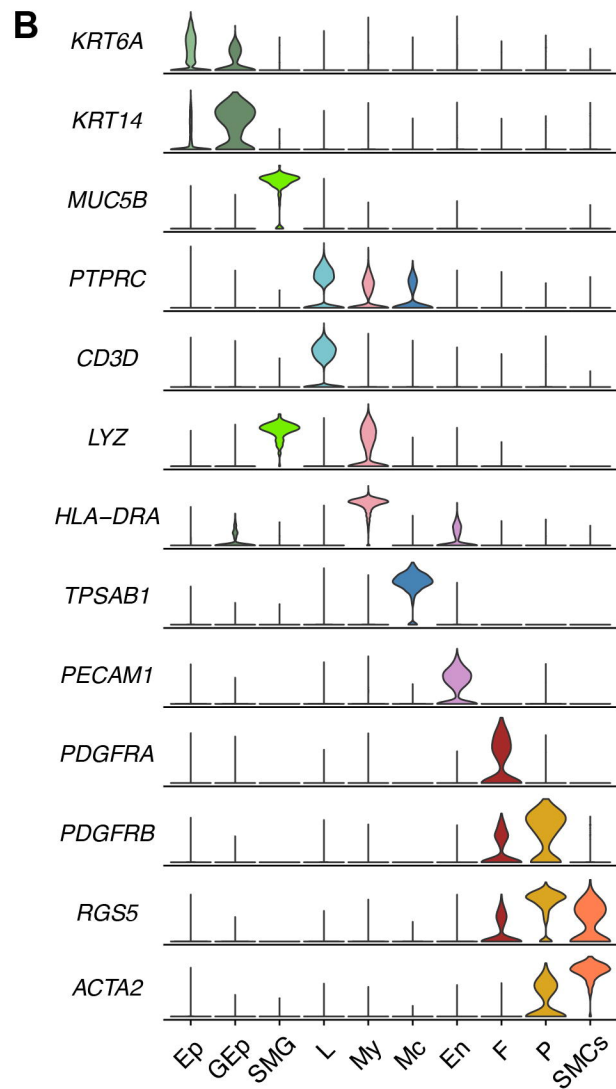
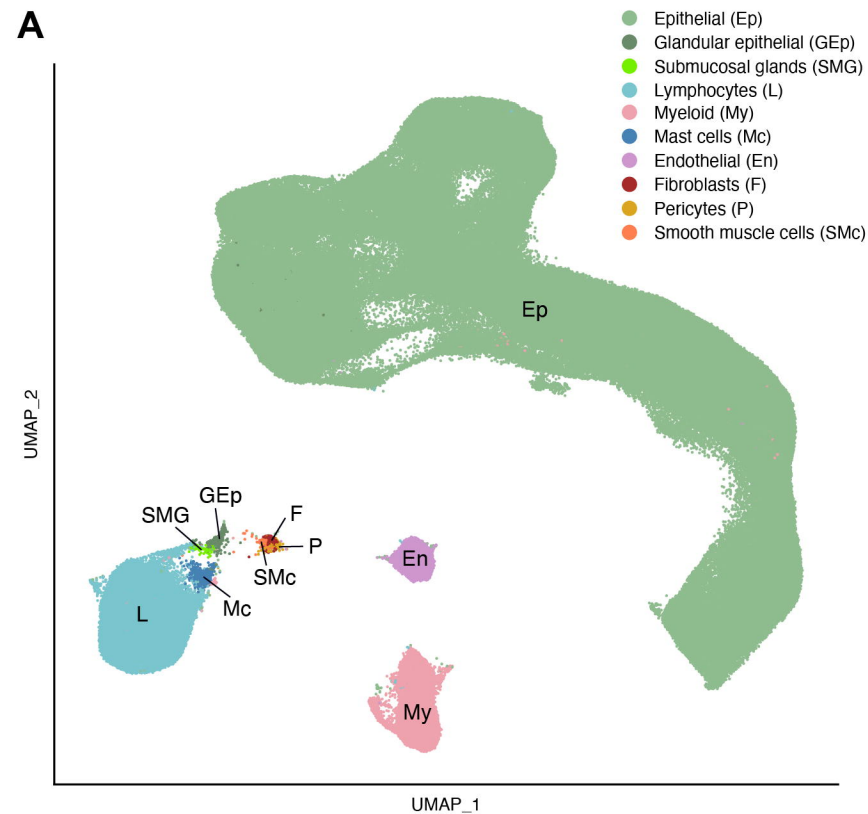
1135

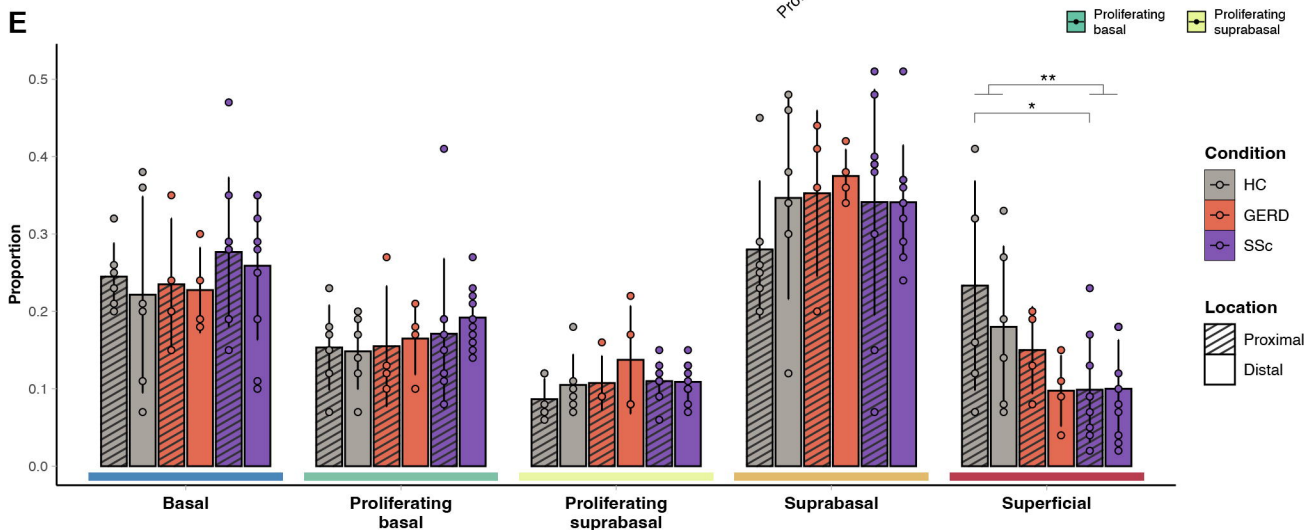
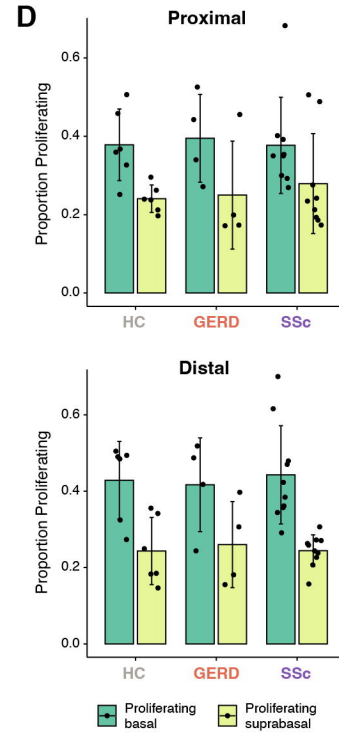
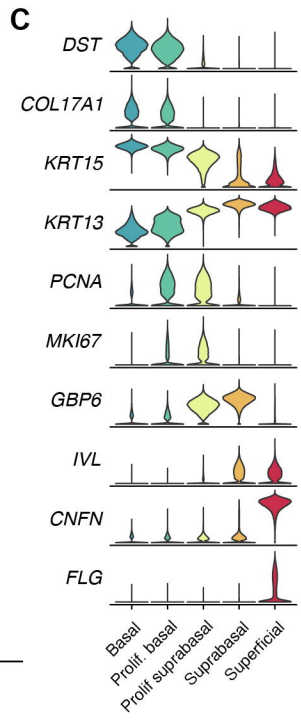
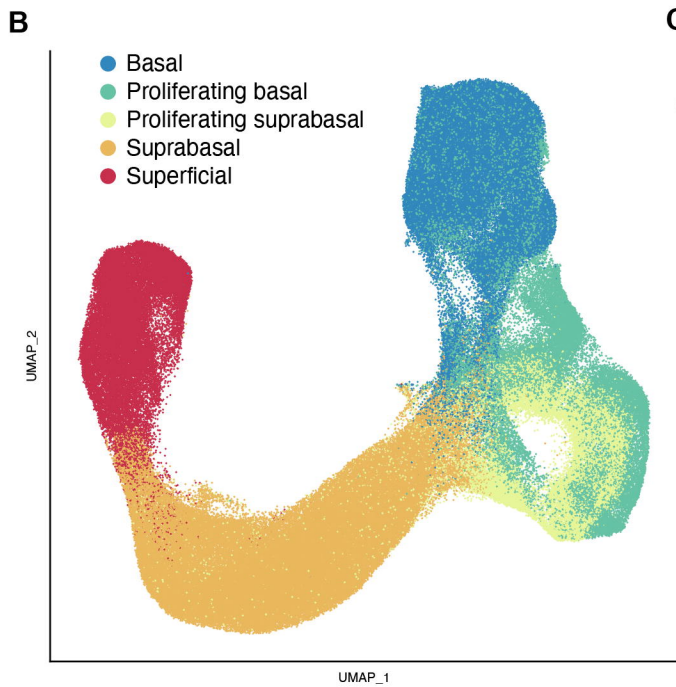
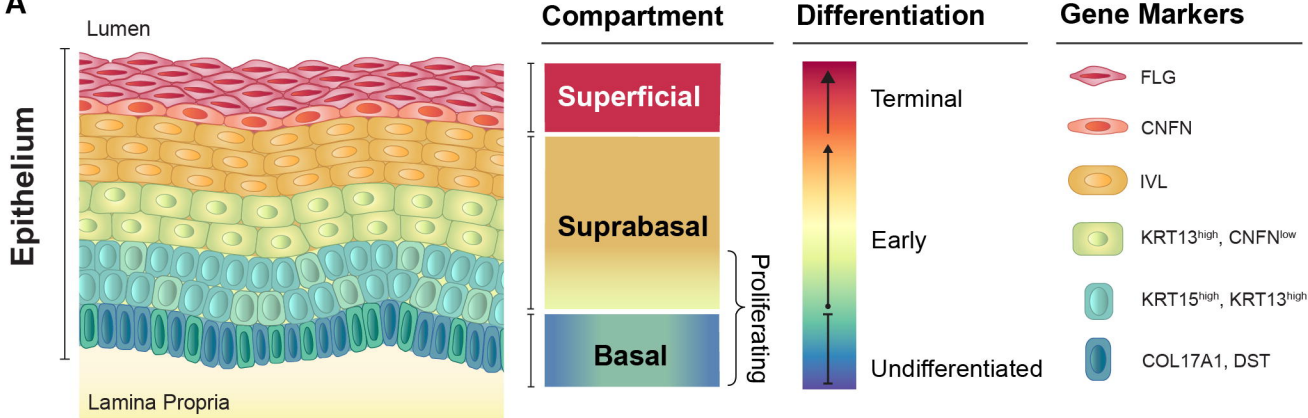
**Table 2. Pairwise transcription factor enrichment in superficial cells in proximal esophagus**

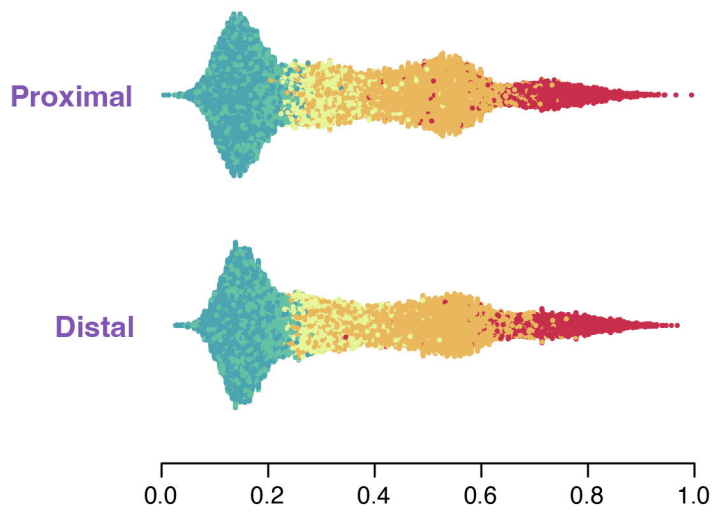
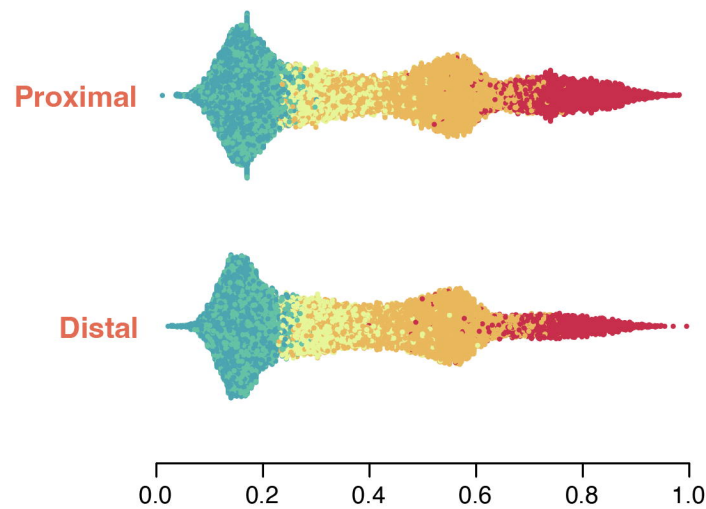
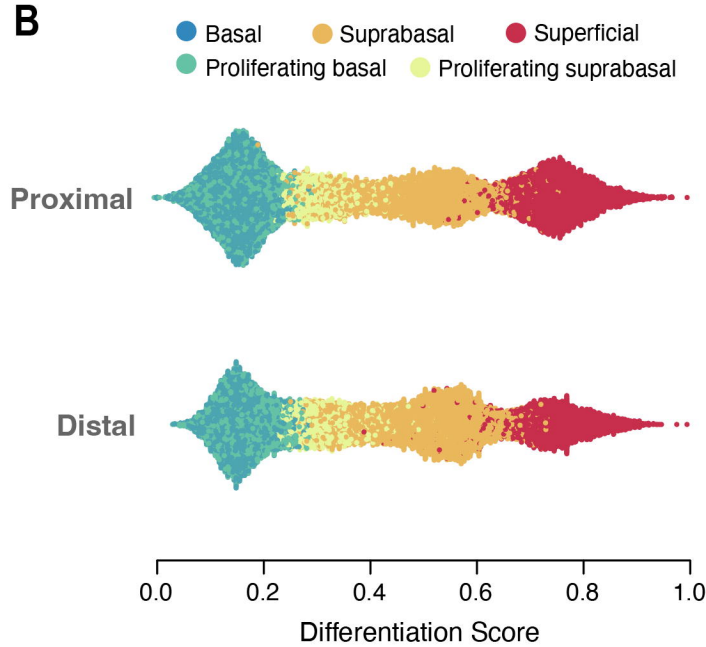
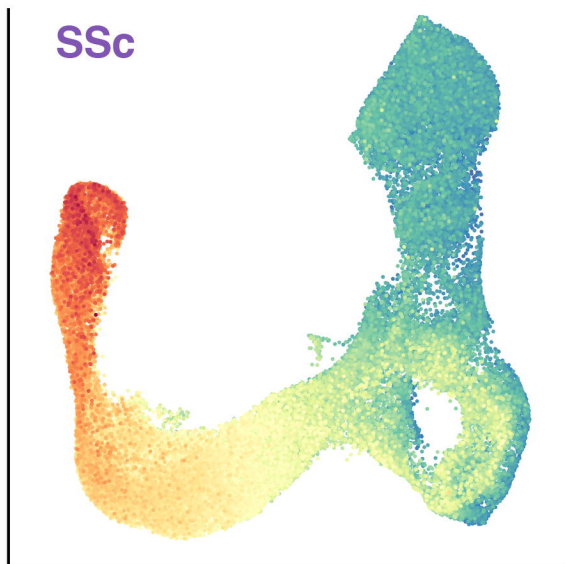
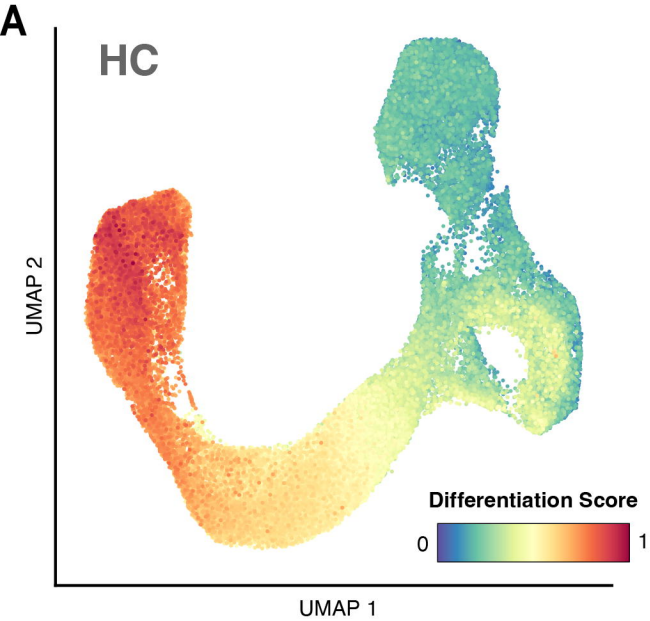
Comparison	TF	Direction	DEG Targets	DEG Targets / DEGs	TF Targets / Background	P <sub>adj</sub>	TF Expr. LogFC	TF Expr. P <sub>adj</sub>
<b>SSc vs. GERD</b>	IRF1	+/-	7	0.11	0.03	2.9×10 <sup>-2</sup>	0.22	9.0×10 <sup>-1</sup>
		-	5	0.19	0.03	8.9×10 <sup>-3</sup>		
<b>SSc vs. HCs</b>	MYC	+	120	0.10	0.06	2.1×10 <sup>-7</sup>	1.64	7.8×10 <sup>-5</sup>
	E2F4	+	116	0.08	0.06	5.5×10 <sup>-5</sup>	0.88	9.8×10 <sup>-4</sup>
	NFE2L2	-	108	0.11	0.07	7.6×10 <sup>-4</sup>	0.25	3.2×10 <sup>-1</sup>

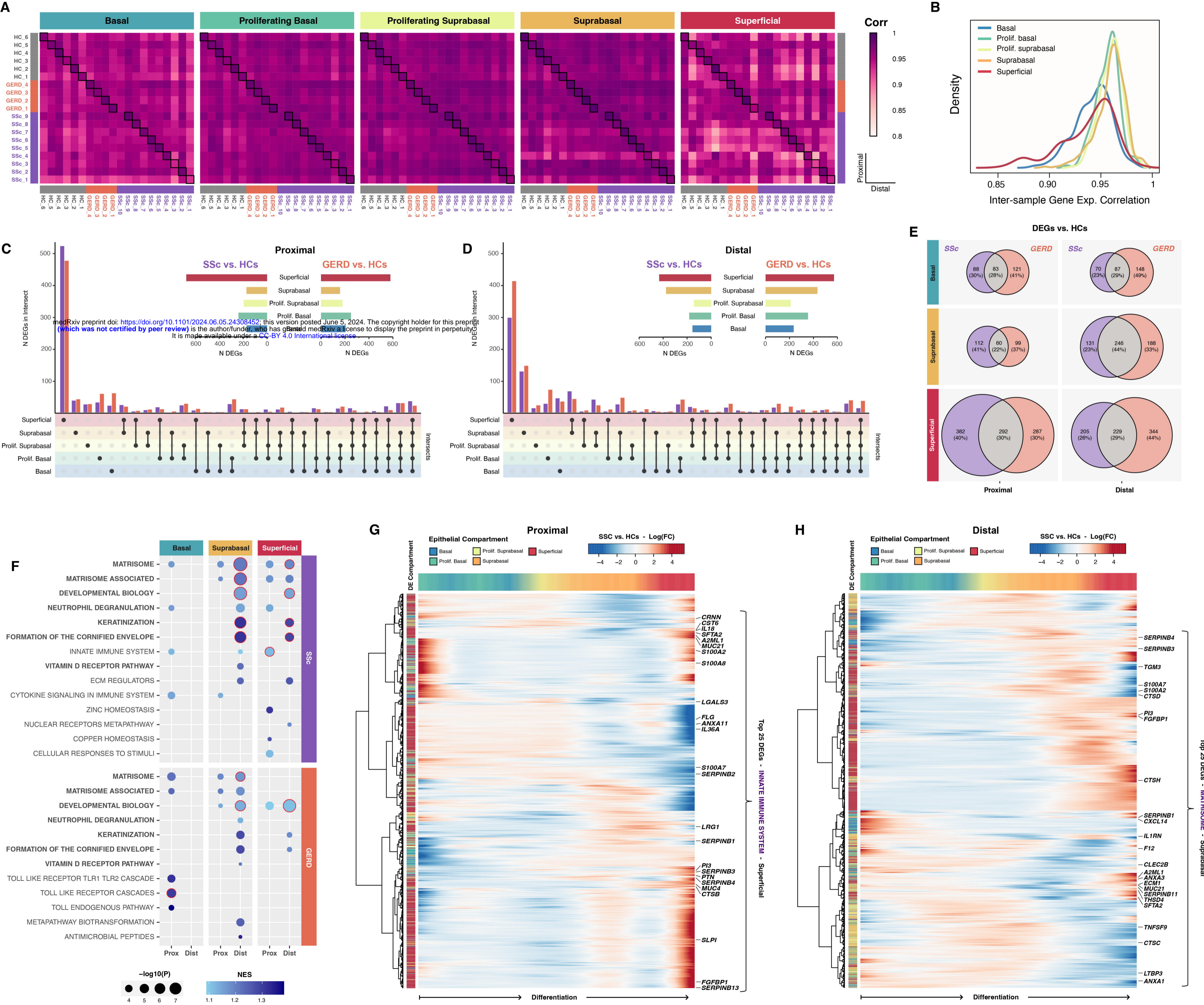
DEG, differentially expressed gene; Expr., expression; GERD, gastroesophageal reflux disease ; HCs, healthy controls; LogFC, log<sub>2</sub>(fold change); SSc, systemic sclerosis; TF, transcription factor.

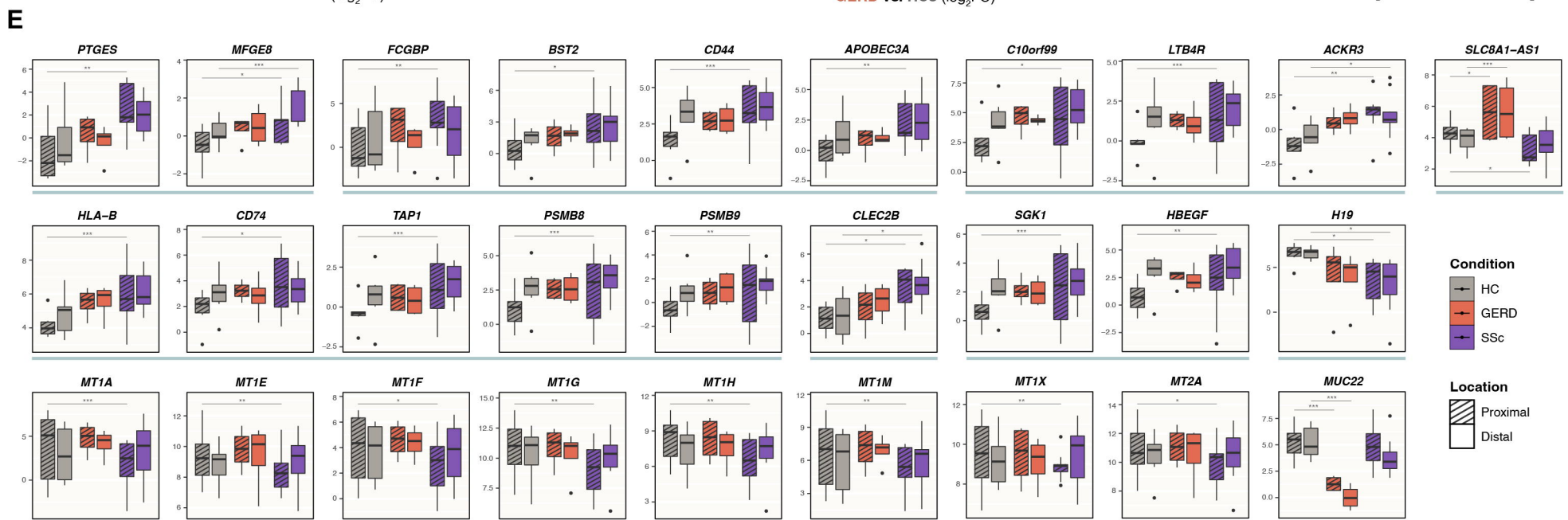
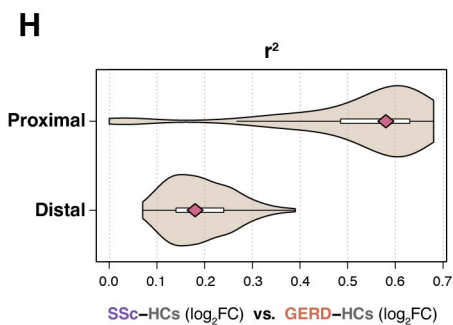
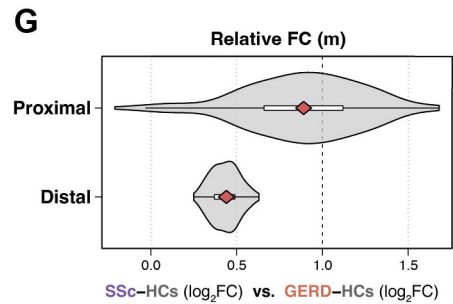
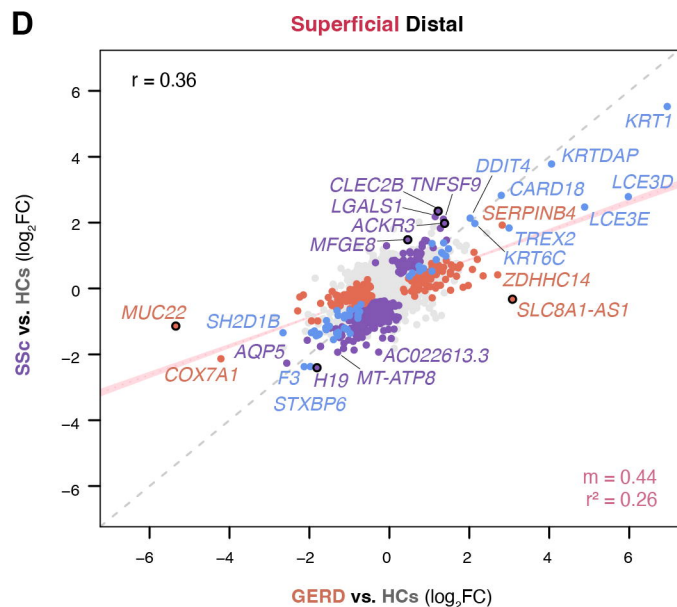
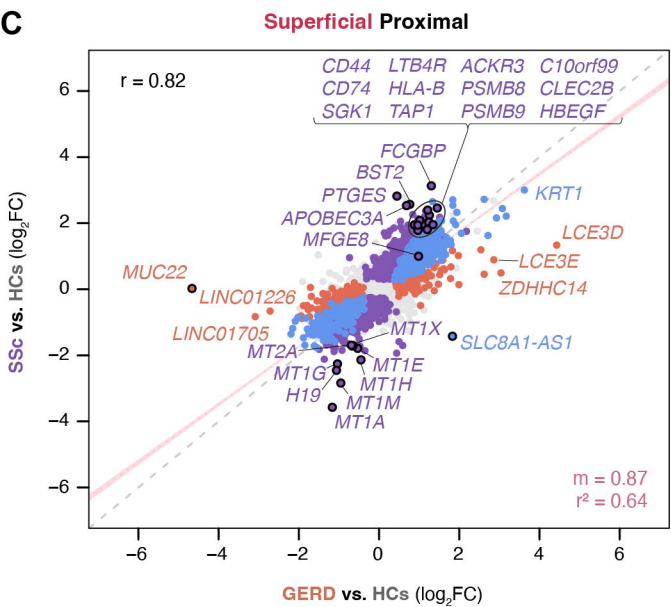
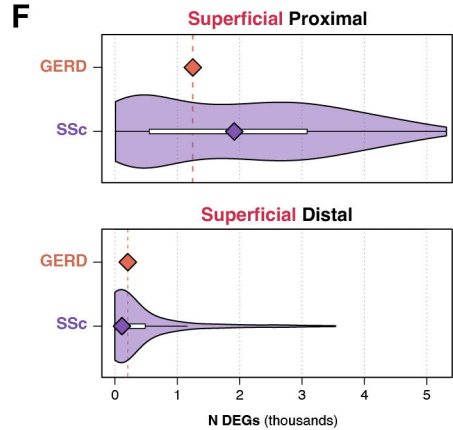
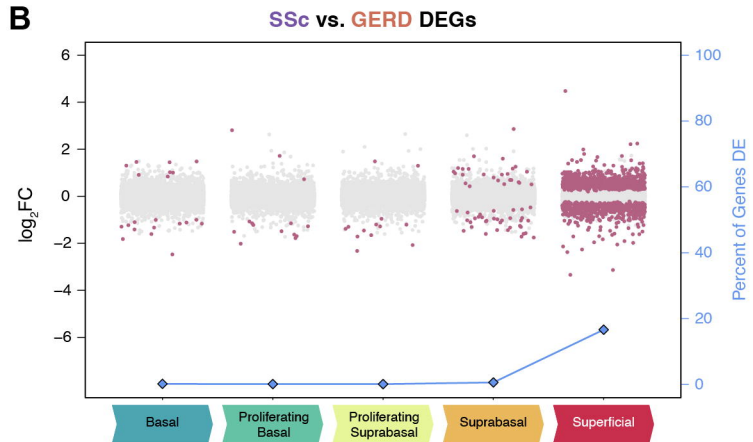
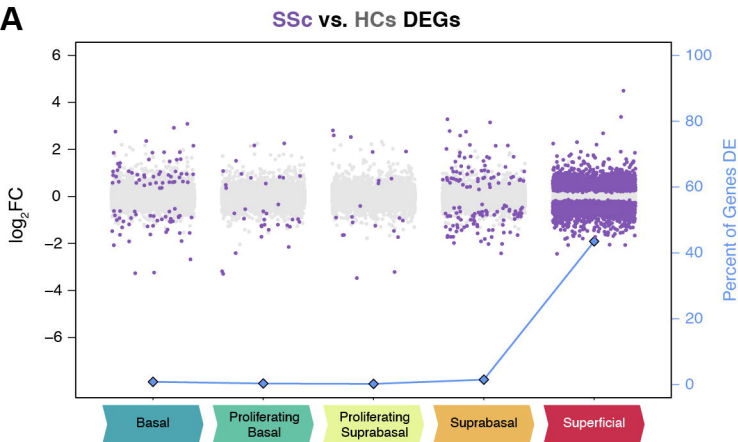
1136

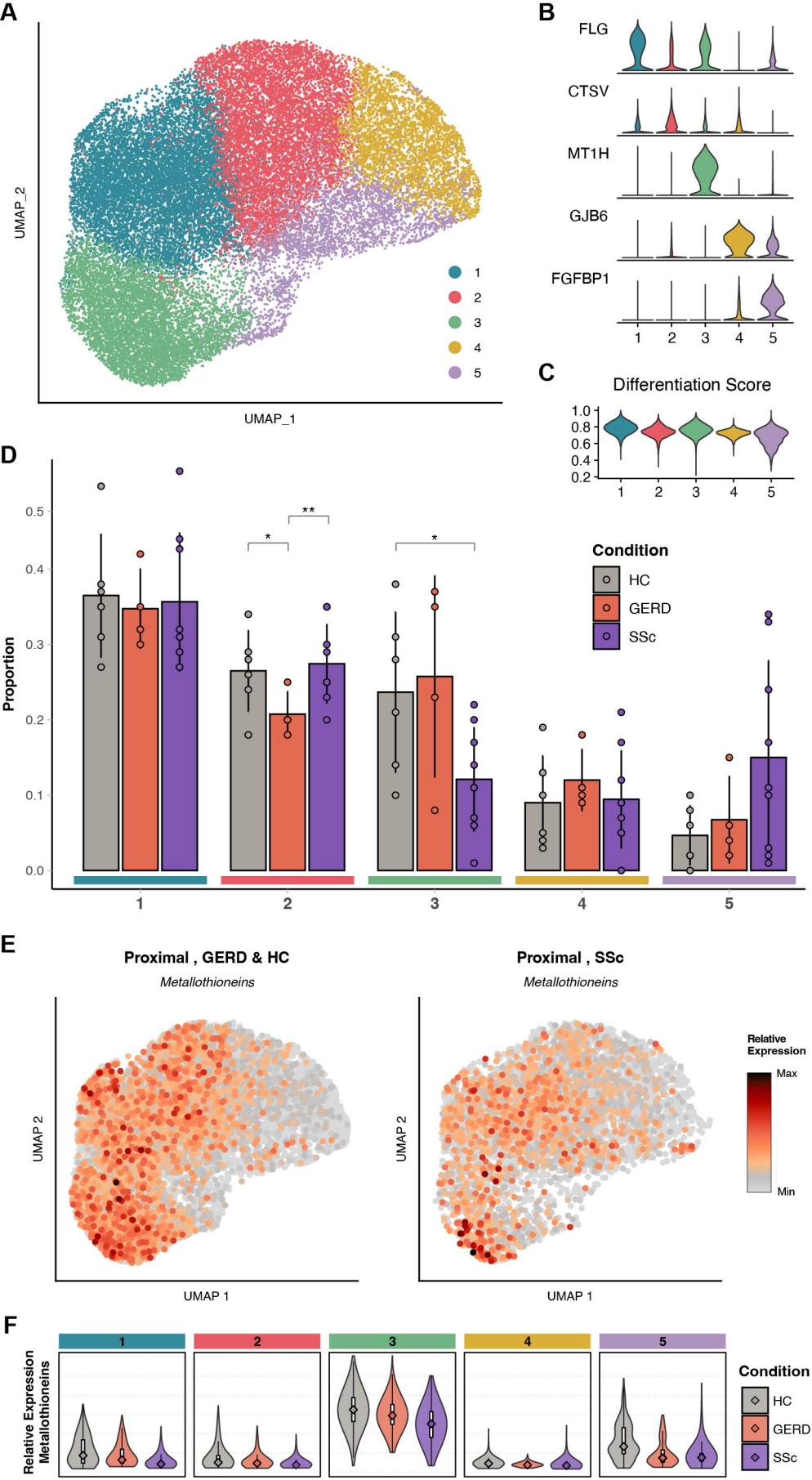


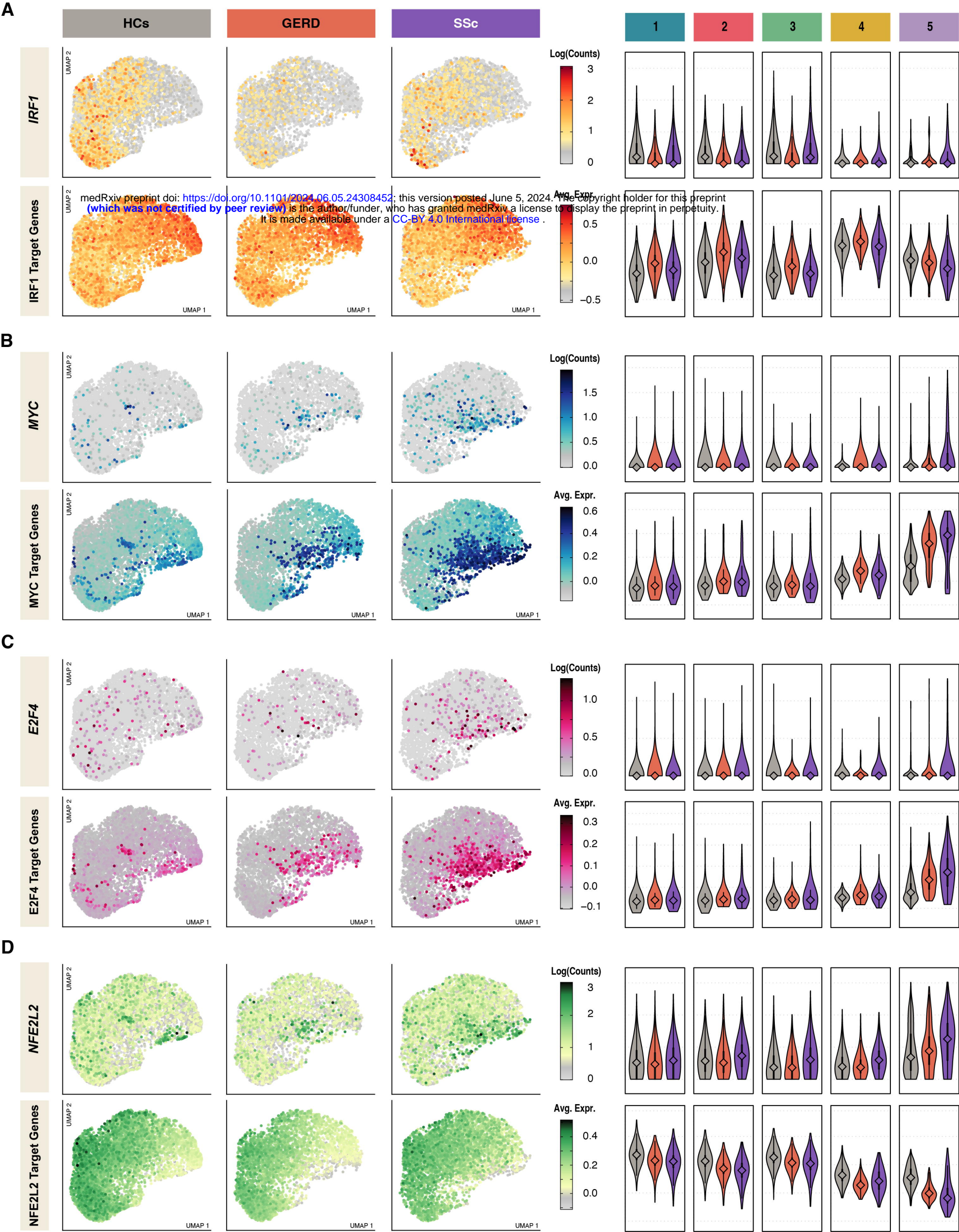




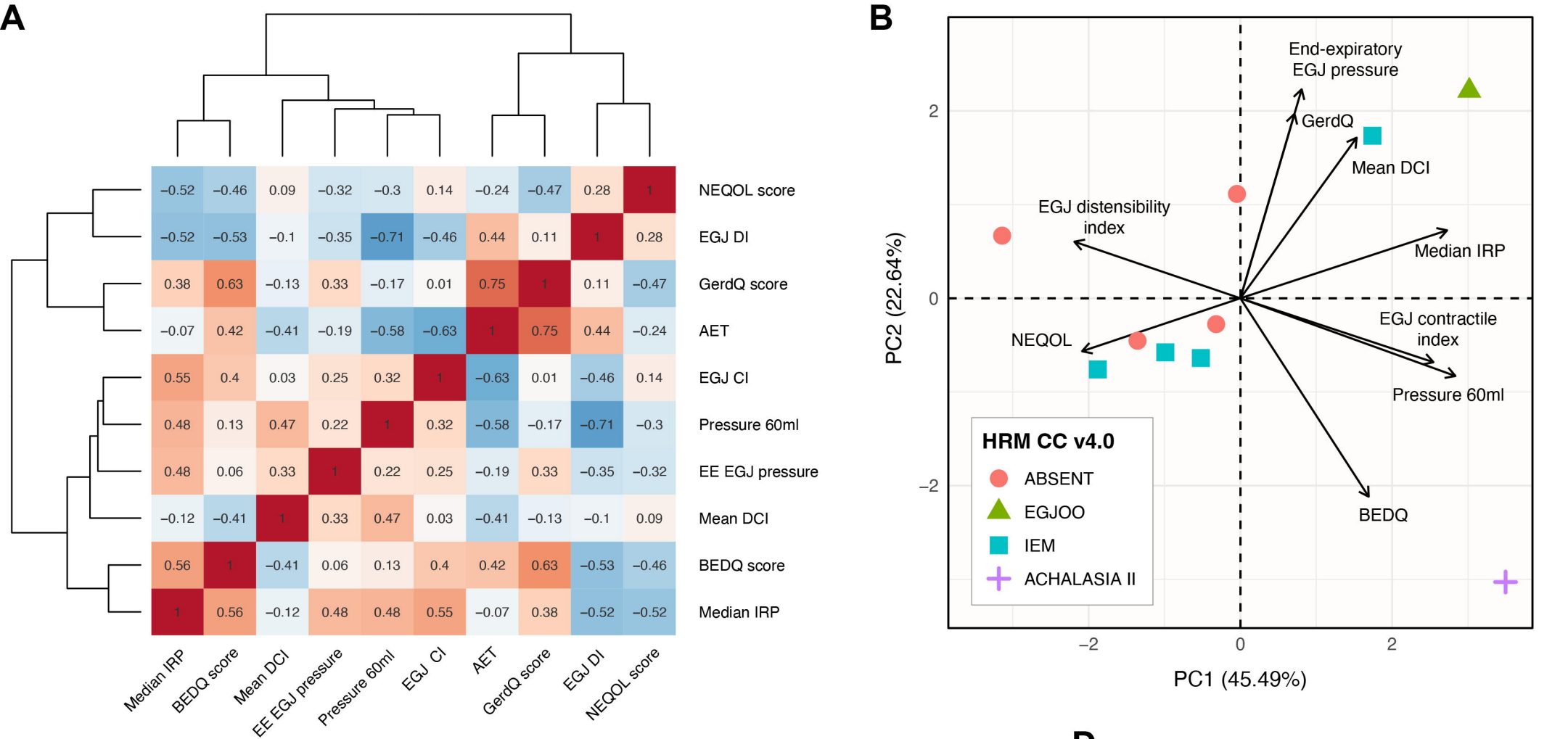




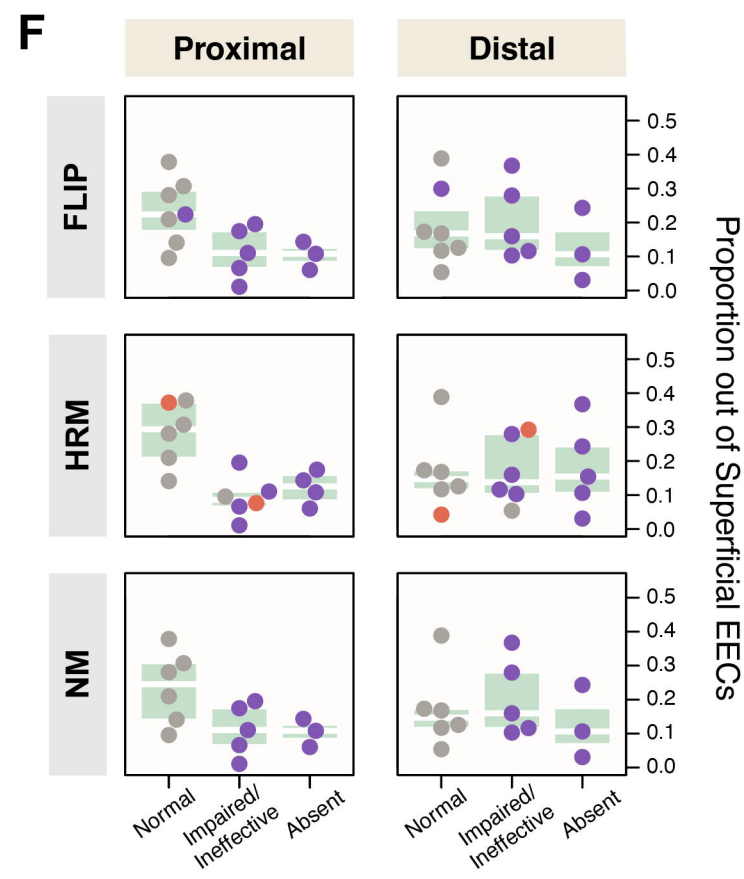
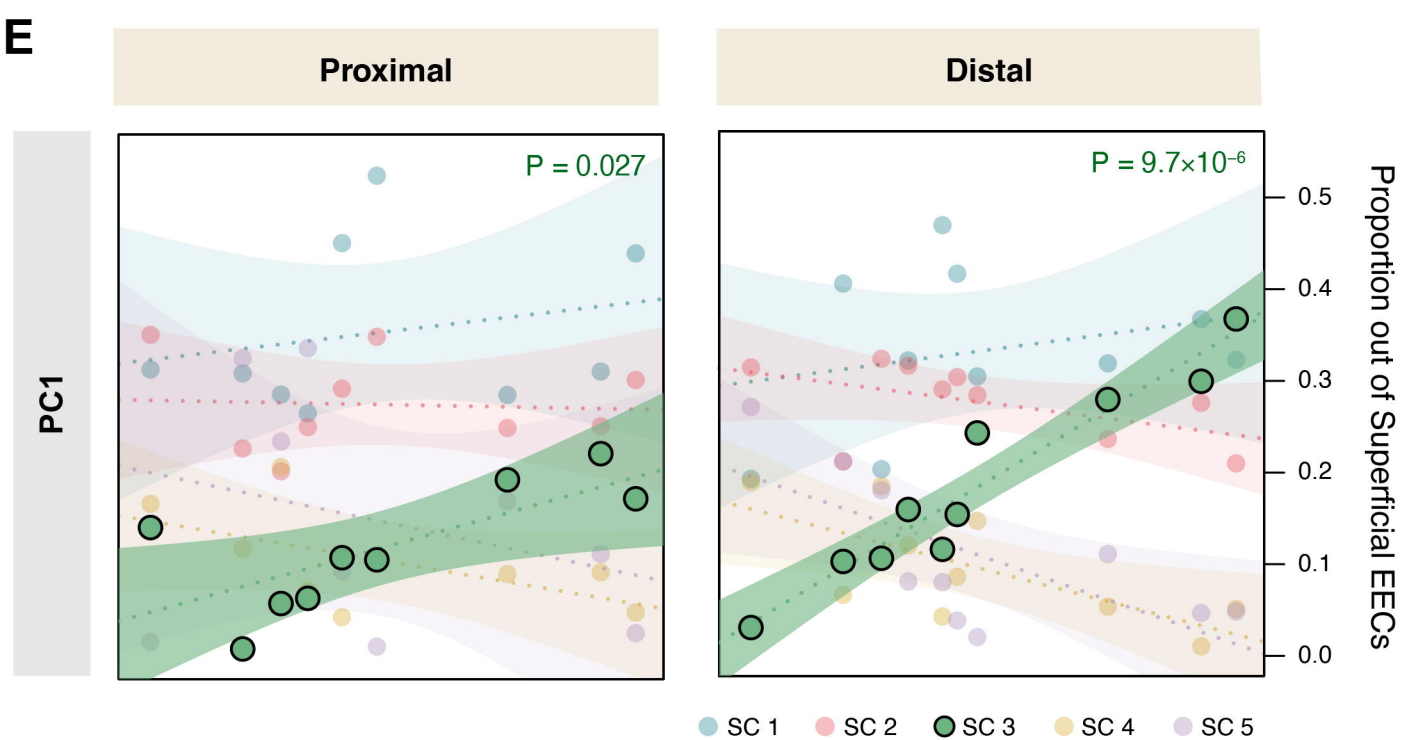
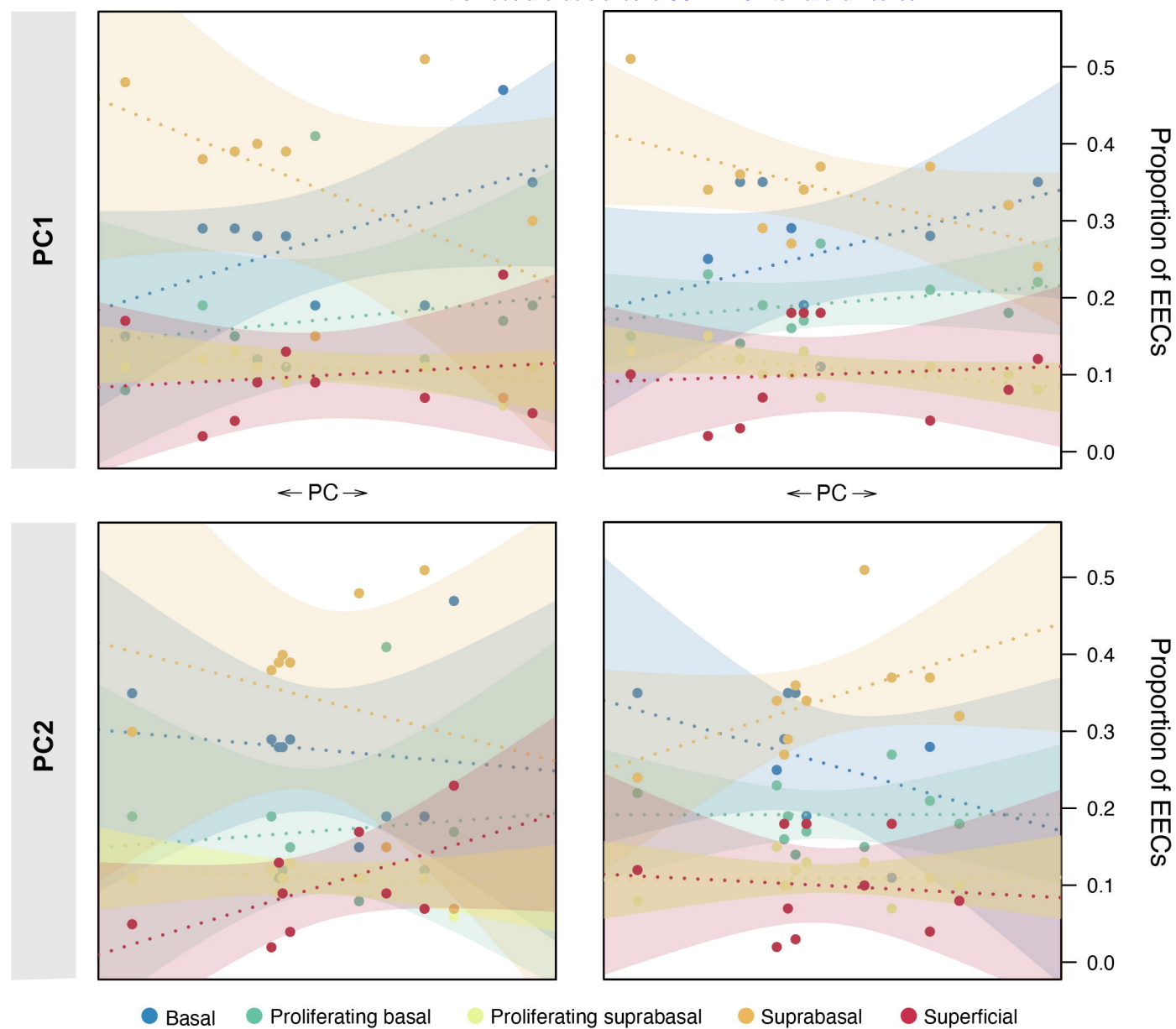


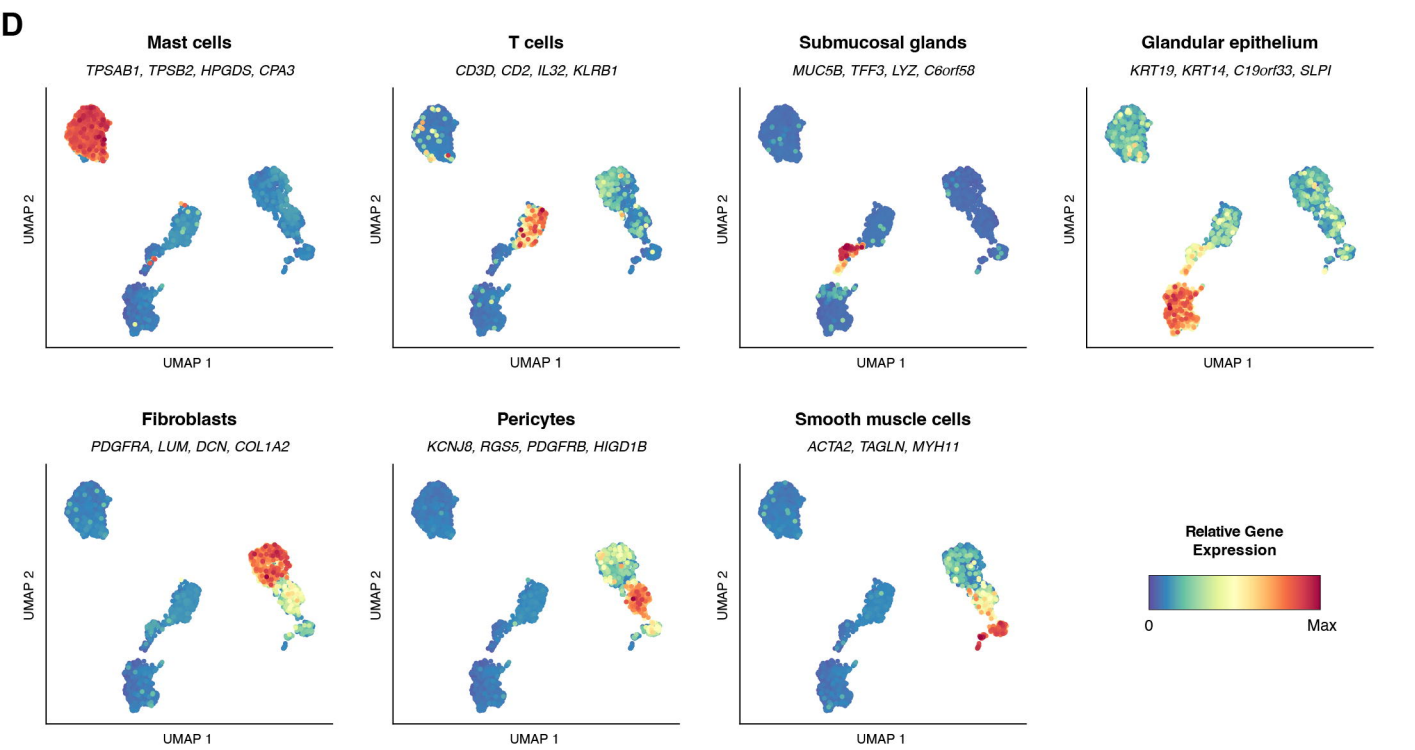
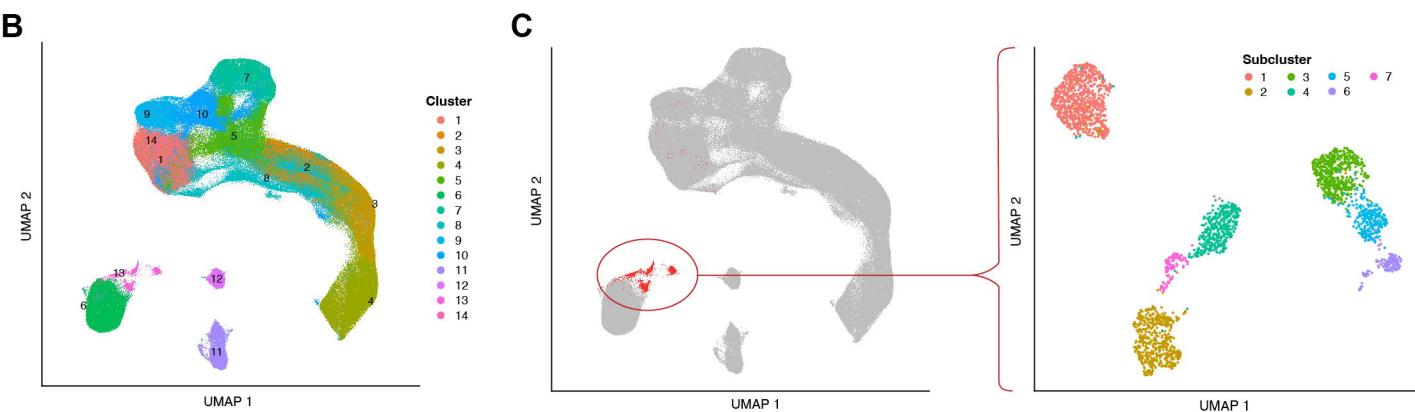
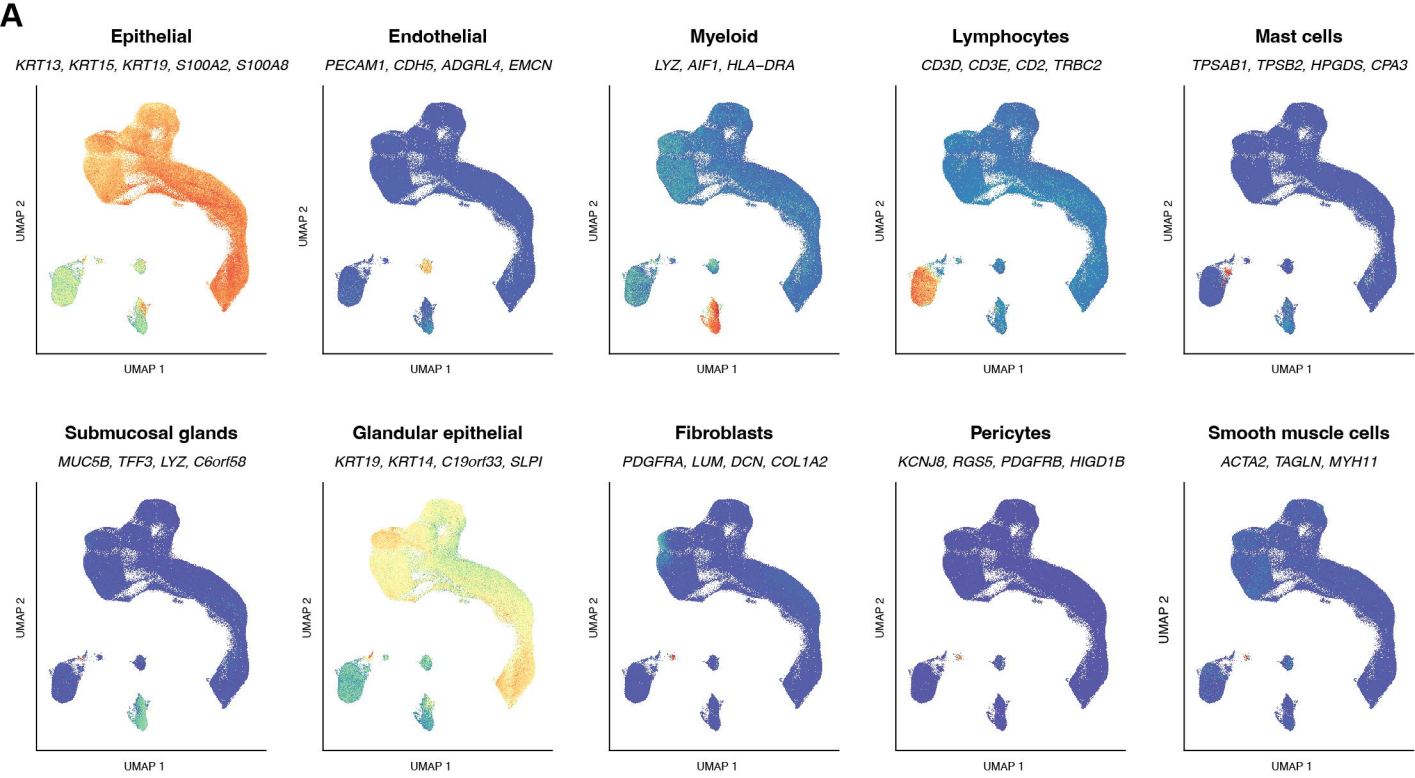


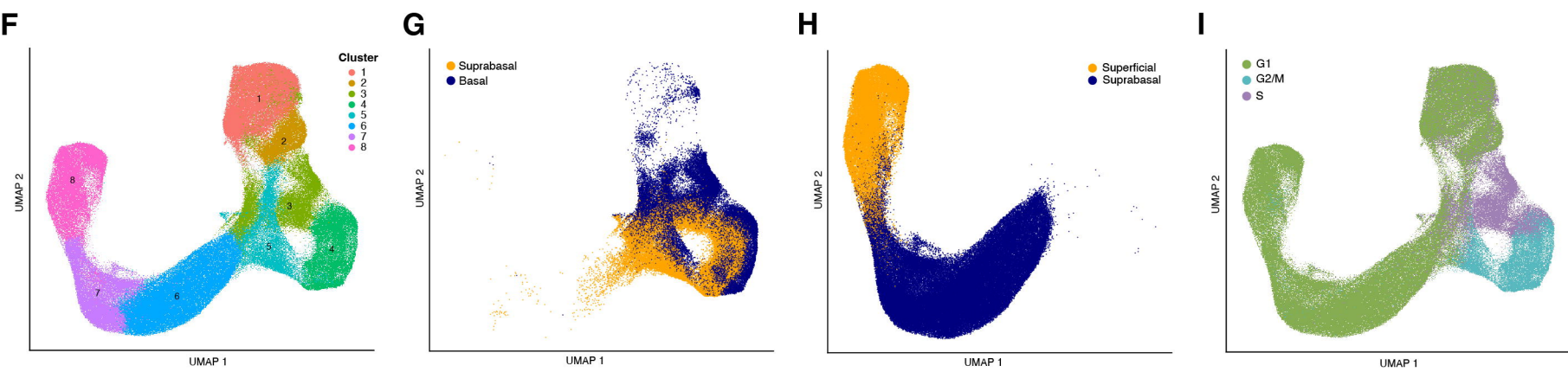
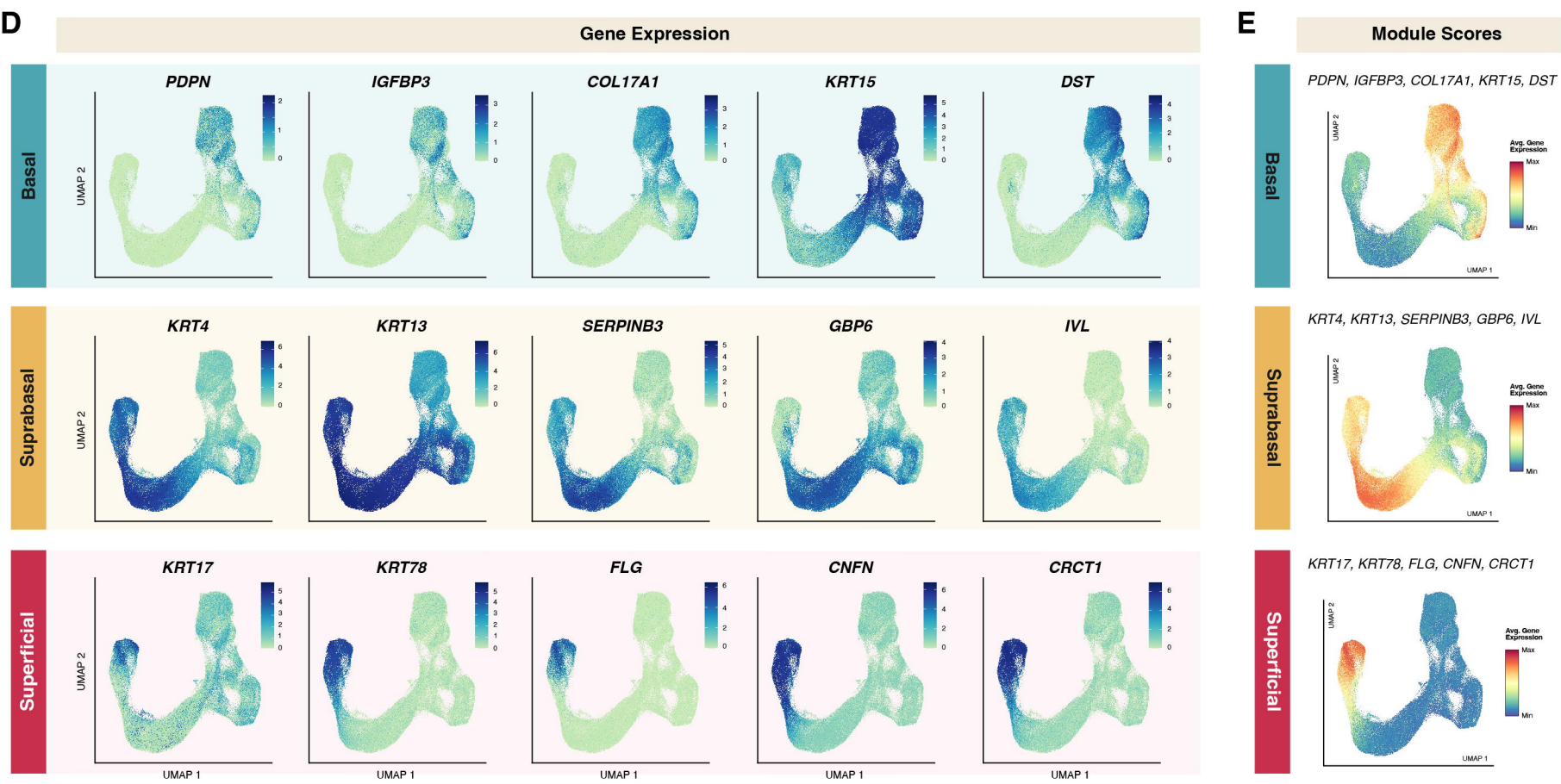
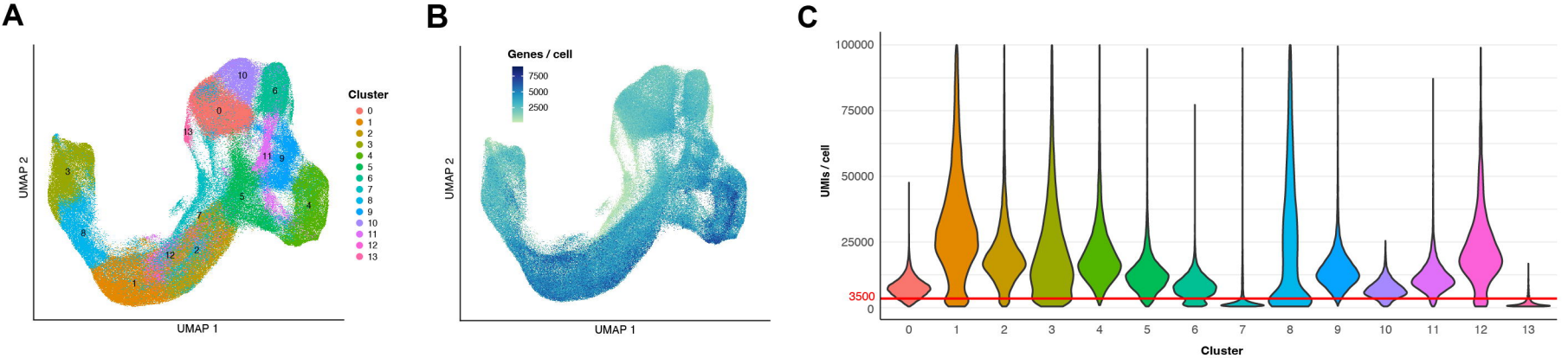


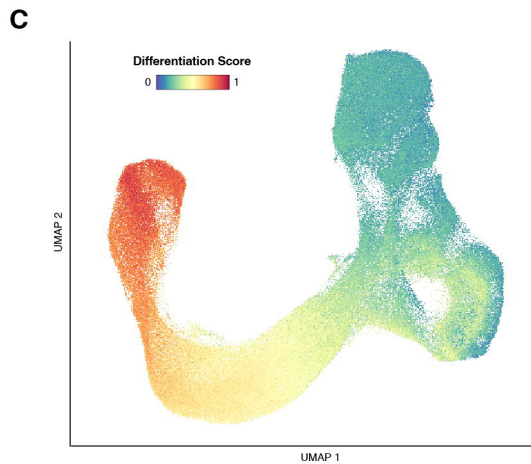
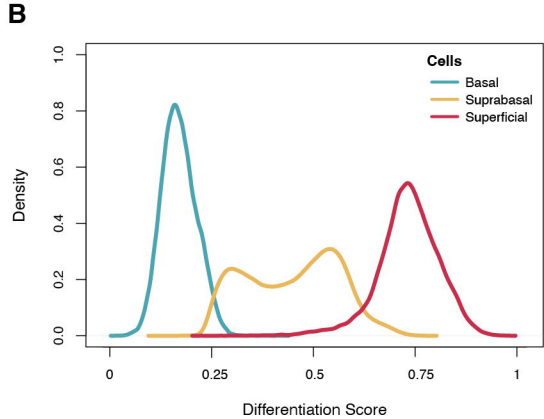
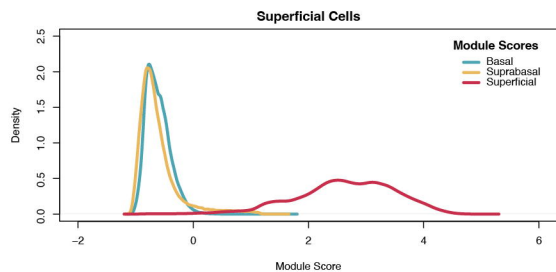
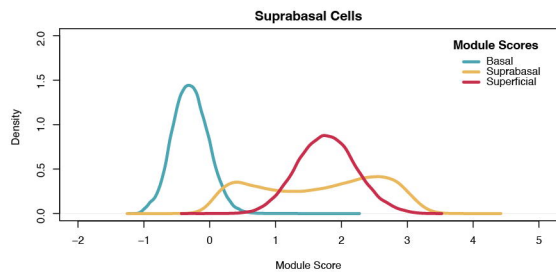
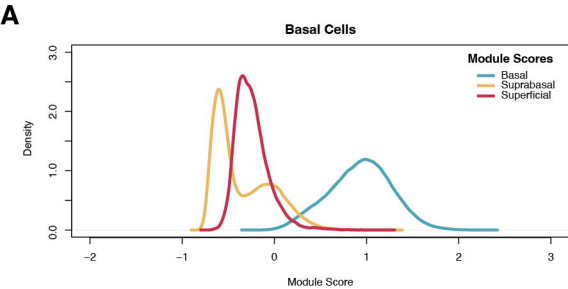


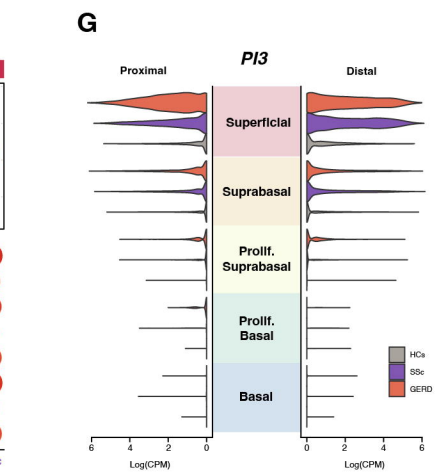
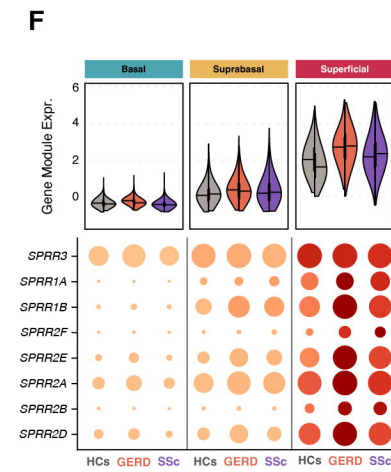
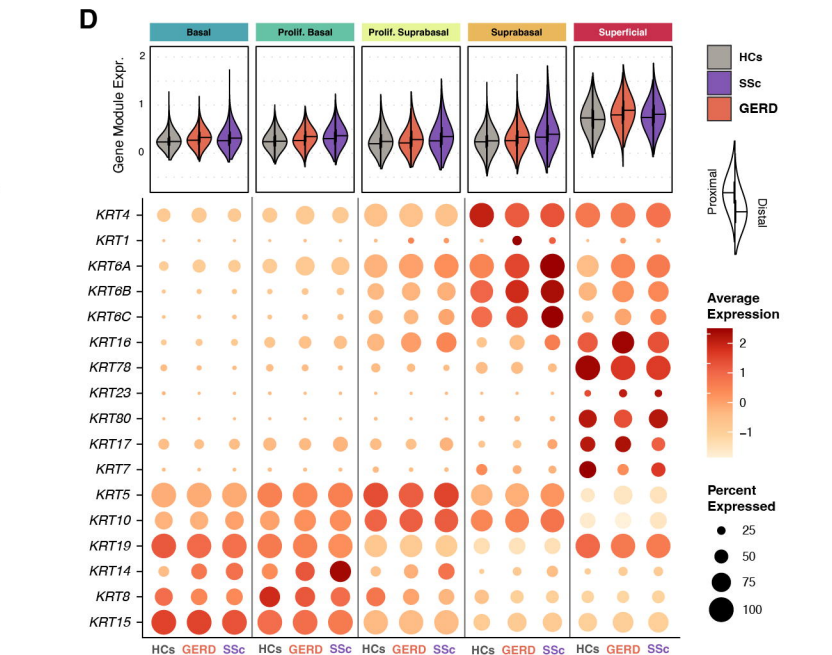
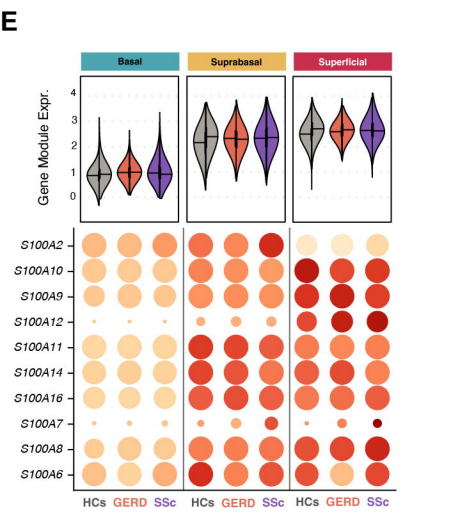
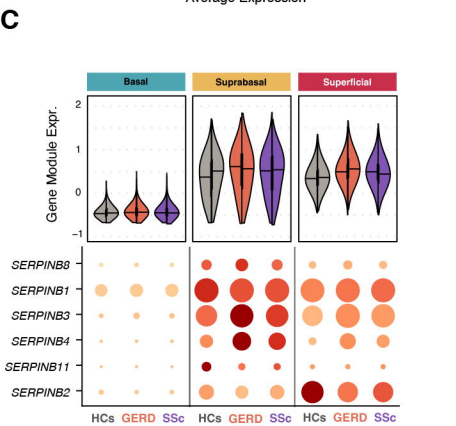
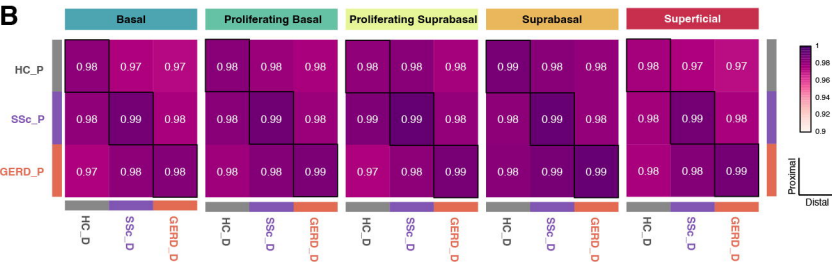
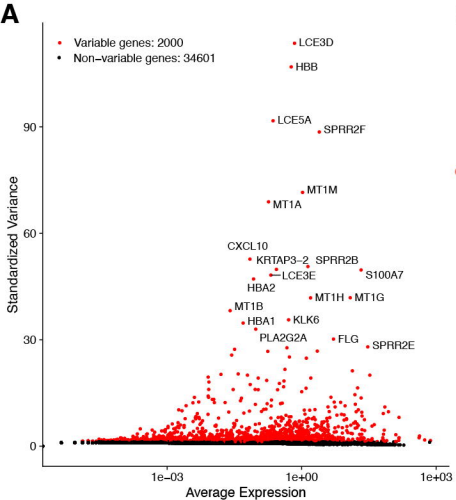
medRxiv preprint doi: <https://doi.org/10.1101/2024.06.05.24308452>; this version posted June 5, 2024. The copyright holder for this preprint (which was not certified by peer review) is the author/funder, who has granted medRxiv a license to display the preprint in perpetuity. It is made available under a [CC-BY 4.0 International license](https://creativecommons.org/licenses/by/4.0/).

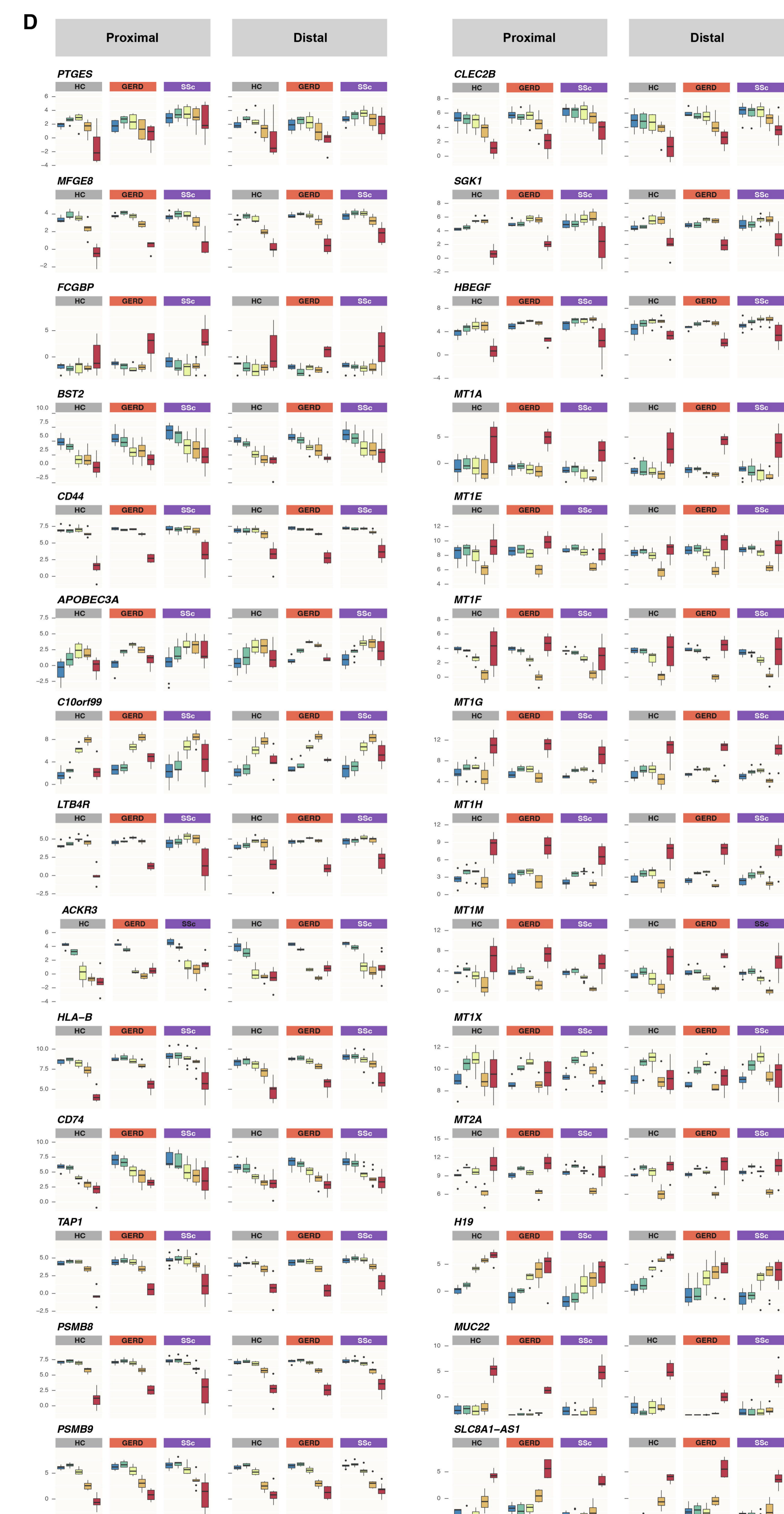
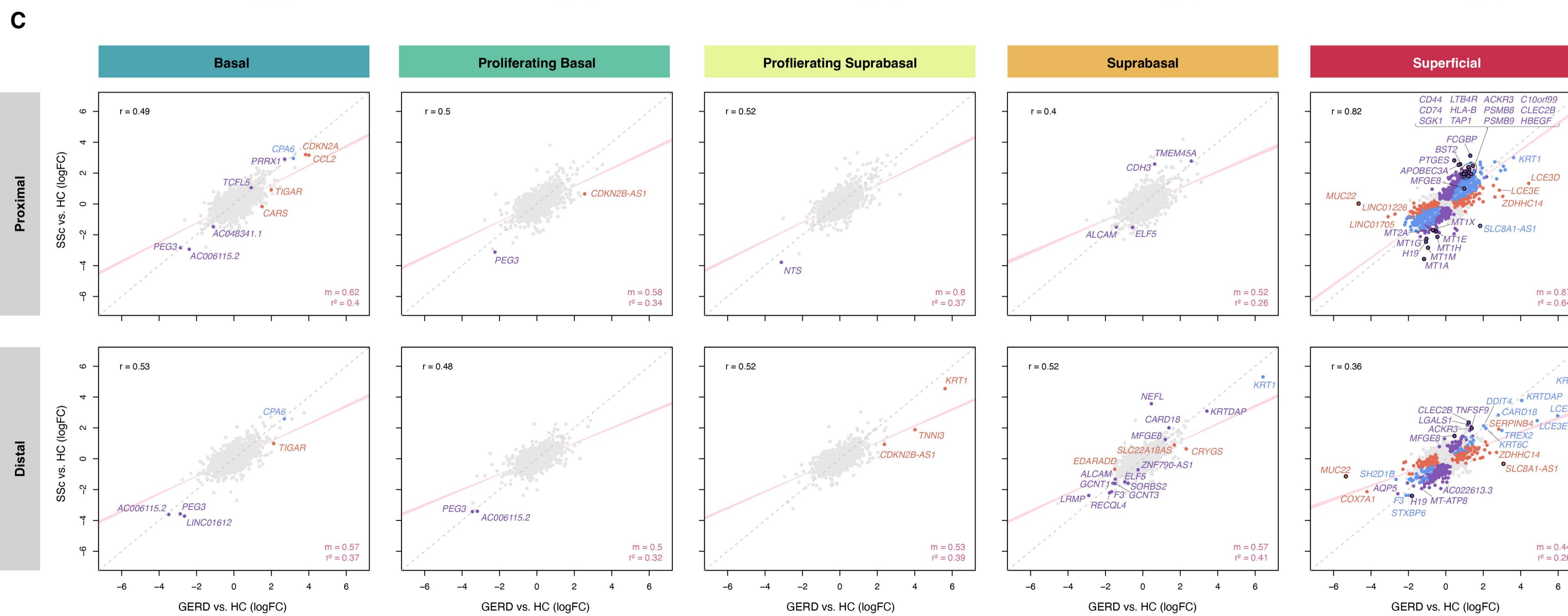
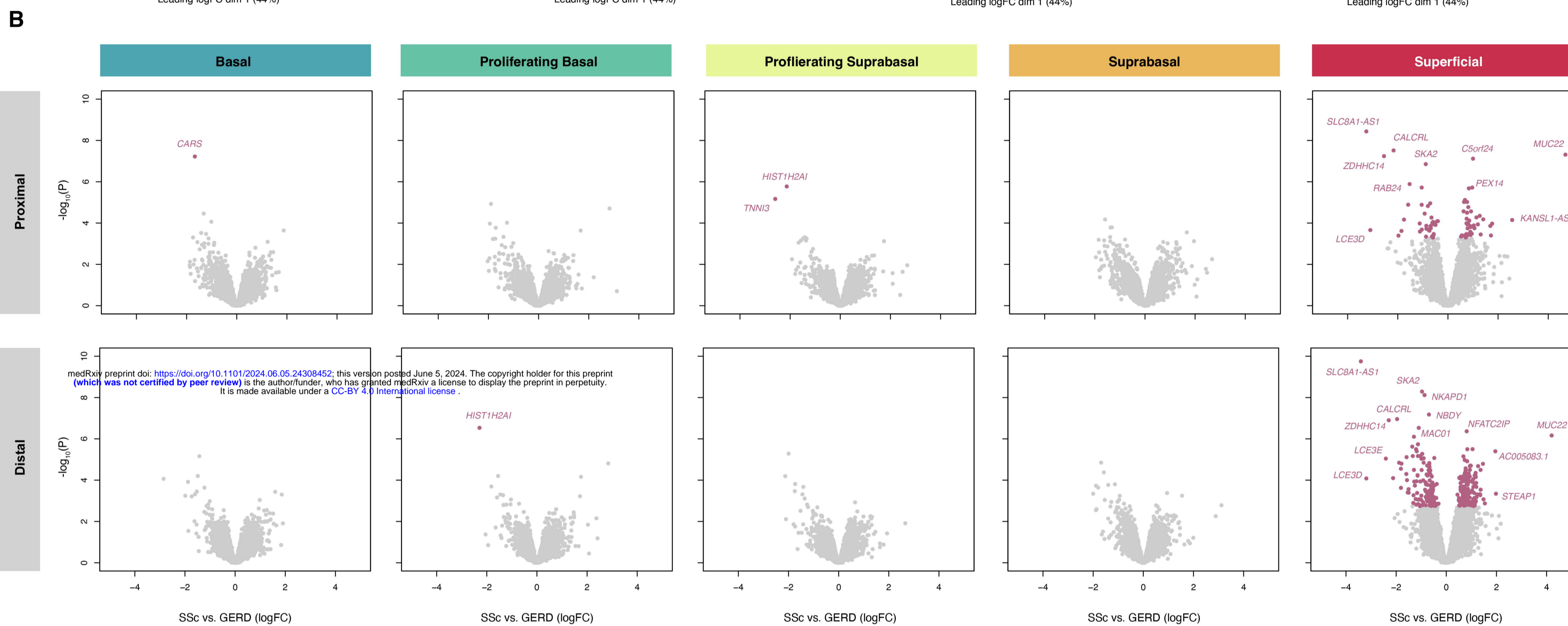
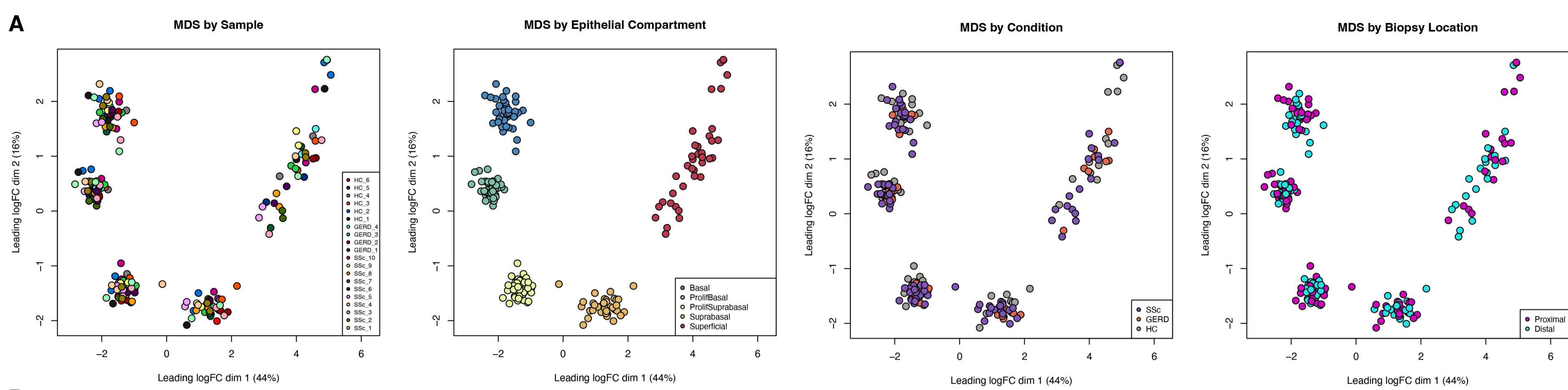






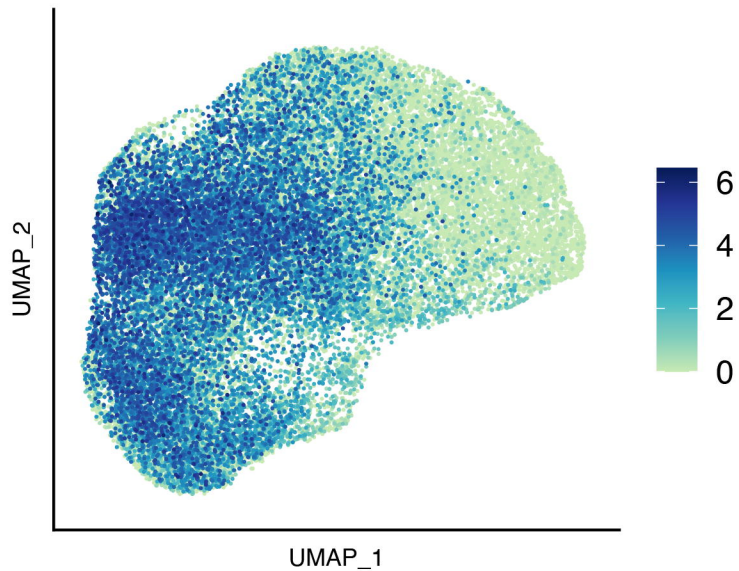




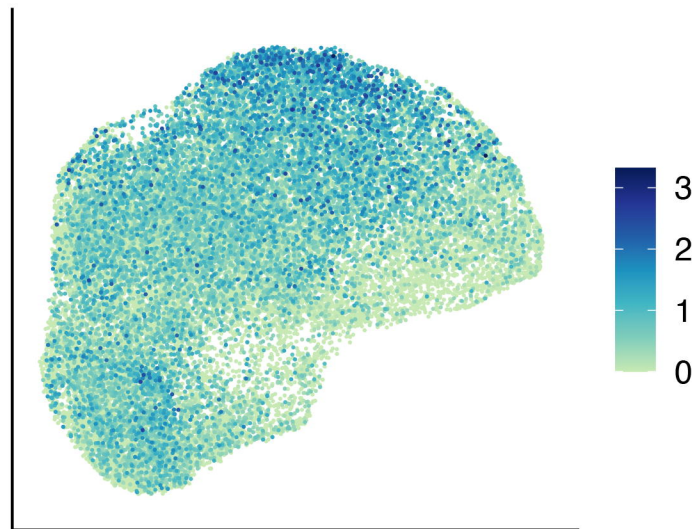


medRxiv preprint doi: <https://doi.org/10.1101/2024.06.05.24308452>; this version posted June 5, 2024. The copyright holder for this preprint (which was not certified by peer review) is the author/funder, who has granted medRxiv a license to display the preprint in perpetuity. It is made available under a CC-BY 4.0 International license.

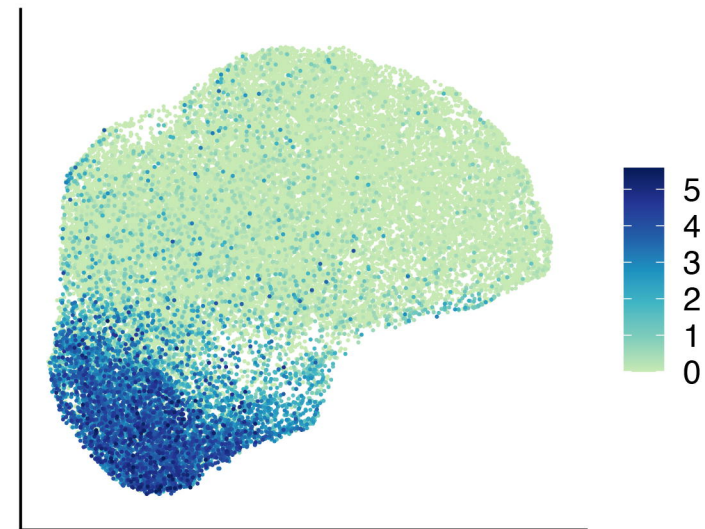
***FLG***



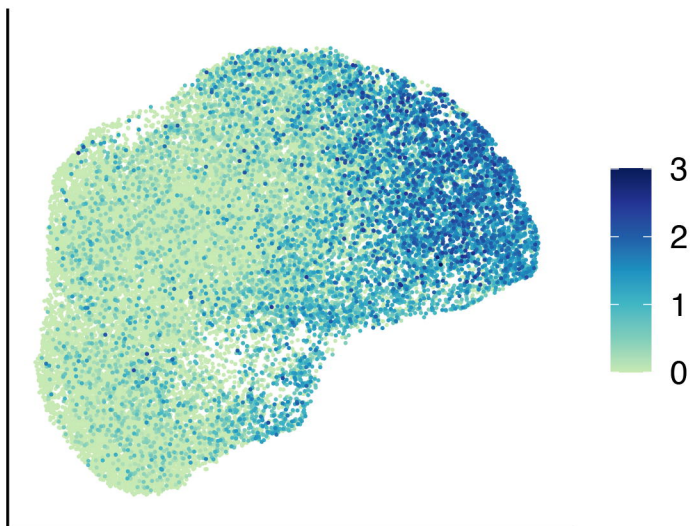
***CTSV***



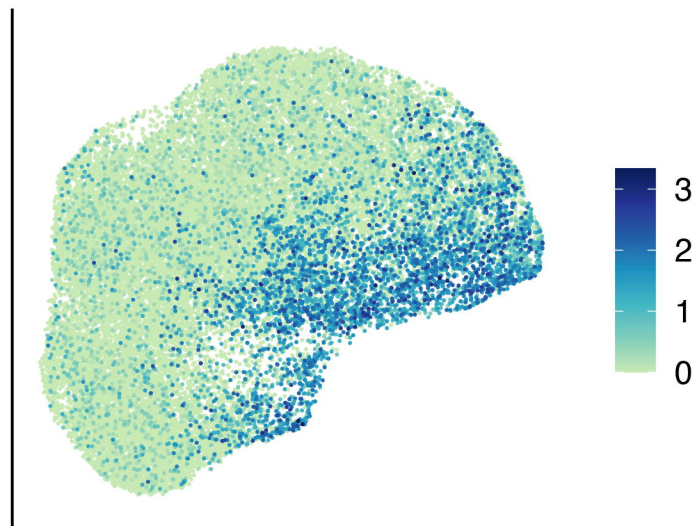
***MT1H***



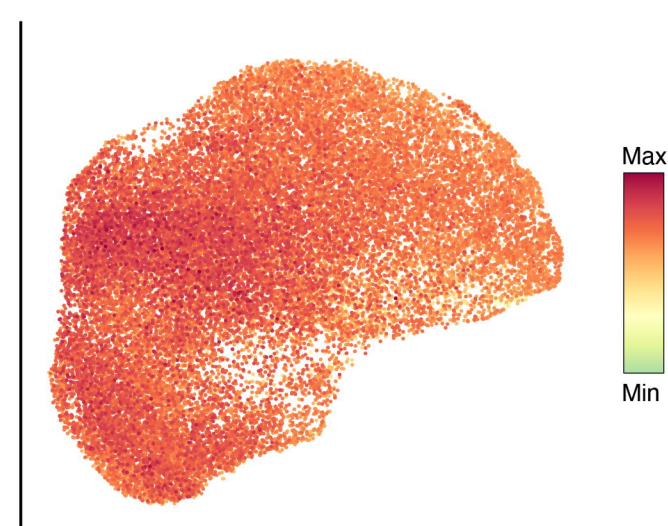
***GJB6***

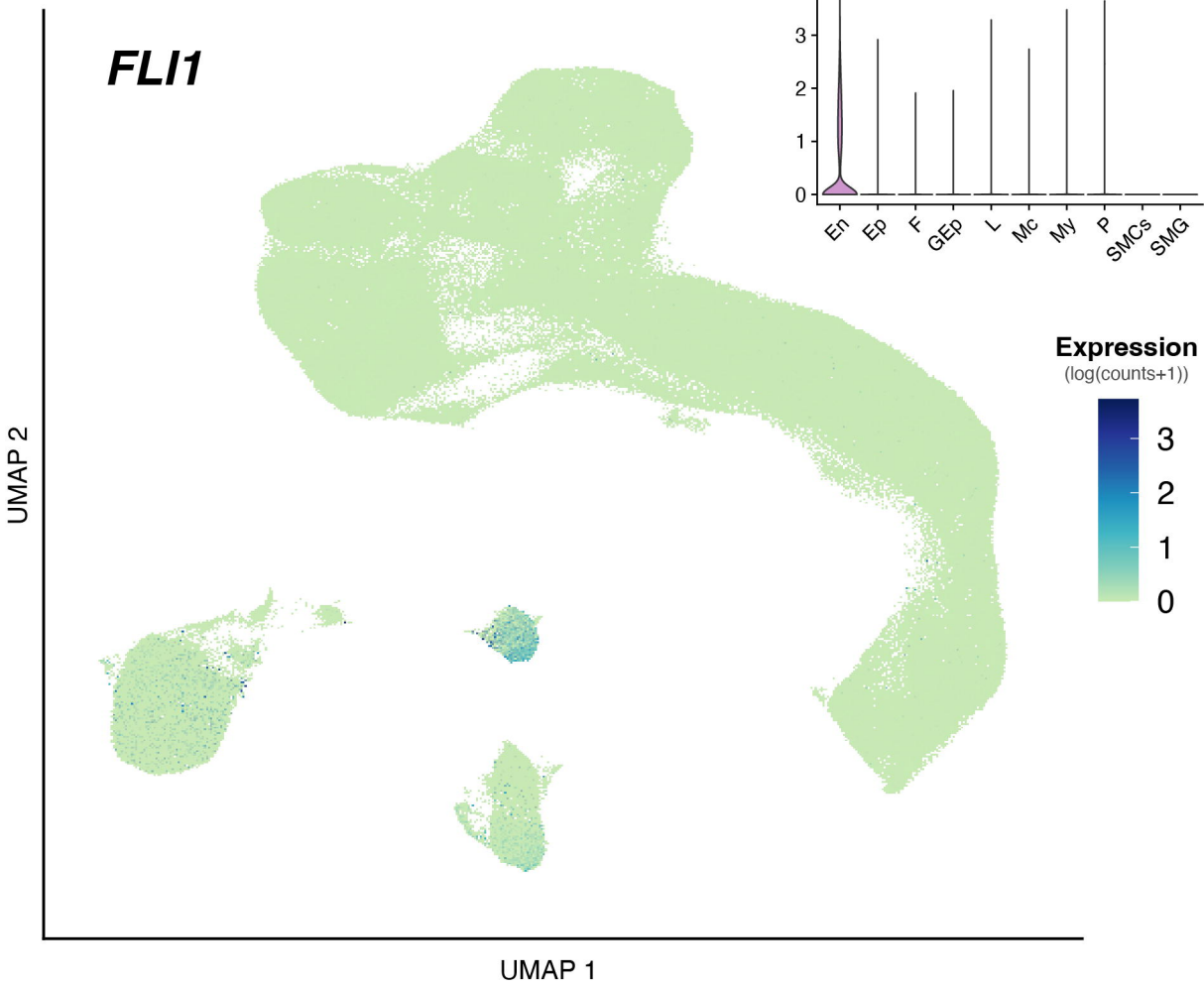
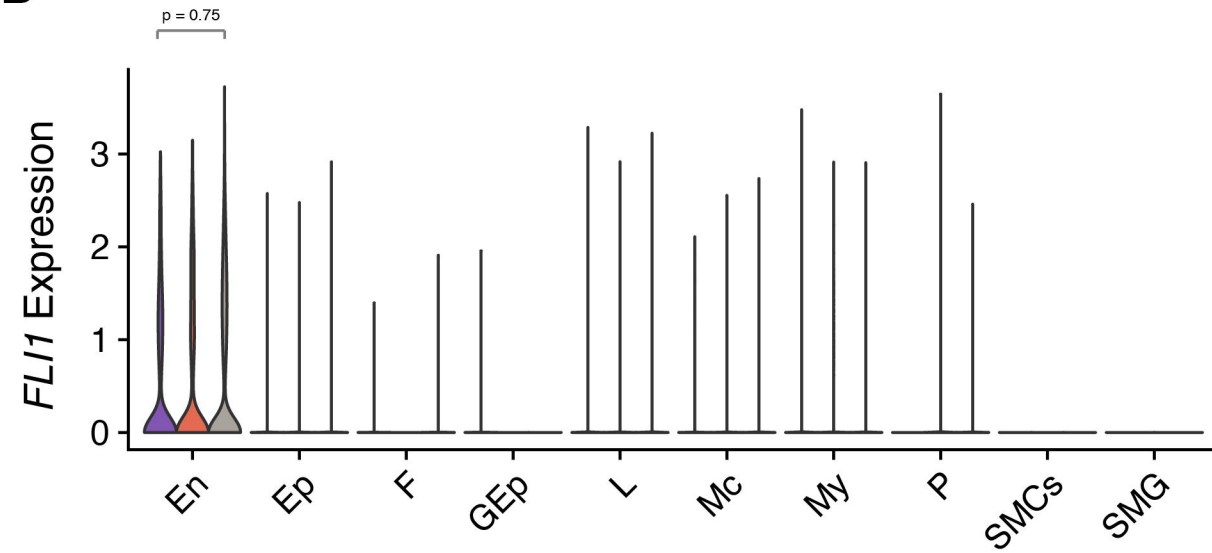


***FGFBP1***



**Differentiation Score**



**A****B****C**